A study of new methods for the simultaneous measurement of diffusion and pore structure in catalyst supports
by Mark Clayton Drake

A thesis submitted in partial fulfillment of the requirements for the degree of Master of Science in Chemical Engineering
Montana State University

Abstract:
Two experimental methods were developed for the simultaneous measurement of both pore structure (i.e., surface area and pore-size distribution) and transport parameters in catalyst supports. One method employed a constant pressure (flow) system, and the other used a variable pressure (batch) system. For the batch method, 2,2-dimethylpropane at 273 K was employed using a “model” spherical support, and carbon dioxide at 303 K was used for the flow system using a commercial cylindrical support.

In the batch method, a step change of adsorbing gas was introduced into the diffusion cell by changing the total pressure of the gas. A finite time was required for equilibrium to occur. By modeling this rate of approach to equilibrium, diffusion coefficients in the support were determined. By measuring the diffusivity over a range of relative pressures, the mode of diffusion was determined (i.e., bulk, Knudsen, or surface). After the mode of diffusion was determined, tortuosity factors were calculated From equilibrium measurements, the surface areas were calculated using the Bruhauer, Emmett, and Teller (BET) equation. Since large quantities of data were generated in this experiment, two techniques were used to match the experimental diffusion data to a “unipore” model. The first technique was the initial slope method, which used experimental data with a normalized weight gain less than 0.5. The second method used moment analysis to match the experimental data over the entire time domain. To determine if the “unipore” model was valid, the value of the effective diffusivity which was calculated from the initial slope method should match that calculated from moment analysis.

In the constant pressure flow process, inert helium was initially introduced into the diffusion cell. A step change in adsorbing gas was accomplished by changing the volume percent carbon dioxide while keeping the total pressure constant with the inert gas. Uptake curves were developed at each step change in adsorbing gas concentration. By modeling this rate of approach to equilibrium, diffusion coefficients in the support may be determined. Three models were attempted to describe the uptake curves that were obtained. The results of the models were inconclusive. Because of the inconclusive results, effective diffusivities could not be determined.

A STUDY OF NEW METHODS FOR THE SIMULTANEOUS MEASUREMENT OF DIFFUSION AND PORE STRUCTURE IN CATALYST SUPPORTS

by

Mark Clayton Drake

A thesis submitted in partial fulfillment
of the requirements for the degree

of

Master of Science

in

Chemical Engineering

MONTANA STATE UNIVERSITY
Bozeman, Montana

August 1984

APPROVAL

of a thesis submitted by

Mark Clayton Drake

This thesis has been read by each member of the thesis committee and has been found to be satisfactory regarding content, English usage, format, citation, bibliographic style, and consistency, and is ready for submission to the College of Graduate Studies.

8/2/84
Date

Chairperson, Graduate Committee

Approved for the Major Department

Aug 2, 1984
Date

John T. Sears
Head, Major Department

Approved for the College of Graduate Studies

8-6-84
Date

Graduate Dean

STATEMENT OF PERMISSION TO USE

In presenting this thesis in partial fulfillment of the requirements for a master's degree at Montana State University, I agree that the Library shall make it available to borrowers under rules of the Library. Brief quotations from this thesis are allowable without special permission, provided that accurate acknowledgment of source is made.

Permission for extensive quotation from or reproduction of this thesis may be granted by my major professor, or in his absence, by the Dean of Libraries when, in the opinion of either, the proposed use of the material is for scholarly purposes. Any copying or use of the material in this thesis for financial gain shall not be allowed without my permission.

Signature Mark C. Quade

Date 7-27-84

ACKNOWLEDGMENTS

The author wishes to thank the faculty and staff of the Chemical Engineering Department at Montana State University for their guidance and assistance.

Special thanks to Dr. Douglas M. Smith for his advice and support throughout the course of this research and thesis preparation.

The author also wishes to thank Dr. Frank P. McCandless and Dr. Robert L. Nickelson for the use of their equipment.

Thanks are also extended to David G. Huizenga for the use of the catalysis supports that he developed.

TABLE OF CONTENTS

	Page
APPROVAL	ii
STATEMENT OF PERMISSION TO USE	iii
ACKNOWLEDGMENTS	iv
TABLE OF CONTENTS	v
LIST OF TABLES	viii
LIST OF FIGURES	ix
NOMENCLATURE	xi
ABSTRACT	xiv
INTRODUCTION	1
BET Surface Area	2
Pore Size Distribution	4
Methods for Measuring Transport Parameters	9
Steady-State Methods	10
Transient Methods	11
Research Objectives	12
DIFFUSION MODELS	13
Mechanism of Transport Into Pores	13
Adsorption Effects	14
"Unipore" Model	14
Surface Concentration Constant	16
Slab	16
Cylinder	17
Sphere	17
Model Matching Techniques	18
Initial Slope Method	18
Moment Analysis	18
Comparison of Initial Slope and Moment Analysis	21

TABLE OF CONTENTS—Continued

	Page
Variable Surface Concentration	21
Slab	22
Cylinder	22
Sphere	22
Moment Analysis	23
EXPERIMENTAL	26
Variable Pressure Batch Method	27
Apparatus	27
Experimental Procedure	29
Constant Pressure Flow Method	30
Apparatus	30
Experimental Procedure	33
Data Acquisition System	34
Data Reduction-Equilibrium	36
Surface Area From Dubinin-Polanyi Theory	36
Surface Area From the BET Equation	37
Pore Size Distribution	37
Data Reduction-Kinetic	39
RESULTS AND DISCUSSION	41
Systems Studied	41
Variable Pressure Batch Method	42
Surface Area	42
Pore Size Distribution	46
Diffusion Coefficients	47
Calculation of Tortuosities	55
Constant Pressure Flow Method	57
Diffusion Coefficients	57
Comparison of Batch and Flow Methods	62
SUMMARY	64
RECOMMENDATIONS FOR FUTURE RESEARCH	65
REFERENCES CITED	66
APPENDICES	69
Appendix 1 – Diffusion Models	70
Slab	71
Sphere	73
Parallel CSTR Model	74

TABLE OF CONTENTS—Continued

Page

Appendix 2 – Computer Algorithms. 76
This program calculates the surface area for porous media using the BET equation with 2,2-dimethylpropane at 273 K 77
This program calculates the surface area for porous media using the BET equation with nitrogen at 77 K 79
This program is a means of computing the pore volume distribution of a powder from isotherm data during either adsorption or desorption. 81
This program evaluates the first through fourth moments. 83
Diffusion model for a slab; Non-steady state; constant surface concentration 85
Diffusion model for a slab; Non-steady state; variable surface concentration 87
Diffusion model for a cylinder; Non-steady state; constant surface concentration 89
Diffusion model for a cylinder; Non-steady state; variable surface concentration 91
Diffusion model for a sphere; Non-steady state; constant surface concentration 93
Diffusion model for a sphere; Non-steady state; variable surface concentration 94
2 CSTR's in parallel model 96
Diffusion model for a cylinder; Non-steady state; 2 CSTR model as the surface concentration 98
This program samples time 100
Appendix 3 – Equilibrium Adsorption Data. 105

LIST OF TABLES

Tables — Page

1. Physical Properties of Adsorbates 41
2. Adsorbents Studied 42
3. Surface Areas Calculated for 2,2-dimethylpropane at 273 K and Nitrogen at 77 K 46
4. Comparison of Times to Given Weight Gain by Initial Slope Method and Moment Analysis 53
5. Linear Regression and 95% Confidence Intervals for D_e versus Total Pressure With 2,2-dimethylpropane at 273 K 55
6. Calculated Knudsen Diffusivities and Tortuosities 57

Appendix Tables

7. Data for Equilibrium Adsorption Experiments for Katalco Alumina Supports 106
8. Data for Equilibrium Adsorption Experiments for $\epsilon = 0.48$ Bimodal Spheres 107
9. Data for Equilibrium Adsorption Experiments for $\epsilon = 0.61$ Bimodal Spheres 108
10. Data for Equilibrium Adsorption Experiments for $\epsilon = 0.38$ Unimodal Spheres 109

LIST OF FIGURES

Figures		Page
1.	Typical type IV adsorption and desorption isotherms showing hysteresis.	6
2.	The five isotherm classifications according to De Boer	8
3.	Sorption curves for slab, cylindrical and spherical geometries with surface concentration C_o	19
4.	The shaded area represents the first statistical moment	20
5.	Sorption curves for slab, cylindrical and spherical geometries for surface concentration given by $C_o (1 - e^{-\beta t})$	24
6.	Calculated sorption curves for surface concentration given by $C_o (1 - e^{-\beta t})$	25
7.	Schematic of variable pressure batch system	28
8.	Schematic of constant pressure flow system	31
9.	Diffusion cell for constant pressure flow system	32
10.	CO_2 calibration curve	35
11.	Adsorption equilibrium data for 2,2-dimethylpropane on unimodal silica spheres at 273 K	43
12.	Adsorption equilibrium data for 2,2-dimethylpropane on bimodal silica spheres at 273 K	44
13.	Adsorption equilibrium data for 2,2-dimethylpropane on bimodal silica spheres at 273 K	45
14.	Experimental sorption curve	48
15.	Reproducibility of experimental sorption curves for the batch method	49
16.	Comparison of effective diffusivities calculated from initial slope method and moment analysis	50

Figures Page

17. Comparison of effective diffusivities calculated from initial slope method and moment analysis 51

18. Comparison of effective diffusivities calculated from initial slope method and moment analysis 52

19. Comparison of initial slope method and moment analysis to an experimental sorption curve 54

20. Reproducibility of experimental uptake curves for the flow method 58

21. Flow diagram for the parallel CSTR model 59

22. Comparison of models with experimental sorption data 60

NOMENCLATURE

A_m	The area occupied per molecule of adsorbate in the complete monolayer
C	Net heat of adsorption
C_o	Initial concentration
C	Concentration
C_2	Concentration into upper chamber in flow method
d_s	Diameter of unimodal spheres
D	Diffusivity
D_e	Effective diffusivity
D_K	Knudsen diffusivity
f	Fraction of molecules which stick to pore wall
F_1	Flow into diffusion cell in flow method
F_2	Flow into upper chamber in flow method
G	Gibbs free energy
h	Linear isotherm coefficient
ierfc	Integral of the complementary error function
I_o	Modified bessel function of the first kind, zero order
I_1	Modified bessel function of the first kind, order one
J_o	Bessel function of the first kind, zero order
J_1	Bessel function of the first kind, order one
$\overline{K}$	Constant determined by the shape of the pore size distribution curve
L	Length of pore
M	Molecular weight of adsorbate

M_t	Total amount of diffusing substance at time t
M_∞	Total amount of diffusing substance at equilibrium
n	0, 1, 2 for slab, cylinder, and sphere
N	6.023×10^{23} molecules/g-mol
P	Pressure
P_0	Saturation pressure
r	Spatial coordinate
$\bar{r}$	Mean pore radius
r_k	Kelvin radius
rp	Actual pore radius
R	Gas law constant
S	Surface area
t	Depth of the adsorbed film
T	Temperature
V	Concentration of sorbate adsorbed on the surface of the porous media
V_1	Volume of diffusion cell in flow method
V_2	Volume of upper chamber in flow method
$\bar{V}$	Molar volume
V_p	Pore volume
W	Weight of adsorbate adsorbed at equilibrium
W_m	Weight of adsorbate at monolayer capacity
α_n	Roots of $J_0(R\alpha_n)$
β	Gas flow rate divided by the diffusion cell volume
γ	Surface tension
δ	Pellet tortuosity factor

ϵ	Void fraction
μ_1	First absolute moment
ρ_p	Particle density
τ	Thickness of one layer
ϕ	Angle of contact between the liquid and the wall of the capillary

ABSTRACT

Two experimental methods were developed for the simultaneous measurement of both pore structure (i.e., surface area and pore-size distribution) and transport parameters in catalyst supports. One method employed a constant pressure (flow) system, and the other used a variable pressure (batch) system. For the batch method, 2,2-dimethylpropane at 273 K was employed using a "model" spherical support, and carbon dioxide at 303 K was used for the flow system using a commercial cylindrical support.

In the batch method, a step change of adsorbing gas was introduced into the diffusion cell by changing the total pressure of the gas. A finite time was required for equilibrium to occur. By modeling this rate of approach to equilibrium, diffusion coefficients in the support were determined. By measuring the diffusivity over a range of relative pressures, the mode of diffusion was determined (i.e., bulk, Knudsen, or surface). After the mode of diffusion was determined, tortuosity factors were calculated. From equilibrium measurements, the surface areas were calculated using the Brunauer, Emmett, and Teller (BET) equation. Since large quantities of data were generated in this experiment, two techniques were used to match the experimental diffusion data to a "unipore" model. The first technique was the initial slope method, which used experimental data with a normalized weight gain less than 0.5. The second method used moment analysis to match the experimental data over the entire time domain. To determine if the "unipore" model was valid, the value of the effective diffusivity which was calculated from the initial slope method should match that calculated from moment analysis.

In the constant pressure flow process, inert helium was initially introduced into the diffusion cell. A step change in adsorbing gas was accomplished by changing the volume percent carbon dioxide while keeping the total pressure constant with the inert gas. Uptake curves were developed at each step change in adsorbing gas concentration. By modeling this rate of approach to equilibrium, diffusion coefficients in the support may be determined. Three models were attempted to describe the uptake curves that were obtained. The results of the models were inconclusive. Because of the inconclusive results, effective diffusivities could not be determined.

INTRODUCTION

Due to the insecurity of petroleum supplies in the Middle East and shortages in world-wide oil reserves, increased attention has been directed toward new sources of energy. The most promising are heavy crude, shale oil, and coal liquids. Due to the large size of these molecules, they provide difficulties as feedstocks for the petroleum refining industry. Since many of the reactions in refining are catalytic (i.e., cracking, reforming, HDS, and HDN), diffusional resistance in the catalyst support pore structure may be significant. This mass transfer resistance can lead to a reduction in the observed activity of the catalyst.

Catalyst supports are normally chosen to be inert with respect to the reacting system, structurally stable at relatively high temperatures and are available in a variety of forms with surface areas ranging from 1 m^2/g to 1300 m^2/g [1]. Typical porosities for catalyst supports range from 10 to 60% with an average pore radius from 1 to 100 nm [1].

One of the most common supports is silica gel, either in the form of granules or powder. Alumina or a composite of silica and alumina are also widely used. Diatomaceous earth, a naturally occurring form of silica having a surface area in the neighborhood of 50 m^2/g, may be utilized as a powdered carrier. Porous carbon is thermally stable to temperatures of 1273 K or more under inert conditions, and certain forms have the highest known surface areas of any material, up to about 1300 m^2/g. These "activated" carbons are commonly used as catalyst carriers for organic reactions [2].

Two methods are commonly used to calculate the total surface area for catalyst supports. For microporosity or pores less than 2 nm, Dubinin-Polyanyi [3,4] potential theory is employed. For pores in the transition range, with diameters between 2 nm and 20 nm, and macropores with diameters above 20 nm the Brunauer, Emmett, and Teller (BET) [5]

theory is used to determine the total surface area. Due to the fact that this research deals with catalyst supports with a mean pore diameter greater than 2 nm, only the BET theory will be considered. This limitation is a result of the large macromolecules used in the refining industry which can approach the size of a 2 nm pore.

Adsorption studies leading to measurements of pore size and pore size distributions employ the Kelvin equation [6]. This relates the equilibrium vapor pressure of a curved surface, such as that of a liquid in a capillary or pore, to the equilibrium pressure of the same liquid on a plane surface.

From equilibrium weight gain measurements of adsorbents as a function of total pressure, adsorption isotherms are developed. Surface area, total pore volume, and pore size distribution can be determined from the methods discussed earlier.

BET Surface Area

To determine surface area by gas adsorption, one needs to calculate the quantity of adsorbate that is equal to a molecular monolayer on the solid surface. Multiplying this quantity by the cross-sectional area occupied by a single adsorbed molecule yields the surface area of the catalyst. This is calculated using the BET equation in which the amount of gas adsorbed on the solid at constant temperature is measured as a function of total pressure of adsorbate gas. The BET equation is [6]:

$$\frac{1}{W[(P_0/P) - 1]} = \frac{1}{W_m C} + \frac{C-1}{W_m C}\frac{P}{P_0} \qquad (1)$$

where

W = weight of adsorbate adsorbed at equilibrium

P = pressure at equilibrium

P_0 = saturation pressure of the adsorbate

W_m = weight of adsorbate at monolayer capacity

C = net heat of adsorption, called the BET **C** value.

A plot of $1/W(P_0/P - 1)$ versus P/P_0 will yield a straight line. Values of W_m and **C** can be calculated from the slope $[(C-1)/W_mC]$ and the intercept $[1/W_mC]$.

The applicability of the BET theory is limited to the range of relative pressures between 0.05 and 0.35, representing the linear BET range. This can be attributed to the assumption that all adsorption sites are energetically equal. The model ignores the influence of lateral adsorbate interactions. Brunauer [7] answers these criticisms by pointing out that lateral interaction between adsorbate molecules increases as the surface becomes more completely covered. The adsorption potential, however, decreases with increasing adsorption up to monolayer coverage. By assuming an energetically heterogeneous surface, the high-energy sites will be occupied at lower relative pressures and occupancy of the lower-energy sites will occur near the completion of the monolayer. These two trends can lead to a nearly constant overall adsorption energy up to completion of the monolayer, which is an implicit assumption of the BET theory. Finally the second and higher layers of molecules have energies assumed to be equal to the heat of liquefaction. For the most reliable measurements the molecules of the gas chosen should be small, approximately spherical, and inert so no chemisorption takes place.

Having determined the monolayer capacity, the specific surface area, $S(m^2/g)$, is calculated by [8]:

$$S = \frac{W_m}{M} N \cdot A_m \times 10^{-20} \qquad (2)$$

W_m = monolayer capacity of adsorbate

M = molecular weight of adsorbate

N = Avogadro's constant

A_m = the area occupied per molecule of adsorbate in the complete monolayer.

In order to use Equation 2, it is necessary to know the value of the cross-sectional area A_m. The value of this quantity is difficult to calculate because of our lack of knowledge as to the exact packing of the adsorbed molecules in a complete monolayer.

Emmett and Brunauer [9] proposed that A_m be calculated from the density of the adsorbate in the liquid form. They assumed that the arrangement of the molecules on the surface was similar to that on a plane surface placed within the bulk of the liquid. For twelve nearest neighbors in the bulk liquid and six on the plane we then have the equation [8]:

$$A_m = 1.091 \left(\frac{M}{\rho N}\right) \times 10^{16} \tag{3}$$

This yields values of 0.162 nm^2, 0.195 nm^2, and 0.625 nm^2 for nitrogen [9] (77 K), CO_2 [11] (273 K), and 2,2-dimethyl propane [10] (273 K), respectively.

Pore Size Distribution

Two methods are commonly used to determine the pore size distribution. One is Mercury Porosimetry, using the Washburn equation and the second is application of the Kelvin equation to adsorption-desorption isotherms.

The Kelvin equation [6], which had been established originally by Thompson [12] (later by Lord Kelvin), relates the vapor pressure of a curved surface, such as that of a liquid in a capillary or pore, to the equilibrium pressure of the same liquid on a plane surface. The increase in the amount of vapor adsorbed onto a catalyst support, as a result of an incremental increase in vapor pressure at constant temperature, represents the filling of capillaries the size of which is given by the Kelvin equation. The size of the largest pore that can be measured is limited by the rapid change of meniscus radius with pressure as the

relative pressure, P/P_0, nears unity. This is generally taken as about 30 nm in diameter, corresponding to a relative pressure of 0.93 [2]. The smallest pore sizes that can be determined by this method are about 1.5-2 nm in diameter. This is because the molecules equipotential lines interact with each other in these small pores and the Kelvin equation no longer applies.

A somewhat different relationship between the amount of vapor sorbed and pressure is usually obtained experimentally upon decreasing rather than increasing the pressure [2]. This difference is known as a hysteresis effect. Figure 1 depicts hysteresis which is typical of porous adsorbents on type IV isotherms [8]. De Boer [13] describes this as a type A hysteresis which is due mainly to cylindrical pores open at both ends. The five types of de Boer's hysteresis will be described later. The line BCD indicates the path followed along the adsorption isotherm, whereas line DFB demonstrates the path followed along the desorption isotherm. The presence of the hysteresis loop introduces considerable complications because there are two relative pressures that correspond to a quantity adsorbed. Figure 1 shows that the weight W adsorbed is at a lower relative pressure on the desorption curve than on the adsorption isotherm. The molar free energy change from the condensation of the vapor into the pore during adsorption is determined by:

$$\Delta G_{ads} = RT(\ln P_{ads} - \ln P_0) \tag{4}$$

For the same quantity on the desorption isotherm, the free energy change is

$$\Delta G_{des} = RT(\ln P_{des} - \ln P_0) \tag{5}$$

Since $P_{des} < P_{ads}$, it follows that $\Delta G_{des} < \Delta G_{ads}$. Therefore, the desorption isotherm is preferred because it is the more stable condition [8].

Several theories have been postulated to describe hysteresis during adsorption and desorption. Zsigmondy [14] attributed hysteresis to a difference in the contact angle during adsorption and desorption. McBain [15] accounted for the hysteresis by assuming the

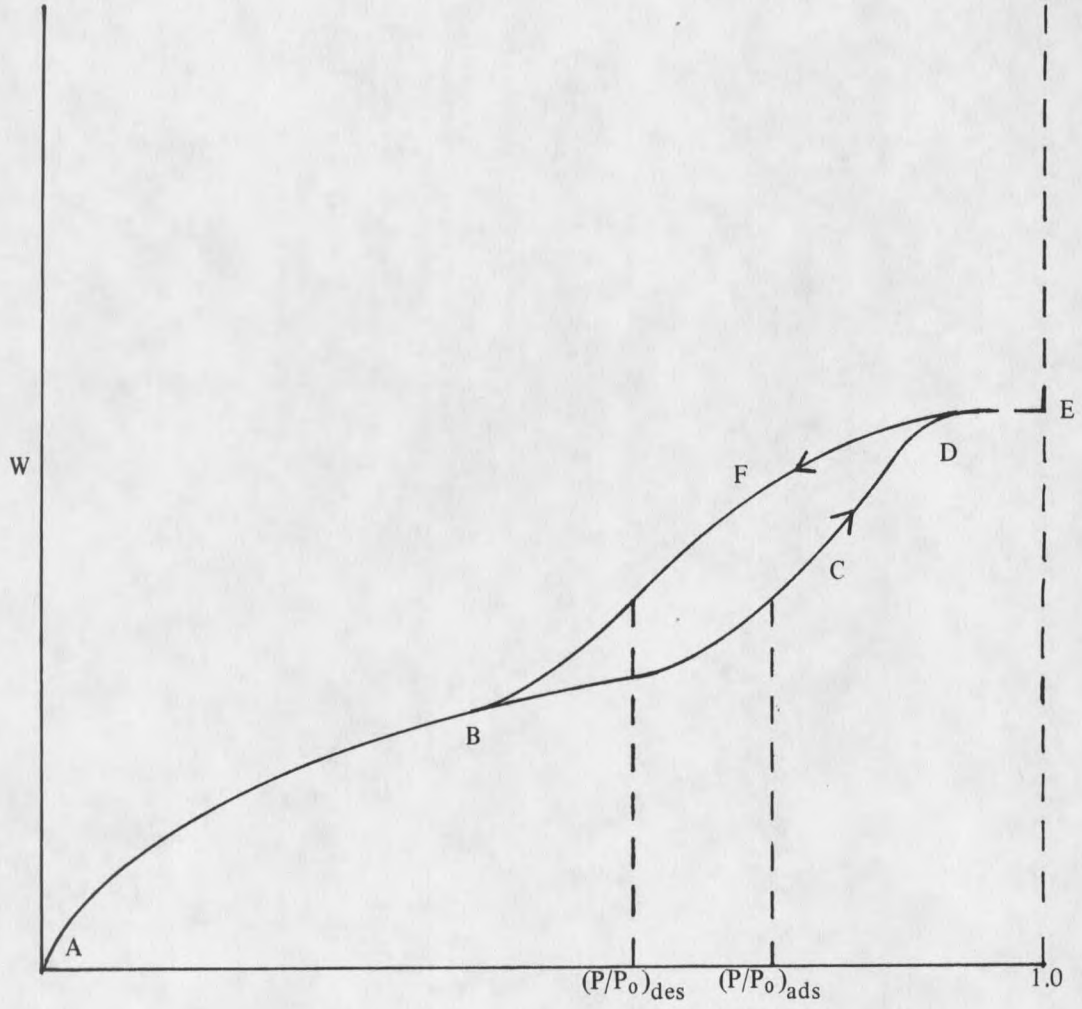

Figure 1. Typical type IV adsorption and desorption isotherms showing hysteresis.

pores contained a narrow opening and a wide body, the so-called "bottleneck" shape. Cohan [16] assumed that condensation occurs by filling the pore from the wall inward. For a cylindrical pore, this would give a cylindrical shaped meniscus whereas evaporation occurs from a hemispherical meniscus once the pore is filled. Foster [17] explained hysteresis by considering the pores to fill by adsorption on the walls while emptying by evaporation from a spherical meniscus. These theories each describe reasons for the occurrence of hysteresis, but no one theory appears to provide a complete explanation.

De Boer [13] has identified five types of hysteresis loops which he has correlated with various pore shapes. Figure 2 shows the five types of hysteresis. Type A is mostly due to cylindrical pores open at both ends. Type B is associated with slit-shaped pores or a space between parallel plates. Type C is produced by a mixture of tapered or wedge-shaped pores with open ends. Type D curves are also produced by tapered or wedge-shaped pores with narrow necks at one or both ends. Type E results from McBain's "bottleneck" pores.

To measure pore size and pore size distributions the Kelvin equation is applied [6,8]

$$\ln\left(\frac{P}{P_0}\right) = -\frac{2\bar{V}\gamma}{rRT}\cos\phi \qquad (6)$$

where

P_0 = saturation vapor pressure

γ = surface tension

$\bar{V}$ = molar volume

ϕ = the angle of contact between the liquid and the walls of the capillary

r = radius of the pore.

Usually knowledge of the pore geometry is not known. Because of this, the assumption of cylindrical pores is made. It is also necessary to assign a value to the angle of contact between the liquid and the pore walls. This quantity is extremely difficult to determine directly in the case of porous solids. The usual assumption is to set the contact angle equal to zero.

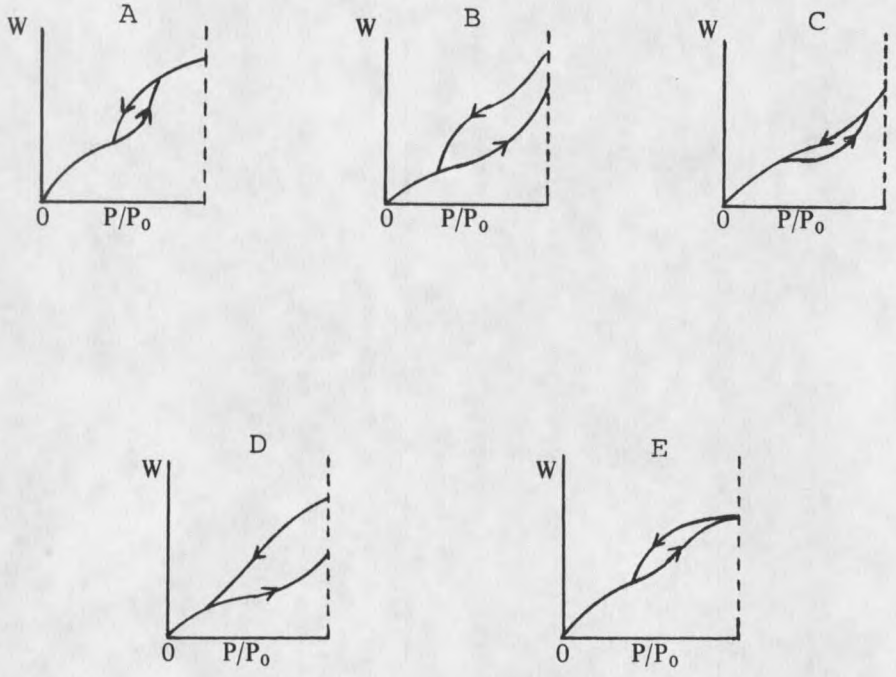

Figure 2. The five isotherms classifications according to De Boer [13].

From Equation 6, the Kelvin radius, r_k, can be calculated. This is not the true radius because adsorption has occurred on the pore wall, prior to condensation, leaving a center core of radius r_k.

With the depth of the adsorbed film being t, then the actual pore radius, r_p, is

$$r_p = r_k + t \tag{7}$$

It is now necessary to calculate t.

Using the assumption that the adsorbed film depth in a pore is the same as on a plane surface for any value of relative pressure, one may write

$$t = \left(\frac{W_a}{W_m}\right) \cdot \tau \tag{8}$$

where W_a and W_m are respectively, the quantity adsorbed at a particular relative pressure and the weight corresponding to the BET monolayer. τ is the thickness of one layer. The value of τ can be calculated by considering the area and volume occupied by one mole of liquid adsorbate if it were spread over a surface to the depth of one molecular layer.

$$\tau = \frac{\bar{V}}{S} \tag{9}$$

where $\bar{V}$ is the molar volume and S is the surface area occupied by one mole of the sorbate when a single layer is formed.

Further details for pore size distribution calculations are given in Lowell [8] and Gregg and Sing [6].

Methods for Measuring Transport Parameters

Several methods are available to measure transport parameters. These methods are divided into two categories, either steady-state or transient. Many unit operations in engineering do not operate in the steady-state. Examples include ion-exchange columns, adsorption towers and packed beds. Therefore, transport parameters must be calculated from

transient methods for these systems. It is the intent of this study to provide a means by which to calculate one particular transport parameter, the effective diffusivity. Comparison of effective diffusivities from steady-state and dynamic experiments can, in principle, provide information about pore structure. For example, dead-end pores should not affect diffusion at steady state, but would influence the diffusion coefficient in dynamic experiments.

Steady-State Methods

Two types of experiments are in common use for studying steady-state diffusion in porous solids. The most frequently used method for steady-state operation is the Wicke-Kallenbach [18] diffusion cell, also known as the constant pressure, counter diffusion cell. In this experiment, the ends of the catalyst pellet are exposed to either an adsorbing or a non-adsorbing gas such that no pressure gradients occur across the sample. Diffusion rates are determined from the flow rates and concentrations of the two outlet streams. The "plug flow" experiment, as the name implies, uses a plug of the porous solid of interest through which the desired gas is forced. By measuring the gas flow rate and the pressure drop across the sample, the diffusivity can be calculated.

The constant pressure, counter diffusion experiment offers advantages over the "plug flow" type experiment. These advantages are [19]:

1. By eliminating the total pressure gradient, the computation of effective diffusivities is simplified.
2. By measuring both gas fluxes simultaneously, the time required for the experiment is halved.

Transient Methods

To determine unsteady-state effective diffusivities, three types of experiments are commonly used. The first method employs volumetric measurements. This is accomplished by introducing a step change of an adsorbing gas into the chamber containing the catalyst support. The size of the chamber and the step change concentration in adsorbing gas must be small to insure that the surface concentration remains constant. The pressure change versus time is then measured. From this data and an appropriate model describing the system, transport coefficients can be determined. The advantage for using the volumetric method is that it can be used for light gases (i.e., low molecular weight) which would not produce a large enough weight gain to be used with gravimetric techniques.

The second method uses pulse tracer (chromatographic) experiments for the determination of diffusivities. Various investigations using these techniques are reviewed by Smith [20] and Satterfield [21]. By passing a pulse of tracer gas through either a fixed-bed, ion-exchange column or a single catalyst pellet, transport coefficients may be obtained by relating the shape of the response pulse to a model describing the system.

The third type of experiment employs gravimetric techniques. Generally, two types of gravimetric balances are used in catalyst research, spring extension [22] and the null beam balance [23,24]. The spring balance usually employs a quartz spiral. Weight change is proportional to the spring extension, the measurement being made visually and intermittently with a cathetometer or automatically by a suitable transformer coupled to electronic equipment giving a continuous voltage output. Disadvantages of the spring balance are limited loading capacity for a given sensitivity and displacement of the sample position with a change in weight [25].

The beam balance uses tare weights, and null principle so that the sample remains in a fixed position. Weight changes are then detected by application of a suitable counterforce

to maintain the null position, the counterforce being converted to voltage which is recorded versus time on a computer acquisition system. To determine transport parameters, a step change in adsorbing gas is introduced into the diffusion cell. A finite time is required for equilibrium to occur. From this rate of approach to equilibrium data an appropriate model is then constructed. Transport parameters can be determined from the model.

The advantages of gravimetric measurements are: only a small sample size is needed; measurements can be made at constant or variable pressure; readings are automatic and continuous; and operation can be static or under flow conditions. The disadvantage is that an adsorbing gas is needed.

Research Objectives

The objective of this research project was to examine an experimental procedure for the simultaneous measurement of both pore structure (i.e., surface area and pore-size distribution) and an effective diffusivity in several catalyst supports. Two different experimental adsorption techniques were to be evaluated, one using a constant pressure flow cell and the other utilizing a variable pressure batch cell. Diffusion models describing each system were to be constructed to evaluate effective diffusivities.

DIFFUSION MODELS

To determine the effective diffusivity in porous media, an appropriate physical model describing the system must be developed. The effective diffusivity calculated via appropriate model matching techniques is put into the solution of the model and a sorption curve is then generated. This is then compared with the experimental data. If the curve generated matches the experimental data the diffusion coefficient calculated is appropriate.

Mechanism of Transport into Pores

The diffusion of an adsorbing gas through porous media may occur due to any of three possible mechanisms. A knowledge of the mechanisms of diffusion is required in order to determine the tortuosity factor and to ascertain the effect of pressure and temperature on the transport rate.

The three possible mechanisms are bulk, Knudsen and surface diffusion. When the pore size is much greater than the mean free path of the gas, intramolecular collisions dominate and gas diffusion is purely bulk diffusion. If the pore size is much smaller than the mean free path of the diffusing gas, Knudsen diffusion will predominate the rate of molecular movement. As a result a molecule within the pore structure will, in general, strike a pore wall before it strikes a second molecule. Intramolecular collisions may thus be neglected. The molecule then travels within the pore by a series of "random flights" interrupted by collisions with the pore wall [26]. When the pore size approaches the mean free path, intramolecular and molecule wall interactions are both important. This is called the transition region. In addition to the two gas phase mechanisms, transport of adsorbed gases along the surface may occur. This surface diffusion has been explained as a flow

of the outer layers as a condensed phase. The overall flux of a gas through porous media may be any one or a combination of the three mechanisms stated above.

Adsorption Effects

Two assumptions were made dealing with adsorption effects. The first is that sorption can be described by the linear isotherm

$$V = hC \tag{10}$$

where

V = concentration of the sorbate adsorbed on the surface of the porous media

h = linear isotherm coefficient

C = concentration of sorbate in the gas phase

This is usually valid at low concentrations. The second is that the rate of adsorption is assumed to be much more rapid than the rate of diffusion (i.e., there is physical adsorption only).

"Unipore" Model

Although the theory of diffusion in a single capillary is well developed, the application of this theory to practical problems is quite complex. In order to apply the findings of capillary theory, a physical model of the porous media must be assumed.

The "unipore" or "parallel pore" model as developed by Wheeler [26] has received wide application in studying porous media due to its conceptual and mathematical simplicity. A porous particle is presumed to be a solid with a system of parallel, nonconnecting cylindrical pores of the same size. A shortcoming of the parallel pore model is its failure to account for intersections and deadends. A modification to the "unipore" model is the addition of a tortuosity factor. This factor is a semiempirical constant employed in an attempt to overcome the above mentioned shortcoming [19].

The following assumptions were made in the development of the "unipore" model:

1. Equilibrium between the gas and adsorbed phases.
2. The diffusion coefficient is constant.
3. Diffusion is one dimensional (no edge effects).
4. The particle has zero concentration initially.

These assumptions were made to minimize the number of parameters considered and will result in findings which may be applied to experiments with multiple particles.

The mass balance for either slab, cylindrical or spherical geometries is

$$\frac{D\epsilon}{\delta r^n} \frac{\partial}{\partial r}\left(r^n \frac{\partial C}{\partial r}\right) = \frac{\partial C}{\partial t} + \frac{\rho_p}{\epsilon} \frac{\partial V}{\partial t} \tag{11}$$

where

n = 0, 1, 2 for slab, cylinder, and sphere

D = diffusion coefficient (i.e., bulk, Knudsen, or surface diffusion)

r = spatial variable

C = concentration

t = time

ϵ = porosity of the particle

ρ_p = particle density

δ = tortuosity

The initial and boundary conditions are as follows

$$C(r,0) = 0, \quad C(R,t) = C_o(t), \quad \frac{\partial C}{\partial r}(0,t) = 0 \tag{12}$$

When the sorbed phase is assumed to be in equilibrium with the gas phase, the source/sink term ($\partial V/\partial t$) is obtained by taking the derivative of the sorption-isotherm Equation 10:

$$\frac{\partial V}{\partial t} = h \frac{\partial C}{\partial t} \tag{13}$$

Substituting Equation 13 into Equation 11 gives

$$\frac{D\epsilon}{\delta r^n}\frac{\partial}{\partial r}\left(r^n\frac{\partial C}{\partial r}\right)=\left(1+\frac{h\rho_p}{\epsilon}\right)\frac{\partial C}{\partial t} \tag{14}$$

Defining an effective diffusivity by

$$D_e=\frac{D\epsilon}{\delta\left(1+\frac{h\rho_p}{\epsilon}\right)} \tag{15}$$

and combining Equation 14 with Equation 15, the governing equation for transient uptake in a porous particle is

$$\frac{D_e}{r^n}\frac{\partial}{\partial r}\left(r^n\frac{\partial C}{\partial r}\right)=\frac{\partial C}{\partial t} \tag{16}$$

The fractional uptake as a function of time is

$$\frac{M_t}{M_\infty}=\frac{{}_0\int^R r^n\,C(r,t)dr}{{}_0\int^R r^n\,C(r,\infty)dr} \tag{17}$$

where

M_t = the total amount of diffusing substance at time t

M_∞ = the total amount of diffusion substance at equilibrium

Surface Concentration Constant

This is the case where the initial concentration in the porous media is zero, and the surface concentration is instantaneously changed to C_o.

The initial and boundary conditions are

$$C(r,0)=0,\quad C(R,t)=C_o,\quad \frac{\partial C}{\partial r}(0,t)=0 \tag{18}$$

Solutions for the slab, cylindrical and spherical geometries are now presented.

Slab. The sorption time curve is given by [27]:

$$\frac{M_t}{M_\infty} = 1 - \sum_{n=0}^{\infty} \frac{8}{(2n+1)^2\,\pi^2}\, e^{-D_e(2n+1)^2\,\pi^2\,t/4R^2} \tag{19}$$

where R = one half of the diffusion path length.

Although Equation 19 predicts the quantity of gas adsorbed as a function of time and the effective diffusivity, convergence problems exist at short times and an alternative form should be used. The corresponding solution useful for small times is [28]

$$\frac{M_t}{M_\infty} = 2\left(\frac{D_e t}{R^2}\right)^{1/2} \left\{ \pi^{-1/2} + 2 \sum_{n=1}^{\infty} (-1)^n \operatorname{ierfc}\left(\frac{nR}{\sqrt{(D_e t)}}\right) \right\} \tag{20}$$

Cylinder. The solution for diffusion into a cylinder is given by [27]:

$$\frac{M_t}{M_\infty} = 1 - \sum_{n=1}^{\infty} \frac{4}{R^2\,\alpha_n^2}\, e^{-D_e\,\alpha_n^2\,t/R^2} \tag{21}$$

where

R = radius of the cylinder

α_n = roots of $J_o(R\alpha_n)$

The corresponding solution for small times is [28]

$$\frac{M_t}{M_\infty} = \frac{4}{\pi^{1/2}}\left(\frac{D_e t}{R^2}\right)^{1/2} - \frac{D_e t}{R^2} - \frac{1}{3\pi^{1/2}}\left(\frac{D_e t}{R^2}\right)^{3/2} + \ldots \tag{22}$$

Sphere. The total amount of diffusion substance entering or leaving a sphere is given by [27]:

$$\frac{M_t}{M_\infty} = 1 - \frac{6}{\pi^2} \sum_{n=1}^{\infty} \frac{1}{n^2}\, e^{-D_e n^2 \pi^2 t/R^2} \tag{23}$$

where R = radius of the sphere.

The corresponding solution for small times is [28]:

$$\frac{M_t}{M_\infty} = 6\left(\frac{D_e t}{R^2}\right)^{1/2}\left\{\pi^{-1/2} + 2\sum_{n=1}^{\infty} \text{ierfc}\left(\frac{nR}{\sqrt{(D_e t)}}\right)\right\} - 3\,\frac{D_e t}{R^2} \qquad (24)$$

Curves comparing the three geometries show M_t/M_∞ as a function of $(D_e t/R^2)^{1/2}$ and are presented in Figure 3.

Model Matching Techniques. Two techniques are presented that allow the determination of an effective diffusivity from experimental data. The first is the initial slope method which uses the experimental data at short times. The second method utilizes moment analysis which uses experimental data over the whole time domain.

Initial Slope Method. For M_t/M_∞ less than 0.5, the following approximations are used:

$$\frac{M_t}{M_\infty} = \frac{2(n+1)}{\sqrt{\pi}}\left(\frac{D_e t}{R^2}\right)^{1/2} \qquad (n=0,1,2) \qquad (25)$$

By plotting the fraction adsorbed, M_t/M_∞, versus $\sqrt{\text{time}}$, an effective diffusivity can be calculated from the linear region.

Moment Analysis. Effective diffusivities may also be determined using the experimental data over the entire time domain. This can be ascertained from moment analysis using the first absolute moment. The solution to Equations 16 to 18 is obtained in the Laplace domain, where the moments are given by [24]:

$$m_i = (-1)^i \left.\frac{d^i(\tilde{M}_t/\tilde{M}_\infty)}{ds^i}\right|_{s=0} \qquad (26)$$

and $\tilde{M}_t/\tilde{M}_\infty$ is the Laplace transform of M_t/M_∞. The solution to this problem for the first absolute moment is [22]:

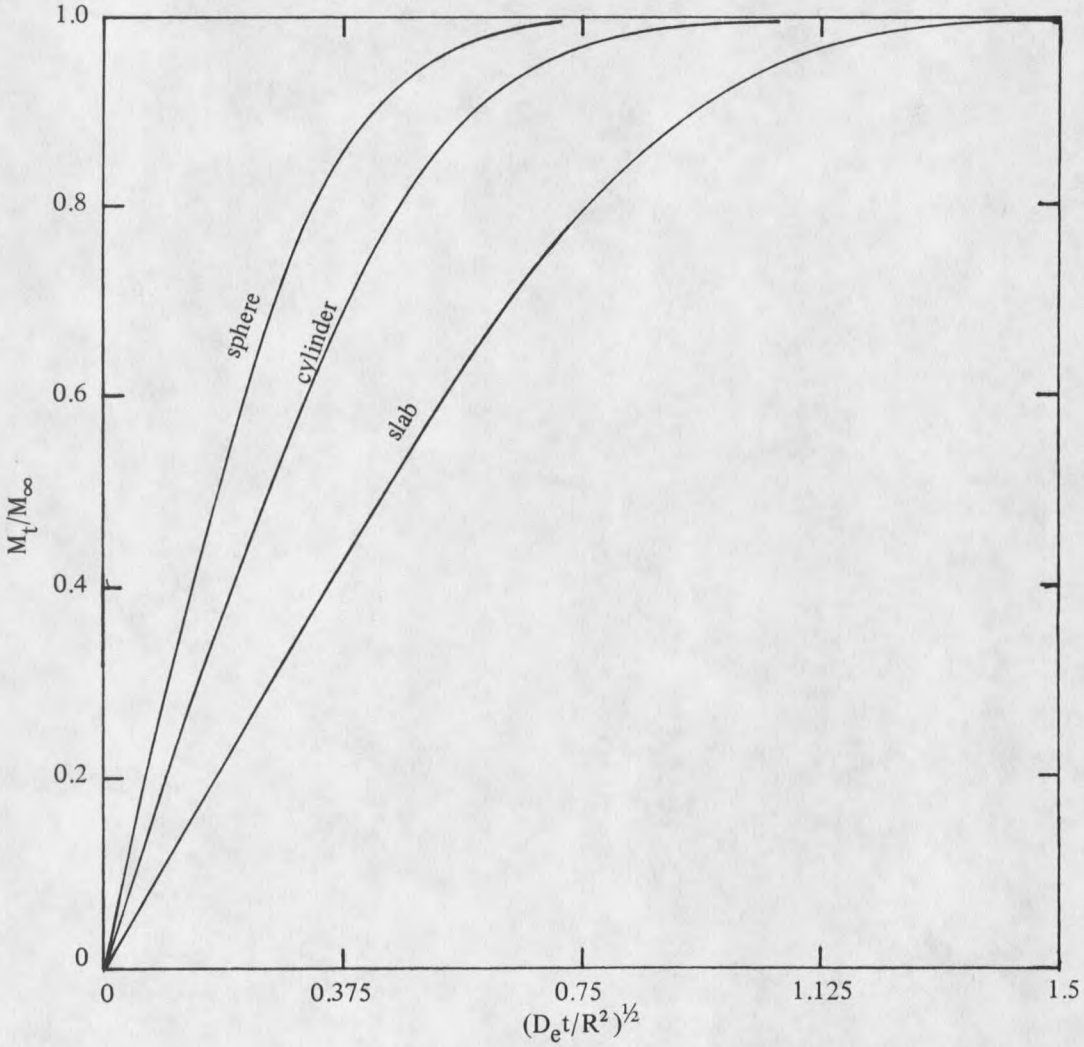

Figure 3. Sorption curves for slab, cylindrical and spherical geometries with surface concentration C_o.

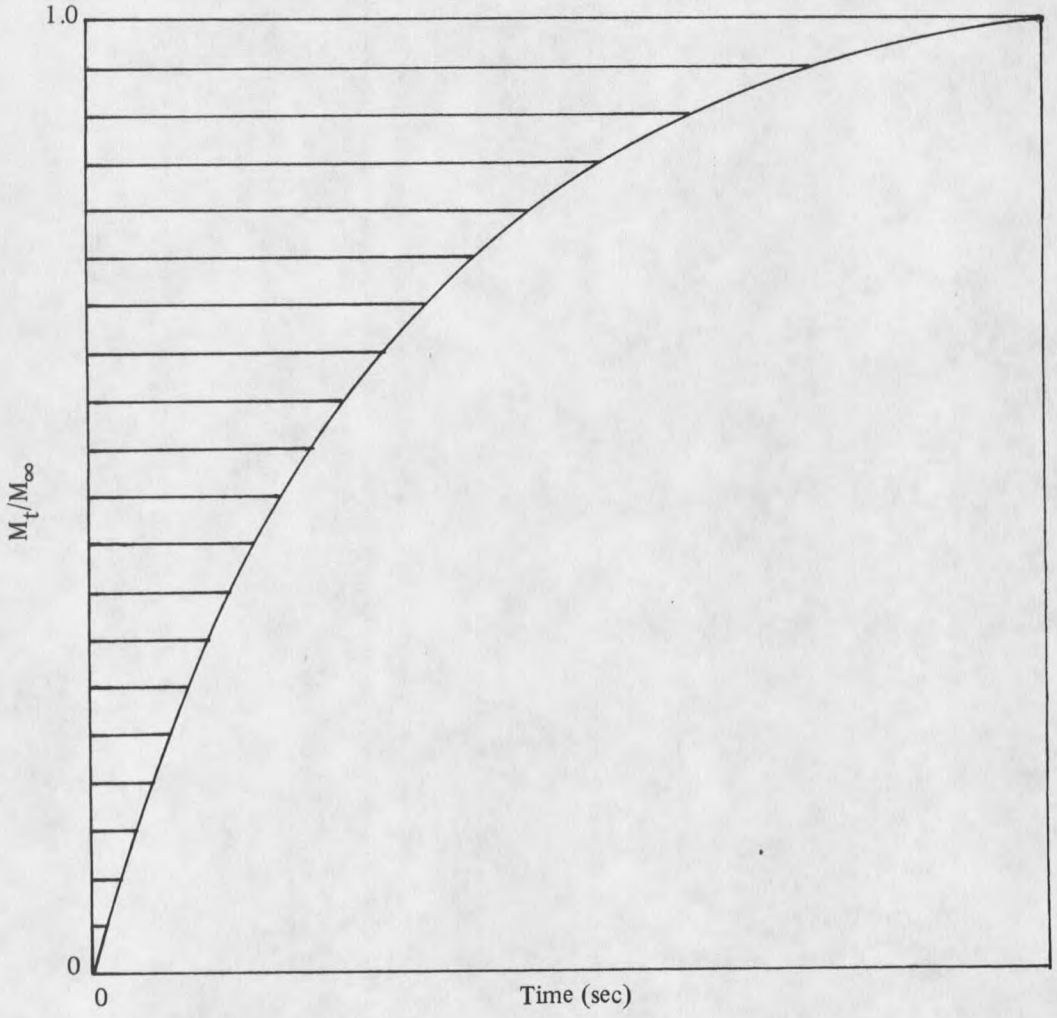

Figure 4. The shaded area represents the first statistical moment.

$$\mu_1 \equiv \frac{m_1}{m_0} = \frac{1}{(n+1)(n+3)} \frac{R^2}{D_e} \qquad (n=0,1,2) \qquad (27)$$

The moments of the experimental (monotonically increasing) curves M_t/M_∞ versus time can be related to the moments of the (monotonically decreasing) complementary curve $(1 - M_t/M_\infty(t))$ versus time, as [24]:

$$m_i = i_0 \int^{\infty} (1 - M_t/M_\infty (t))\, t^{i-1}\, dt \qquad (28)$$

The shaded area in Figure 4 represents the moments calculated from Equation 28. Equating Equations 27 and 28, an analytic expression involving the diffusion coefficient is obtained. Appendix 2 contains an algorithm that will evaluate the first through fourth moments from M_t/M_∞ versus time data.

Comparison of Initial Slope and Moment Analysis. To determine if the "unipore" model is valid for the porous media in question, the value of D_e, which is calculated for short times only should match that calculated from data over the whole time domain. If the effective diffusivities calculated from the two methods do not match, then the "unipore" model is not adequate for this material and another model should be developed.

Variable Surface Concentration

This is the case where the initial concentration in the porous media is initially zero, and the surface approaches an equilibrium concentration C_o exponentially. This can represent a surface concentration which is changed rapidly but not instantaneously, a situation which usually arises when an instantaneous change is attempted in an experiment.

The initial and boundary conditions are:

$$C(r,0) = 0, \quad C(R,t) = C_o(1 - e^{-\beta t}), \quad \frac{\partial C}{\partial r}(0,t) = 0 \qquad (29)$$

where

β = F/V

V = diffusion cell volume

F = volumetric flow rate

Presented are solutions for the slab, cylindrical and spherical geometries for diffusion when each surface approaches an equilibrium concentration, C_o, exponentially.

Slab. The sorption time curve is given by [27]:

$$\frac{M_t}{M_\infty} = 1 - e^{-\beta t}\left(\frac{D_e}{\beta R^2}\right)^{1/2} \tan\left(\frac{D_e}{\beta R^2}\right)^{1/2} - \\ - \frac{8}{\pi^2} \sum_{n=0}^{\infty} \frac{e^{-(2n+1)^2 \pi^2 D_e t/4R^2}}{(2n+1)^2\left[1 - (2n+1)^2\left\{\frac{D_e \pi^2}{4\beta R^2}\right\}\right]} \qquad (30)$$

where R = one half the path length, and β is not equal to $D_e(2n+1)^2\pi^2/4R^2$.

Cylinder. The sorption versus time curve is given by [27]:

$$\frac{M_t}{M_\infty} = 1 - \frac{2J_1\left\{(\beta R^2/D_e)^{1/2}\right\} e^{-\beta t}}{(\beta R^2/D_e)^{1/2} J_0\left\{(\beta R^2/D_e)^{1/2}\right\}} + \frac{4}{R^2} \sum_{n=1}^{\infty} \frac{e^{-D_e \alpha_n^2 t}}{\alpha_n^2\left\{\frac{\alpha_n^2}{(\beta/D_e)} - 1\right\}} \qquad (31)$$

where

R = radius of the cylinder

α_n = roots of $J_0(R\alpha_n)$

Sphere. The sorption-time curve is given by [27]:

$$\frac{M_t}{M_\infty} = 1 - \frac{3D_e}{\beta R^2} e^{-\beta t}\left[1 - \left(\frac{\beta R^2}{D_e}\right)^{1/2} \mathrm{Cot}\left(\frac{\beta R^2}{D_e}\right)^{1/2}\right] +$$

$$+ \frac{6\beta R^2}{\pi^2 D_e} \sum_{n=1}^{\infty} \frac{e^{-D_e n^2 \pi^2 t/R^2}}{n^2(n^2\pi^2 - \beta R^2/D_e)} \qquad (32)$$

where R = radius of the sphere.

Figure 5 compares uptake curves for slab, cylindrical and spherical geometries plotted against $(D_e t/R^2)^{1/2}$ with the parameter $\beta R^2/D_e$ equal to 3. Figure 6 depicts uptake curves for cylindrical geometry with different values of the parameter $\beta R^2/D_e$ plotted against $(D_e t/R^2)^{1/2}$. When $\beta = \infty$, the surface concentration rises instantaneously to C_o and the curve of Figure 6 has the characteristic initial linear portion followed by the approach to the equilibrium value, M_∞. The uptake curves for finite values of $\beta R^2/D_e$, for which the surface concentration rises at a finite rate, all show points of inflexion. At first the rate of uptake increases as sorption proceeds but later decreases as the final equilibrium is approached. Curves of this kind are often referred to as sigmoid sorption curves [20].

Moment Analysis. Since finite values of $\beta R^2/D_e$ give sigmoid sorption curves, the small time portion of the uptake curve is not linear, therefore the initial slope method cannot be used. Effective diffusivities are determined using Equations 26 and 27 to evaluate the first absolute moment.

The solution of Equations 16, 17, and 29 is

$$\mu_1 \equiv \frac{m_1}{m_o} = \frac{1}{\beta} + \frac{1}{(n+1)(n+2)} \frac{R^2}{D_e} \qquad (n=0,1,2) \qquad (33)$$

Derivations for the first absolute moment for all three geometries is given in Appendix 1.

The effective diffusivities are determined using Equation 33 and μ_1 is calculated from the moment algorithm given in Appendix 2.

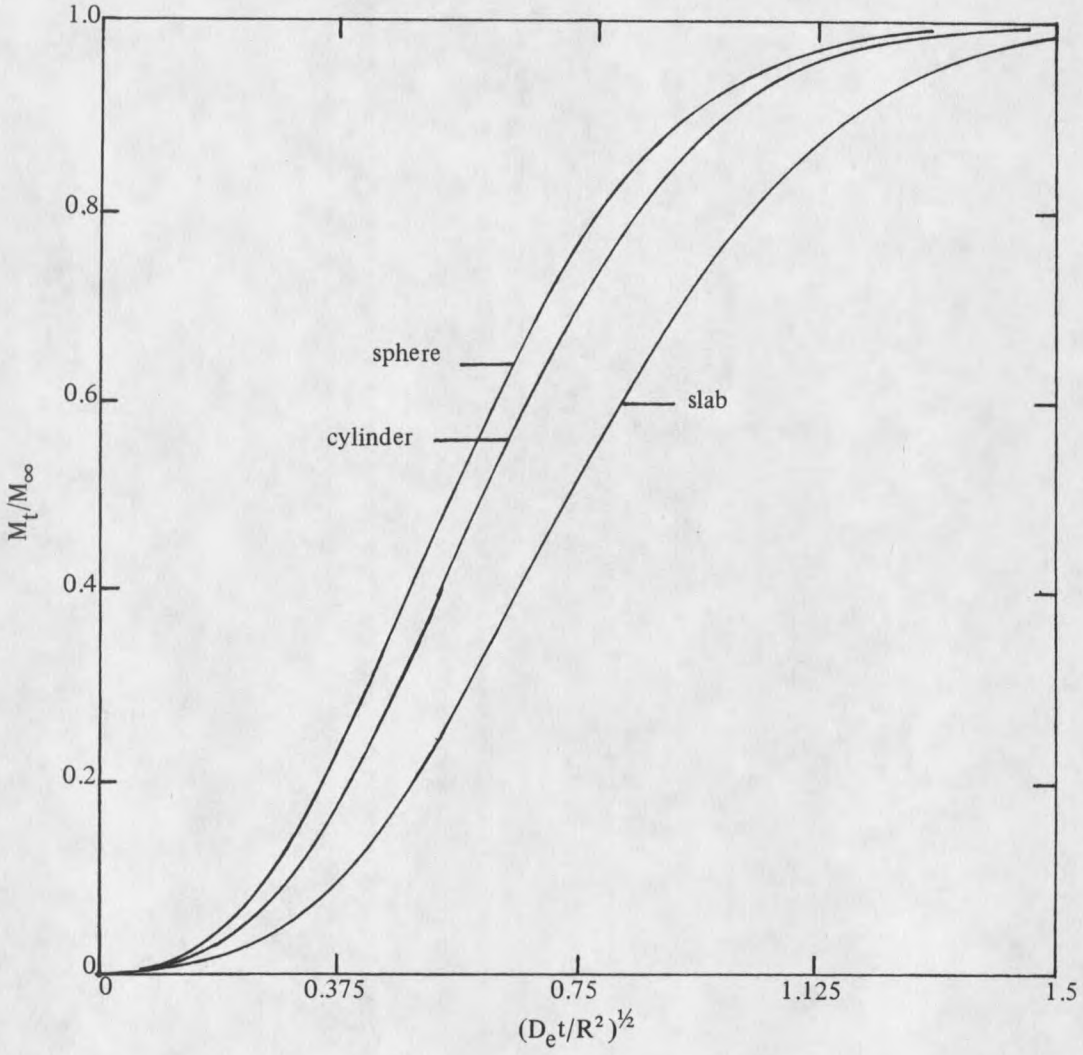

Figure 5. Sorption curves for slab, cylindrical and spherical geometries for surface concentration given by $C_o \left\{ 1 - \exp(-\beta t) \right\}$.

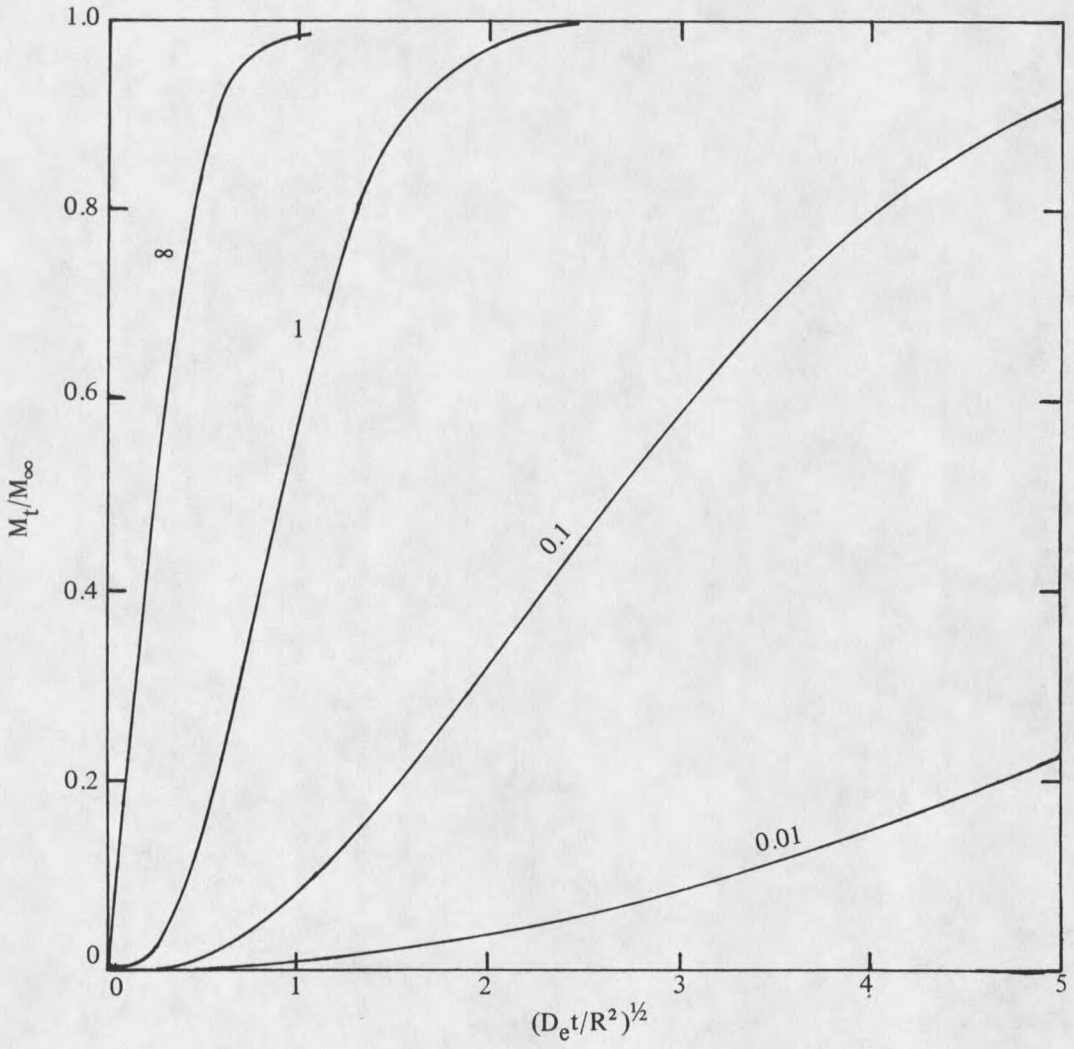

Figure 6. Calculated sorption curves for surface concentration given by $C_o(1 - e^{-\beta t})$. Numbers on curves are values of $\beta R^2 / D_e$.

EXPERIMENTAL

Two different experimental methods were examined to determine the pore structure and transport parameters in porous media. The first one is a variable pressure batch system, and the second is a constant pressure flow method.

In the batch system, a step change of a single adsorbing gas is introduced into the diffusion cell by changing the total pressure of the gas. A finite time is required for equilibrium to occur. This rate of approach to equilibrium (i.e., an uptake curve which is the weight gain of adsorbed gas on the porous media versus time) is acquired by a data acquisition system. From this uptake curve, transport parameters are calculated from the methods discussed in the modeling section. By determining the equilibrium weight as a function of pressure, adsorption isotherms are developed. Step changes in the adsorbing gas pressure are continued until the saturation pressure is approached. The effective diffusivities are determined over a range of pressures from near zero up until the saturation pressure is approached. By plotting the diffusion coefficients versus pressure, the mechanism of diffusion (i.e., bulk, Knudsen or surface) can be determined. If the diffusion coefficients are constant over the entire pressure range the mechanism of diffusion is pure Knudsen. If there is an upward trend in the coefficients, then it is possible that the mechanism of pure Knudsen diffusion is coupled with surface diffusion [20]. If there is a downward trend in the diffusion coefficients, then the mechanism of diffusion is in the "transition" region. The mechanism of diffusion is purely bulk if the diffusion coefficients are inversely proportional to pressure.

In the constant pressure flow process, helium is initially introduced into the diffusion cell. Helium is used to keep the process at a constant pressure, also it is inert so it will not

adsorb onto the porous media. The step change in adsorbing gas concentration is accomplished by changing the volume percent of the adsorbing gas while keeping the total pressure constant with inert gas. This is repeated for different inlet concentrations until the saturation pressure is approached. As described in the variable pressure system, uptake curves are developed at each step change in adsorbing gas concentration. By fitting these curves with the model derived describing the system, diffusion coefficients are determined. From equilibrium weight measurements, adsorption isotherms are also developed. Having a high enough flow rate in the diffusion cell will insure there is a negligible bulk film resistance on the surface of the porous media.

Variable Pressure Batch Method

Apparatus

A schematic of the apparatus is shown in Figure 7. The system consisted of a CAHN/Ventron R-100 null beam electrobalance. The balance detects sample weight gain by application of a counterforce to maintain the null position. The counterforce is converted to voltage which was recorded by the data acquisition system. A Sargent-Welch model 1400 vacuum pump was used to evacuate the system and desorb gases from the porous media. Two different adsorbing gases were employed; nitrogen at 77 K and 2,2-dimethylpropane at 273 K. The step change in the inlet gas was controlled by a pressure regulator and a needle valve in series. The cell was immersed in a Masterline 2095 constant temperature bath with ethylene glycol as the fluid for experiments at 273 K. Liquid nitrogen was used to reach temperatures of 77 K. The sample weight versus time curves were monitored by an Apple II computer with a Cyborg/Isaac analog to digital interface. The algorithms used to sample the uptake curves is given in Appendix 2. Equilibrium gas pressure measurements were determined using a mercury manometer.

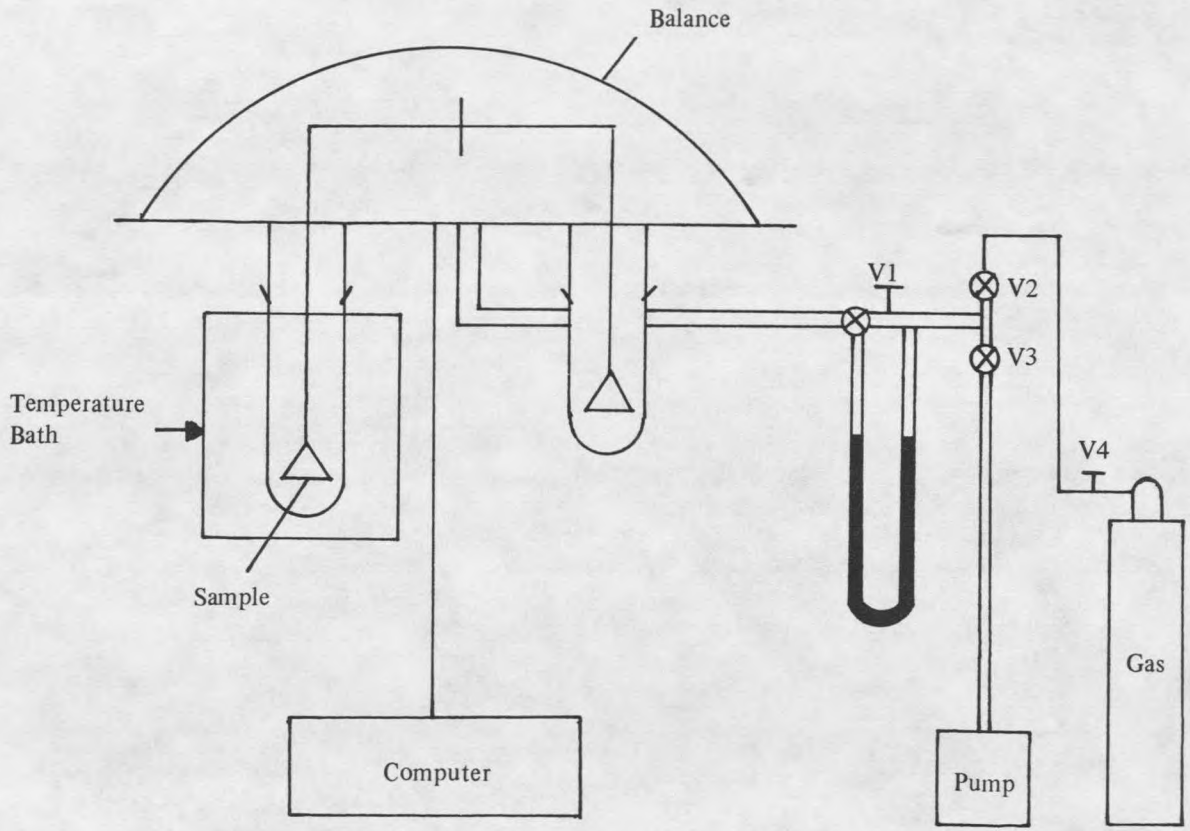

Figure 7. Schematic of variable pressure batch system.

Experimental Procedure

To initiate the experiment, the diffusion cell was loaded with 0.1 to 1.0 grams of sample. All valves were closed except V1 and V3, and the cell was evacuated for approximately 24 hours at room temperature. The weight loss was monitored to determine when equilibrium is attained. Then the cell was cooled with the constant temperature bath for about an hour until its equilibrium temperature was reached. If 2,2-dimethylpentane was used, the cell was cooled to 273 K and if nitrogen was employed, it was cooled to 77 K. A step change of 20 to 40 torr of adsorbing gas was introduced into the reaction cell. The experimental procedure is:

1. Close valves V1 and V3 to terminate the desorption.
2. Tare the scale to zero and record the zero value.
3. Start the computer program.
4. Open valves V1 and V2.
5. Introduce a 10 to 40 torr step change of gas by adjusting the needle valve V4.
6. After the desired amount of gas is obtained, close valves V1 and V2. Open valve V3 and measure the total pressure of the gas introduced from the mercury manomenter.
7. After the sample weight reached equilibrium, print out the voltage versus time results from the computer.
8. The equilibrium weight gain was recorded from the Cahn electrobalance.
9. Steps 2 through 8 were repeated until the saturation pressure of the adsorbing gas was approached.

The rate of approach to equilibrium was automatically sampled by the data acquisition system. At the completion of the final run, the diffusion cell was evacuated overnight at room temperature to remove the adsorbed gas to prepare for a new set of sorption runs.

The weight gains recorded from the electrobalance had a sensitivity of ±0.5 micrograms. The pressure was measured to within ±1 torr of their stated values, and the temperature of the diffusion cell was maintained at ±1 K of its setpoint.

Constant Pressure Flow Method

Apparatus

Figure 8 shows a schematic of the experimental system. The system consists of a CAHN/Ventron R-100 null beam electrobalance; a Sargent-Welch model 1400 vacuum pump; and an Apple II computer with a Cyborg/Isaac analog to digital interface which monitored the sample weight versus time curves.

Inert helium was initially input into the system at the desired flow rate to ensure good mixing within the diffusion cell itself. CO_2 was then fed in a step-wise manner through a metering valve, a rotameter, the diffusion cell and finally through a gas chromatograph. The diffusion cell is surrounded by a chamber that has ethylene glycol flowing from a Masterline 2095 constant temperature bath at 303 K. The step change in the inlet gas concentration was accomplished by adding CO_2 while adjusting the flow rate of helium to keep the total flow of the mixture constant. The effluent stream was analyzed for % CO_2 after every run with a gas chromatograph (Varian Aerograph Series 1400) equipped with a chart recorder to record the peak heights and a manual sampling valve to introduce the gases.

Figure 9 shows the diffusion cell itself. It was enclosed in a chamber surrounded by ethylene glycol flowing to keep the diffusion cell isothermal. The sample was contained in stainless steel wire baskets having three tiers. This allowed for increased gas contact with the catalyst support. The helium-carbon dioxide mixture was fed through a copper 1/8" tube that extended to the bottom of the diffusion cell. The purpose for this was to ensure there was sufficient mixing in the diffusion cell so the concentration was uniform throughout.

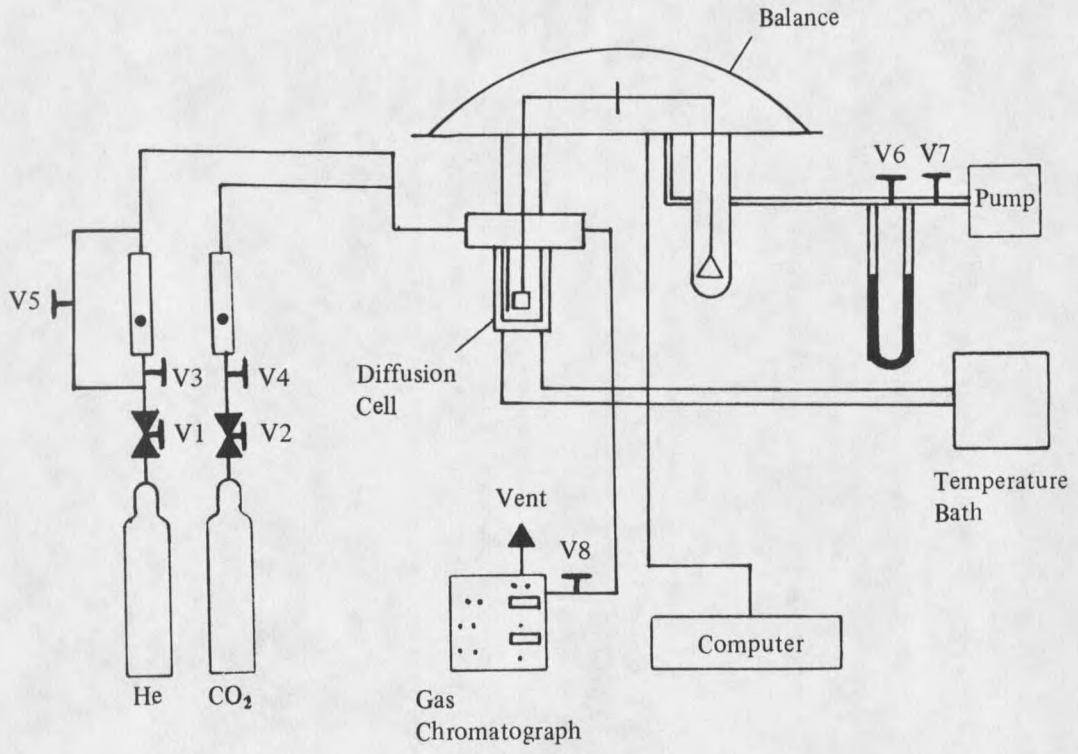

Figure 8. Schematic of constant pressure flow system.

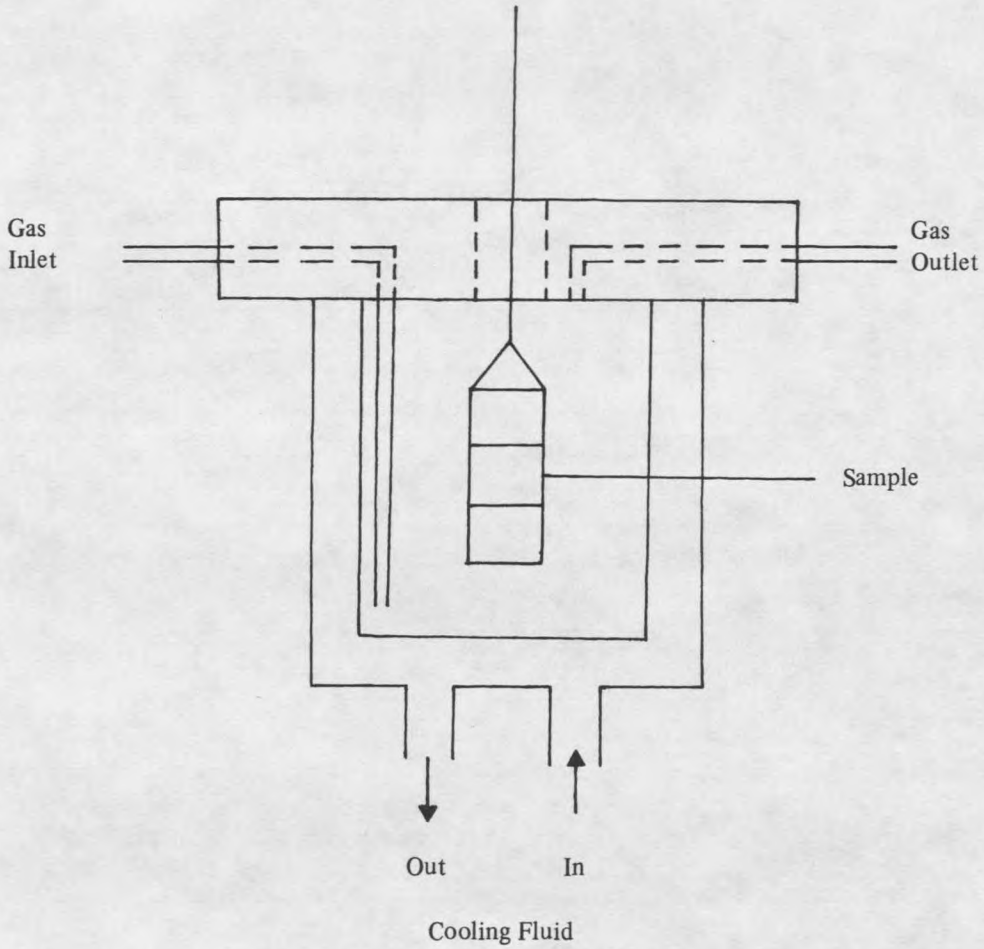

Figure 9. Diffusion cell for constant pressure flow system.

Experimental Procedure

After the diffusion cell was loaded with 0.2 to 0.5 grams of sample, the system was desorbed for approximately 24 hours. The cell was heated to 303 K by the constant temperature bath. Both of the Matheson Model 70 series low pressure line regulators on the carbon dioxide and the helium cylinders, valves V1 and V2, were set at 5 psig. Helium was then added to pressurize the system to atmospheric pressure. Due to the restricted flow rate of the rotameter, pressurization was accomplished through the helium bypass valve V5. This reduced the time required to pressurize the system to atmospheric pressure. After the diffusion cell reached its equilibrium temperature, which took approximately one hour, the experiment was initiated. The helium flow was then adjusted to one of two flow rates studied, either 30 cc/min or 60 cc/min at STP. The sequence of steps was as follows:

1. Tare the scale to zero.
2. Start the computer program.
3. Input the carbon dioxide by opening valve V4 while adjusting the helium valve V3 to keep the gas mixture flow rate constant.
4. The sample weight versus time was sampled by the data acquisition system. When the system reached equilibrium the voltage versus time data were printed out from the computer.
5. The equilibrium weight gain was recorded from the Cahn electrobalance.
6. The volume percent carbon dioxide was determined by gas chromatograph (GC) analysis.
7. The gas stream volumetric flow rate was then determined from a soap-film flow meter.
8. A new run was begun by repeating steps 1 through 7 to a higher volume percent carbon dioxide.

At the completion of the final run, the cell was evacuated overnight to ensure complete removal of all adsorbed carbon dioxide.

Data Acquisition System

During the course of each sorption run, the uptake curve was sampled periodically by the Apple II/Cyborg data acquisition system. The algorithm is given in Appendix 2. This algorithm samples the voltage increase that is required to keep the balance in a null position. The output signal from the electrobalance ranges from 0 to 100 mV. This is then amplified with an Omega D.C. millivolt amplifier from 0 to 5 (± 0.0024) volts and digitized by the Cyborg data acquisition system.

The gases used for this study were analyzed by a Varian Aerograph Series 1400 gas chromatograph using hydrogen as a carrier gas. The two choices for a carrier gas are helium and hydrogen. Since helium and carbon dioxide were the gases to be separated, hydrogen was the logical choice for the carrier gas. Hydrogen was supplied at 40 psig and was adjusted to flow through the chromatograph at an exit flow rate of 40 ml/min. The chromatographic separation was performed using a 1/8" × 12' column packed with Chromosorb 102 80/100 mesh particles. The composition of the separated gases are then determined using a thermal conductivity detector. The transient output signal from the detector (0 to 10 mV) is received by a chart recorder. The peak height from the CO_2 peak was measured and the % CO_2 determined from the calibration curve shown in Figure 10, a plot of percent carbon dioxide versus peak height. The column temperature was operated at 308 K. The detector was heated to 348 K and operated and 150 mA. The chromatograph was allowed to operate at least 3 hours before samples were analyzed so steady-state operation was attained.

Calibration of the gas chromatograph was accomplished by correlating the gas composition with the peak height of carbon dioxide measured on a chart recorder. Gas standards

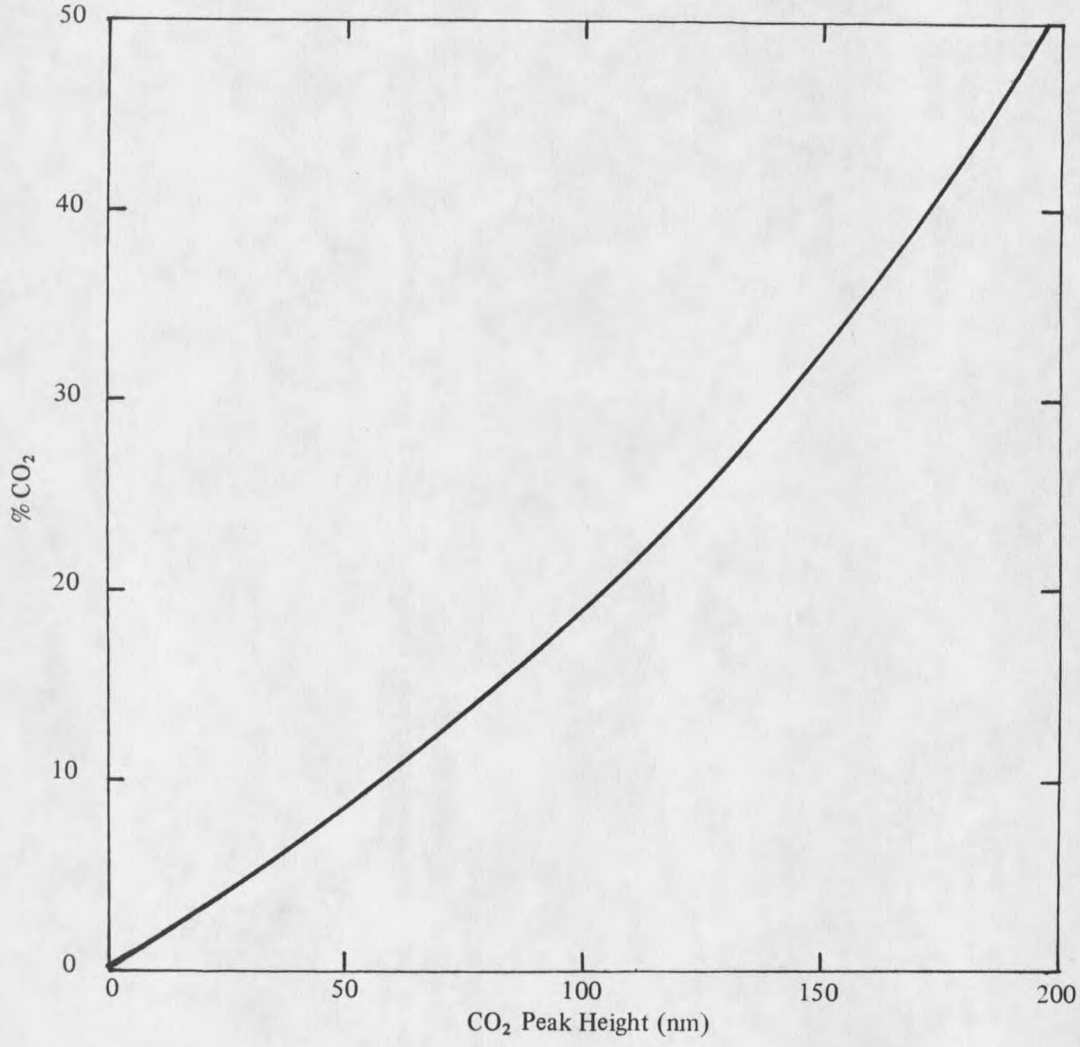

Figure 10. CO_2 calibration curve.

were made by placing a 1 liter cylinder in series between the gas feed and the gas chromatograph. The cylinder and all connected lines were evacuated. Carbon dioxide was then added to the cylinder at the desired pressure. The pressure was determined from the mercury manometer. The cylinder valve was closed and the gas lines were again evacuated. Helium was then added and the final pressure was measured. Three to five peak height determinations were made for each of the gas standard.

The gas stream volumetric flow rate was determined with a soap-film flow meter. This meter was a 10 ml glass buret containing a 0.05 percent soap solution. The flow rate was determined by timing the soap film as it traveled from the 0 to the 10 ml mark.

Data Reduction-Equilibrium

Presented are two methods for the calculation of surface area of porous materials. One is the Dubinin-Polanyi theory for microporous substances and the other is the BET equation. Calculations are also presented for pore size distribution.

Surface Area From Dubinin-Polanyi Theory

Many catalyst supports have pore with radii less than 1.5 nm. These pores are generally classified as "micropores". To determine the surface area of a microporous material, the Dubinin-Polanyi [3,4] theory can be used. The governing equation is

$$\log W = \log W_m - \bar{K} \log \left(\frac{P_0}{P}\right)^2 \qquad (34)$$

where

$\bar{K} = 2.303 * \bar{k} * (RT)^2$

W = weight of adsorbate at equilibrium

W_m = weight of adsorbate at monolayer capacity

P = pressure at equilibrium

P_0 = saturation pressure of adsorbate

A plot of log W versus $(\log P_0/P)^2$ should yield a straight line with an intercept of log W_m from which the surface area can be calculated by Equation 2. The linear range of these plots are usually at very low relative pressures, less than 10^{-2}.

Surface Area From the BET Equation

The BET equation was used to determine the monolayer coverage on the catalyst supports. Having determined the monolayer capacity, the specific surface area, $S(m^2/gm)$, is calculated by Equation 2.

The BET equation in its final form is:

$$\frac{1}{W[(P_0/P) - 1]} = \frac{1}{W_m C} + \frac{C-1}{W_m C}\frac{P}{P_0} \qquad (1)$$

A plot of $1/W(P_0/P) - 1)$ versus P/P_0 will yield a straight line. Values of W_m and C can be calculated from the slope $[(C-1)/W_m C]$ and the intercept $[1/W_m C]$. The applicability of the BET theory is limited to the range of relative pressures between 0.05 and 0.35.

Computer programs for both nitrogen and 2,2-dimethylpropane BET surface area determination can be found in Appendix 2. To use the algorithms, the sample weight is entered in grams. Then the experimental data is entered as pressure in torr and the weight of adsorbate adsorbed at equilibrium in grams. The programs will fit the data to a straight line, y=ax+b, and determine the slope and y-intercept. The monolayer capacity, heat of adsorption and specific surface area is calculated.

Pore Size Distribution

The following steps are calculation details for pore size distribution [6,8]. The adsorbed volumes are normalized for one gram of adsorbent. Relative pressures are chosen using small decrements at high values, where r is very sensitive to small changes in relative pressure and where the slope of the isotherm is large, such that small changes in relative pressure produce a large change in volume.

1. The Kelvin radius is calculated from the Kelvin equation assuming a zero wetting angle.

2. The film depth t, is calculated using Equation 8.

3. The pore radius r_p, is calculated using Equation 7.

4. $\bar{r}_k$ and $\bar{r}_p$ are determined by calculating the mean value in each decrement from successive entries.

5. The change in film depth is calculated by taking the difference between successive values of t.

6. ΔV_{ad}, is the change in adsorbed volume between successive P/P_o values and is determined by subtracting successive values from V_{ad}.

7. ΔV_{liq}, is the volume of liquid corresponding to V_{ad}, it is calculated by the known moles of V_{ad} and multiplied by the liquid molar volume. For nitrogen at STP this is given by:

$$\Delta V_{liq} = \frac{\Delta V_{gas}}{22.4 \times 10^3} \times 34.6 \ (cm^3) \tag{35}$$

8. The volume change of the adsorbed film remaining on the walls of the pores is the product of the film area ΣS and the decrease in the film depth Δt. By assuming no pores are present larger than the size of the pore corresponding to a relative pressure of 0.99, the first ΣS can be set to zero, since there exists no film area from the previously emptied pores. Subsequent values are calculated as the product of Δt for a decrement, and ΣS from the values corresponding to the adsorbed film area exposed by evaporation of the center cores of all the previous decrements.

9. The actual pore volume is evaluated from the following equations:

$$\Delta V_{liq} = \pi \bar{r}_k^{\,2} L + \Delta t \Sigma S \tag{36}$$

where

L = length of the pore

$\bar{r}_k$ = average Kelvin pore radius

Δt = decrease in film depth

ΣS = film area

Equation 36 represents the volume evaporated out of the center cores plus the volume desorbed from the film left on the pore walls. The actual pore volume is given by

$$V_p = \pi \bar{r}_p^2 L \tag{37}$$

where $\bar{r}_p$ is the average pore radius. Combining Equations 36 and 37 results to form

$$V_p = \left(\frac{\bar{r}_p}{\bar{r}_k}\right)^2 [\Delta V_{liq} - (\Delta t \Sigma S)(10^{-4})]\,cm^3 \tag{38}$$

10. The surface area of the pore walls is calculated from the pore volume by

$$S = \frac{2V_p}{\bar{r}_p} \times 10^4\ (m^2) \tag{39}$$

with V_p in cubic centimeters and $\bar{r}_p$ in Angstroms. It is this value of S which is summed in part 8.

11. ΔV_p, the increment of actual pore volume, is calculated by subtracting successive values.

12. Calculate $\Delta V_p/\Delta r_p$.

13. Plot $\Delta V_p/\Delta r_p$ versus $\bar{r}_p$.

In Appendix 2, a computer program for the calculation of pore volume distribution from nitrogen sorption isotherms is given.

Data Reduction-Kinetic

After the kinetic data was acquired from a given sorption experiment, the following analysis was applied. First, the data was entered into a data file and normalized. Second, the normalized weight gain versus time data was plotted. From the weight gain versus time

plot, the time corresponding to zero weight gain was determined. All later times were then offset by the time corresponding to zero weight gain. The normalized and offset data was then used for the model matching techniques.

To calculate diffusivities by the initial slope method, the fraction adsorbed, M_t/M_∞, versus time was plotted. The slope is then determined from the linear region at low times. An effective diffusivity is then calculated from Equation 25.

To calculate diffusivities from moment analysis, the first absolute moment is determined from the algorithm in Appendix 2 which evaluates Equation 28 using experimental data over the whole time domain. To determine the effective diffusivity for constant surface concentration in the batch method Equation 27 was used, and for variable surface concentration in the flow method Equation 33 was employed.

The mechanism of transport into the pores was then determined. This was accomplished by plotting the effective diffusivity as a function of pressure. If the diffusion coefficients are constant over the entire pressure range the mechanism of diffusion was purely Knudsen. If there was a downward trend in the diffusion coefficients, then the mechanism of diffusion is in the "transition" region. If there was an upward trend in the diffusion coefficients, then the mechanism of Knudsen diffusion is coupled with surface diffusion.

Knowing the mechanism of diffusion, porosity, and the effective diffusivity, the tortuosity can be calculated using Equation 15.

RESULTS AND DISCUSSION

Systems Studied

Physical properties for the adsorbates used in this study at experimental conditions are presented in Table 1. 2,2-Dimethylpropane at 273 K was used because it is symmetrical, nonpolar and has a suitable saturation pressure. Nitrogen at 77 K was chosen because it is the standard for calculating surface area and pore size distribution. Carbon dioxide at 273 K was used to determine surface areas by applying Dubinin-Polanyi [3,4] theory. For the flow method, carbon dioxide at 303 K was chosen because it is symmetric, commonly used for adsorption studies and is easily available.

Table 1. Physical Properties of Adsorbates.

Adsorbate	Temperature (K)	Sat. Press. Po (atm)
Batch Method		
2,2-dimethylpropane	273	0.697
Nitrogen	77	0.842
Carbon dioxide	273	34.397
Flow Method		
Carbon dioxide	303	71.166

Table 2 presents the four adsorbents used in this study. Huizenga [29] has fabricated assemblages of silica spheres with unimodal and bimodal size distributions. By randomly packing these spheres into metal casings, a porosity of 0.38 was attained for the unimodal spheres, and porosities of 0.48 and 0.61 were created for the bimodal spheres by varying the packing pressure. Only the ends of the assemblages of spheres were exposed in the metal casings allowing these catalyst supports to be modeled for calculating diffusivities

using a one dimensional slab geometry. The Katalco alumina pellets used are a representative catalyst support in the cracking industry.

Table 2. Adsorbents Studied.

Adsorbent	Porosity	Sphere Diameter (nm)
Silica Spheres		
Unimodal	0.38	107±9
Bimodal	0.48	15 and 94±8
Bimodal	0.61	15 and 94±8
		Mean Pore Diameter (nm)
Katalco Alumina Support	0.46	9.0

Variable Pressure Batch Method

Surface Area

To determine pore structure (i.e., surface area and pore size distribution), adsorption isotherms were developed for the unimodal and bimodal silica adsorbents. Figures 11 through 13 present experimental adsorption isotherms developed from 2,2-dimethylpropane at 273 K adsorbed onto the silica supports. Surface areas were calculated by using the BET equation and the adsorption-equilibrium data in the range of relative pressures between 0.05 and 0.35. The results are given in Table 3. Nitrogen at 77 K was used to check the validity of the surface areas calculated from 2,2-dimethylpropane. The agreement of the surface areas calculated using nitrogen and that for 2,2-dimethylpropane was within experimental error. This demonstrated that 2,2-dimethylpropane is an adequate choice for calculating surface areas.

Adsorption experiments were performed to determine the surface area for the Katalco alumina supports. Carbon dioxide at 273 K was first attempted applying Dubinin-Polanyi

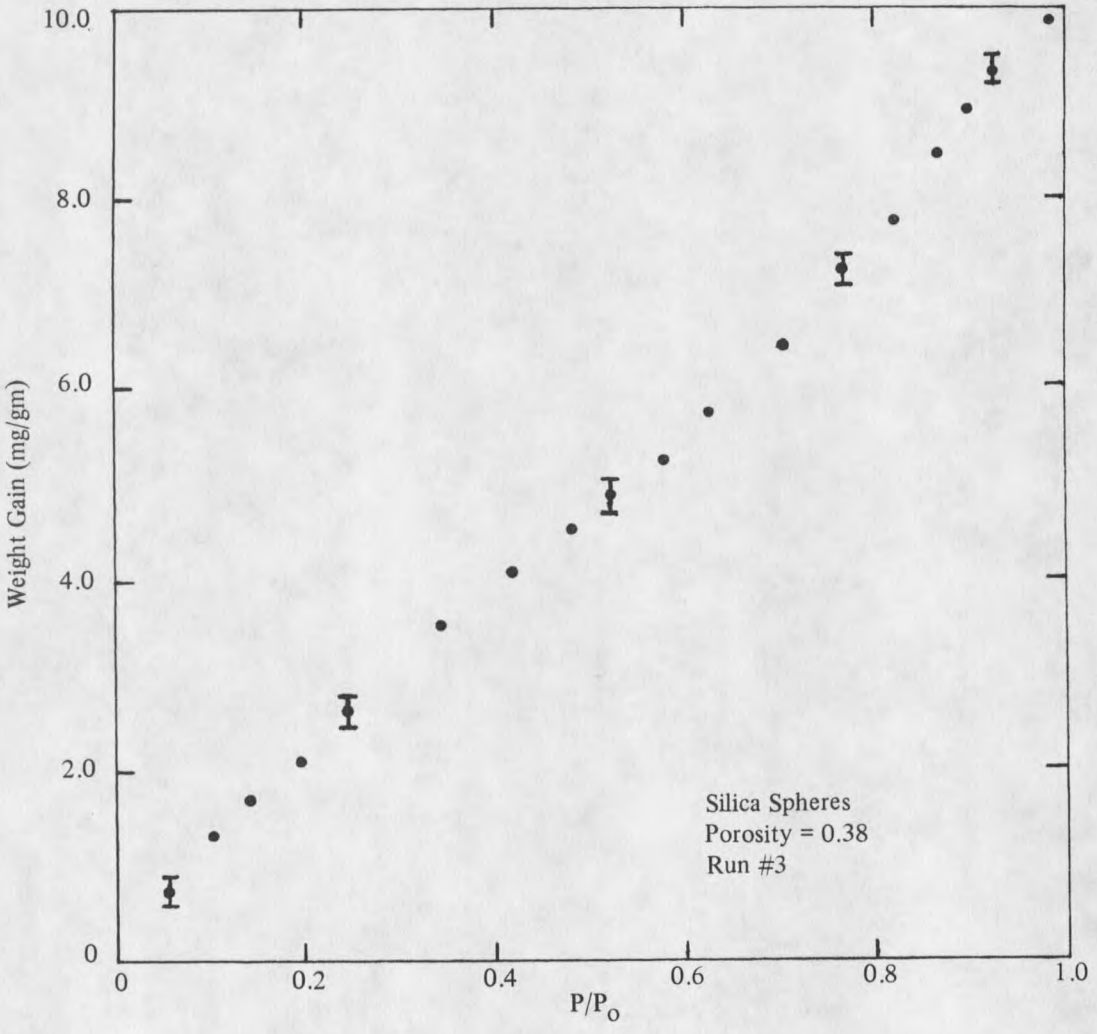

Figure 11. Adsorption equilibrium data for 2,2-dimethylpropane on unimodal silica spheres at 273 K.

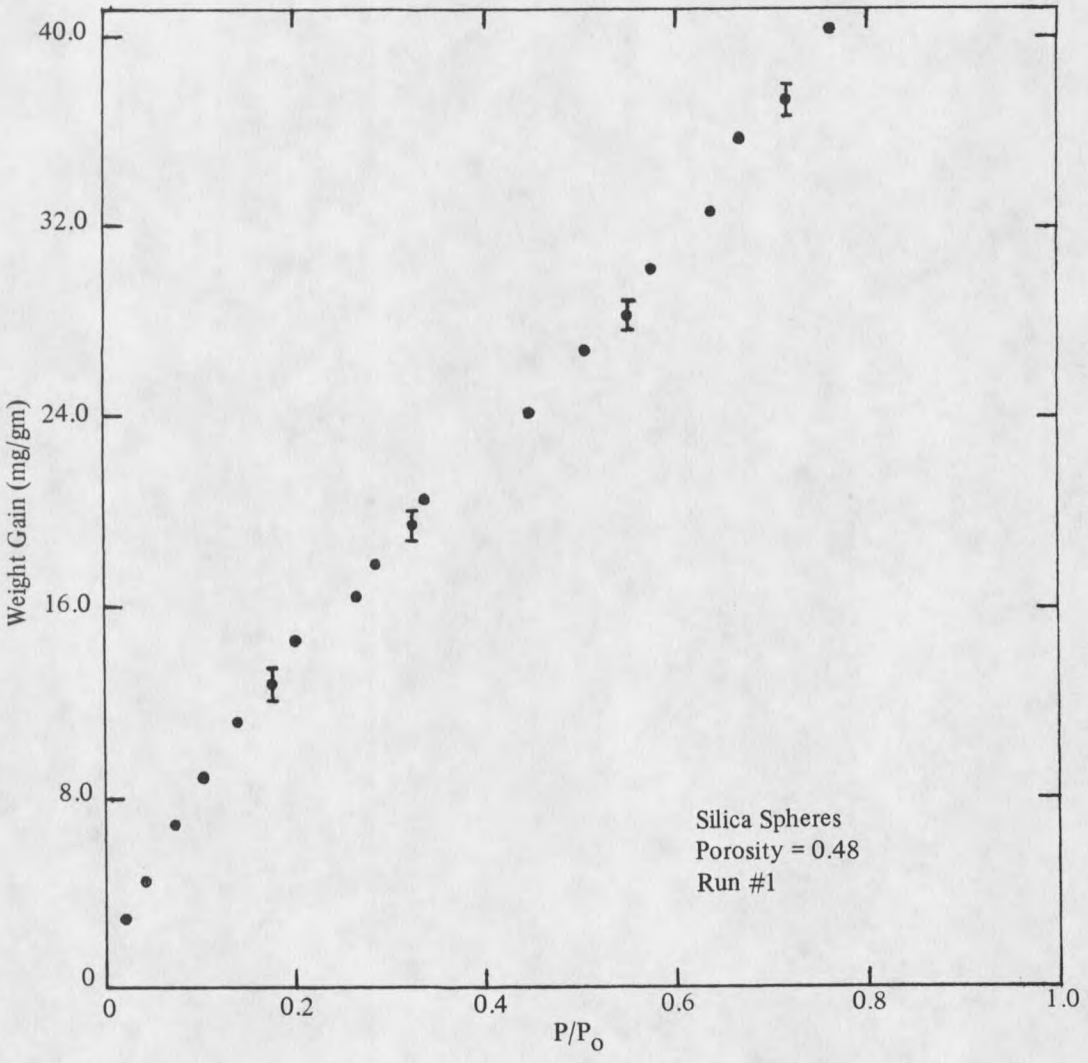

Figure 12. Adsorption equilibrium data for 2,2-dimethylpropane on bimodal silica spheres at 273 K.

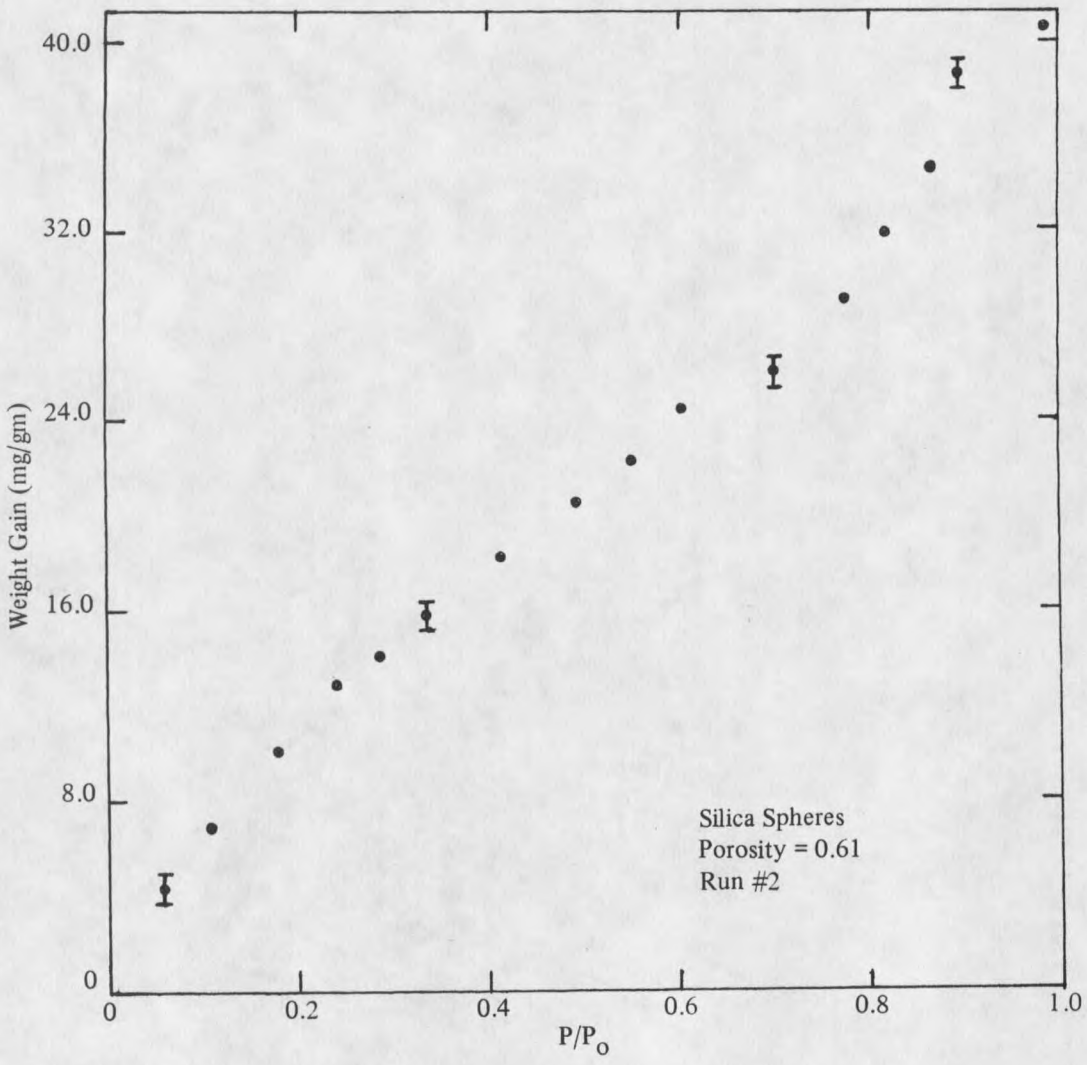

Figure 13. Adsorption equilibrium data for 2,2-dimethylpropane on bimodal silica spheres at 273 K.

Table 3. Surface Areas Calculated for 2,2-Dimethylpropane at 273 K and Nitrogen at 77 K.

Porosity	Adsorbate	Surface Area (m^2/gm)
Unimodal Spheres		
0.38	2,2-dimethylpropane	18.0±3.7
0.38	Nitrogen	15.2±2.1
Bimodal Spheres		
0.48	2,2-dimethylpropane	90.4±3.4
0.61	2,2-dimethylpropane	74.6±4.4
Katalco Alumina Supports		
0.46	Carbon dioxide	151.8±13.8*
0.46	2,2-dimethylpropane	309.2±32.2
0.46	Mercury Porosimetry	251.2**
0.46	Nitrogen	337.3**

*Surface area calculated using Dubinin-Polanyi theory.
**From manufacturer (Micronerities).

theory. The surface areas calculated using carbon dioxide were only 50% of the values calculated employing 2,2-dimethylpropane with application of the BET equation. The results are presented in Table 3. The Dubinin-Polanyi theory did not give proper surface areas for the Katalco alumina supports. The reason for this is that the Katalco support is not microporous, so the Dubinin-Polanyi theory would not be expected to give the proper surface areas.

Pore Size Distribution

To compute the pore size distribution of porous media, nitrogen or 2,2-dimethylpropane and adsorption or desorption data from an isotherm is needed. Appendix 2 has an algorithm developed by colleague Arden M. Edwards for computing the pore size distribution of porous media using nitrogen as the adsorbate. To use the algorithm the ambient pressure and adsorbent sample weight must be entered. The successive data pairs (pressure and adsorbent weight) are then read from a data file. The pore volume distribution is then determined. A complete discussion is given in the Experimental section.

Diffusion Coefficients

As a result of its simplicity, the "unipore" model was the first choice for comparison to experimental adsorption data. Each equilibrium point on Figures 11 through 13 represents experimental uptake curves. Figure 14 presents a typical uptake curve. Figure 15 shows the excellent reproducibility of two sorption curves run at the same total pressure.

With a constant surface concentration, the simplest form of the "unipore" model may be used, thus simplifying the matching of experimental adsorption data to the model. Effective diffusivities have been calculated for three samples by using the initial slope method, Equation 25, and by moment analysis, Equations 27 and 28. The calculated values of D_e are presented in Figures 16 through 18. These figures show how the diffusivities calculated from data at short times only can correlate with diffusivities calculated from data over the entire time domain. The agreement is excellent for all three catalyst supports, showing that the "unipore" model is appropriate for these catalyst supports.

It is necessary to consider which model-matching technique is more accurate; the initial slope method or moment analysis. To determine this, the diffusivities calculated were put into the solution of the "unipore" model. The curves generated were then compared with the experimental data. This was accomplished by evaluting the average derivations for time values for M_t/M_∞ from 0.1 through 0.9 at intervals of 0.1. Table 4 presents the definition for the average deviation and the average deviations calculated. Two sorption runs for each of the three samples were evaluated. The average deviations were not significantly different for the two methods. The initial slope method would be the obvious choice for calculation of the effective diffusivities because it is computationally less complex.

One difficulty encountered in using the initial slope method and moment analysis was determining when equilibrium was attained. This introduced error in calculating the effective diffusivities for the two methods. Choosing the equilibrium value is more of a problem

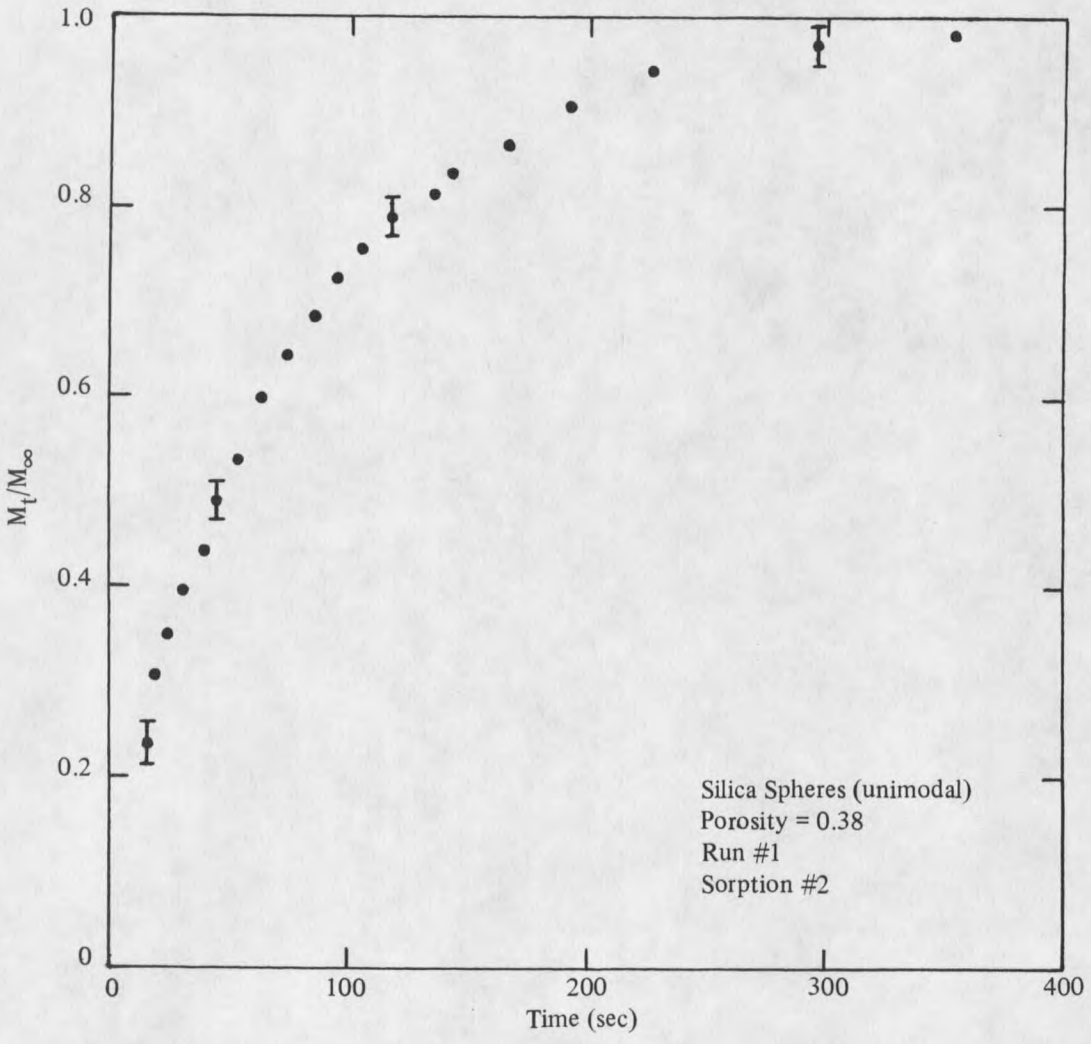

Figure 14. Experimental sorption curve (batch method).

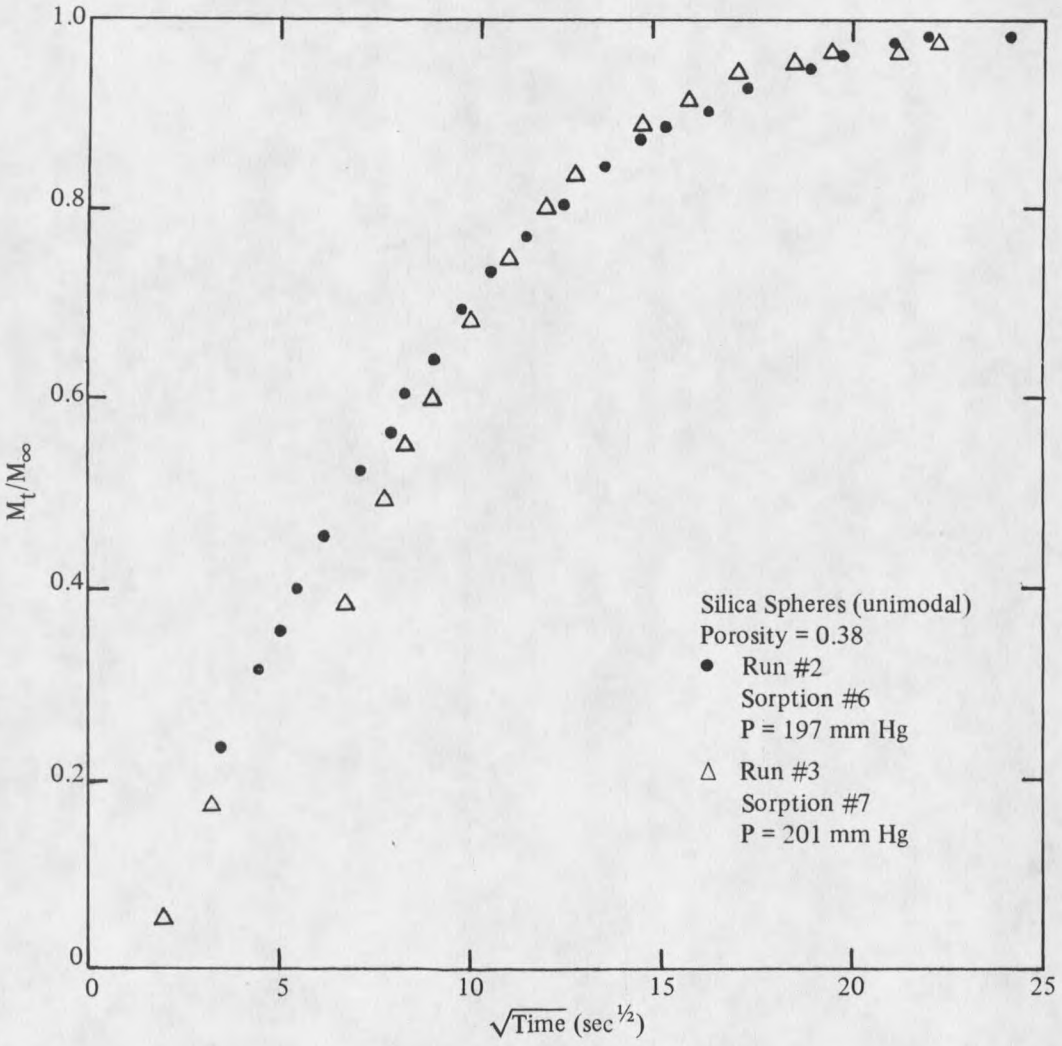

Figure 15. Reproducibility of experimental sorption curves for the batch method.

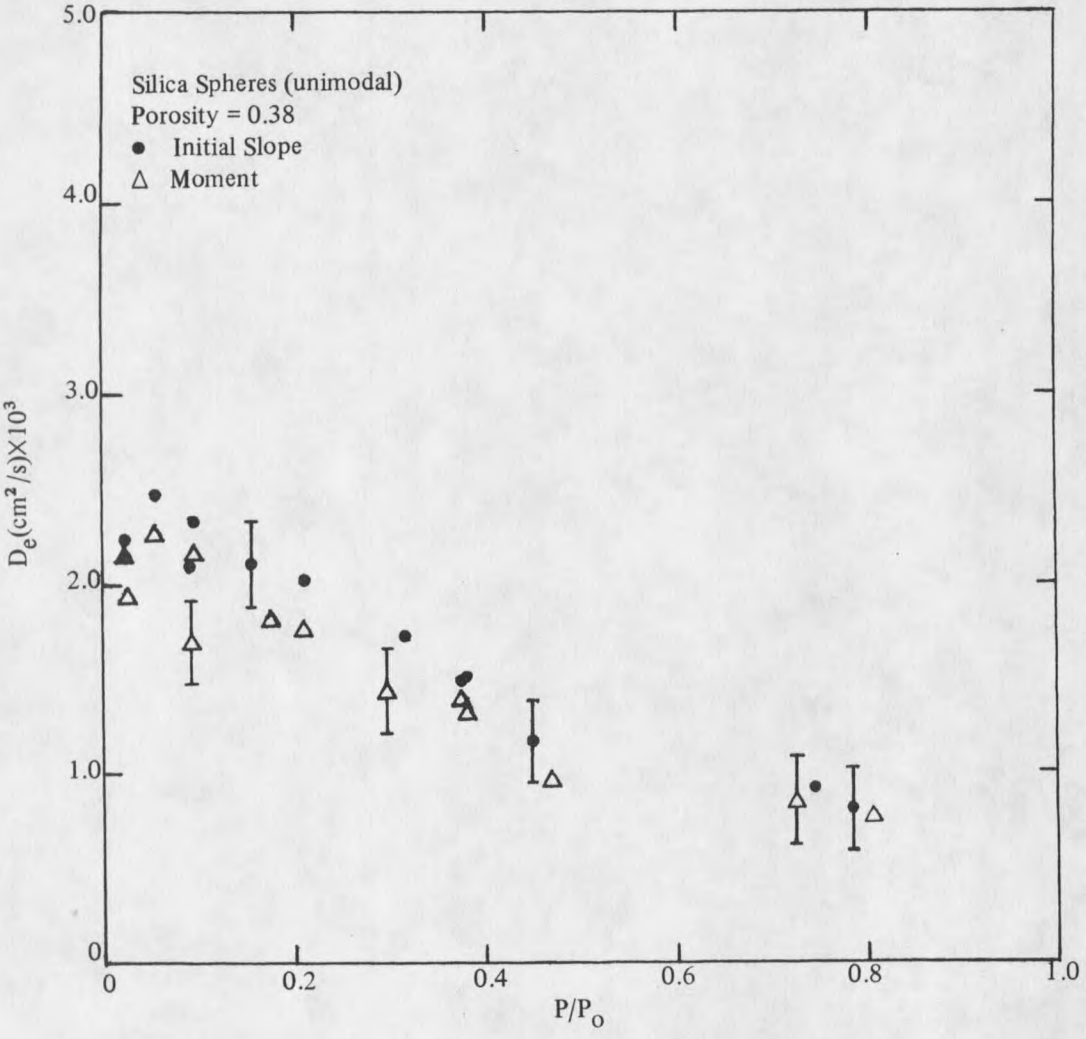

Figure 16. Comparison of effective diffusivities calculated from initial slope method and moment analysis (2,2-dimethylpropane at 273 K).

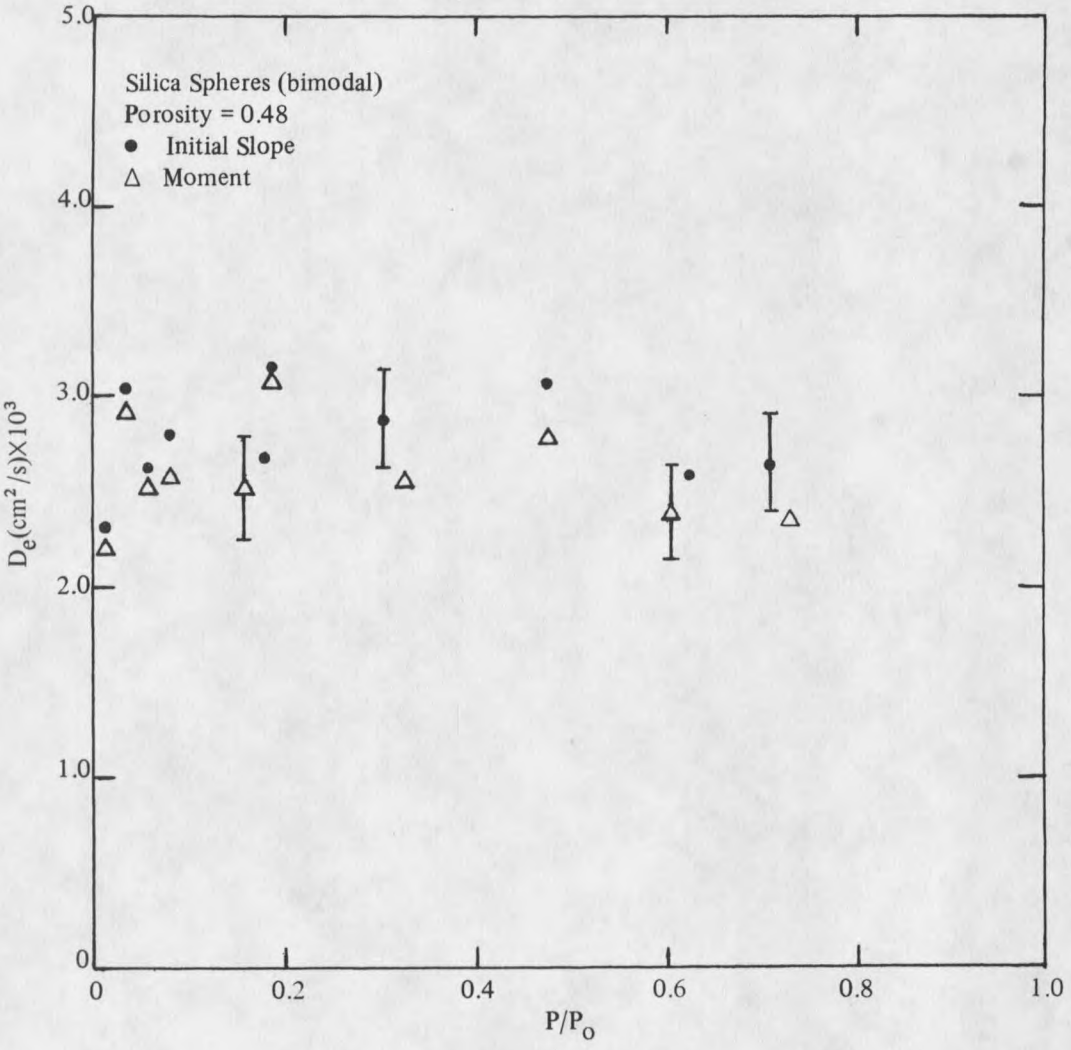

Figure 17. Comparison of effective diffusivities calculated from initial slope method and moment analysis (2,2-dimethylpropane at 273 K).

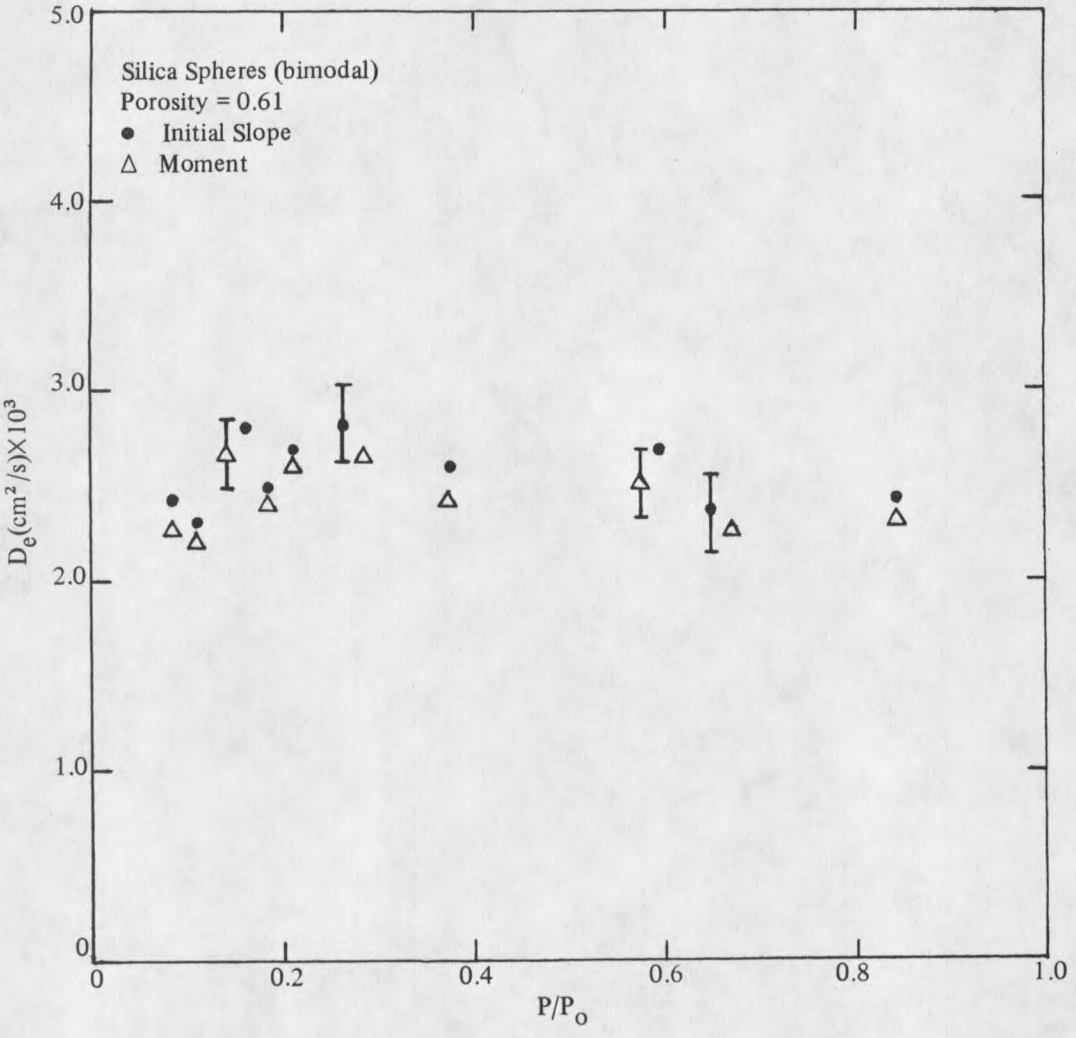

Figure 18. Comparison of effective diffusivities calculated from initial slope method and moment analysis (2,2-dimethylpropane at 273 K).

Table 4. Comparison of Times to Given Weight Gain by Initial Slope Method and Moment Analysis.

Porosity	Run No.	Sorption #	Average Deviation*	
			Initial Slope	Moment
Unimodal Spheres				
0.38	2	1	2.34	1.88
0.38	3	13	1.07	0.76
Bimodal Spheres				
0.48	1	6	1.54	1.41
0.48	1	13	2.08	1.81
0.61	1	11	0.38	0.42
0.61	2	3	2.28	2.00

*Average deviation = $\Sigma^n[(x_i - x_{exp})/\bar{x}]^2$.

with moment analysis than with the initial slope method. This is due to the fact that the area used to determine the first absolute moment for moment analysis is more sensitive to a different equilibrium value than the slope that is used in the initial slope method. To be consistent with all experiments, equilibrium was chosen as the point when the uptake rate was less than 1% of the initial rate. The exact choice of the equilibrium point is uncertain due to the low signal to noise ratio of the balance and acquisition system.

Figure 19 compares the initial slope method and moment analysis to experimental sorption data. This figure shows the excellent agreement of the unipore model to that of the experimental sorption curve.

Figure 16 shows a downward trend of the D_e versus pressure for the unimodal spheres with $\epsilon = 0.38$. This indicates that after a relative pressure of 0.2 is reached, the mechanism of diffusion is in the transition region between bulk and Knudsen diffusion. Figures 17 and 18 both show that for bimodal assemblages of silica spheres, D_e versus pressure does not follow an upward or downward trend. This indicates that the mode of diffusion is Knudsen. Because of the scatter of data in these figures, 95% confidence intervals [30] were determined for the slopes and the y-intercepts. The method of least squares was applied to fit the data to the linear equation:

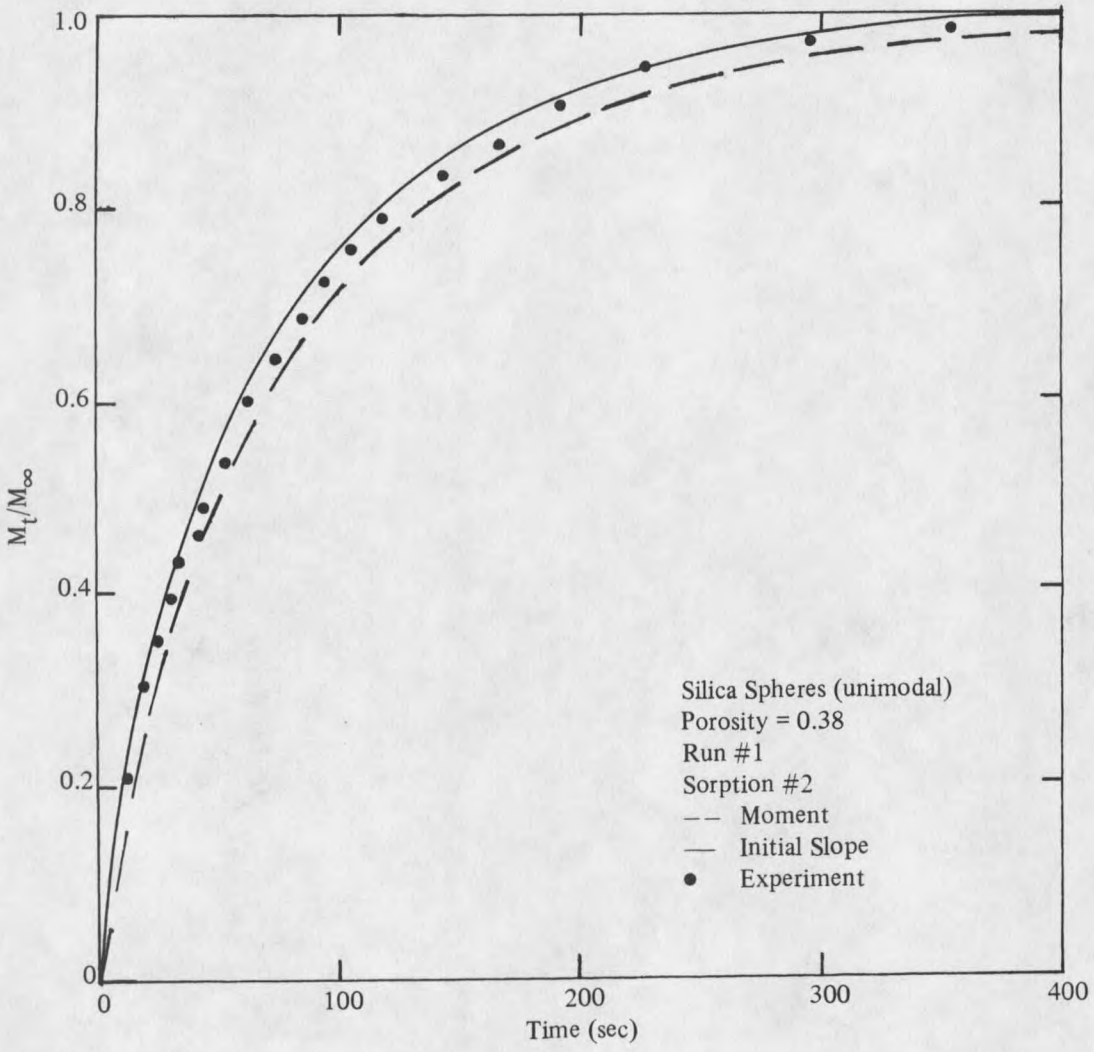

Figure 19. Comparison of initial slope method and moment analysis to an experimental sorption curve.

$$D_e = a + b(P/P_o) \tag{40}$$

where a = y-intercept

b = slope of the line.

This analysis indicates that for $\epsilon = 0.48$ and 0.61 bimodal spheres a straight line with zero slope fits the experimental data within a 95% confidence interval, which indicates the mode of diffusion is purely Knudsen over the entire pressure range studied. This analysis for the $\epsilon = 0.38$ unimodal spheres indicated that the diffusion was in the "transition" regime at higher pressures. These findings are expected from the mean free path of the gas and the estimated pore size.

The effective diffusivities calculated for the Knudsen regime are given in Table 5.

Table 5. Linear Regression and 95% Confidence Intervals for D_e versus Total Pressure With 2,2-Dimethylpropane at 273 K.

Porosity	D_e (cm^2/s)
Unimodal Spheres	
0.38	$2.1\times10^{-3} \pm 0.2\times10^{-3}$
Bimodal Spheres	
0.48	$2.1\times10^{-3} \pm 0.8\times10^{-3}$
0.61	$2.5\times10^{-3} \pm 0.7\times10^{-3}$

Values of effective diffusivities for $\epsilon = 0.48$ and 0.61 bimodal spheres were calculated over the entire pressure range. The value for D_e calculated for $\epsilon = 0.38$ unimodal spheres was for relative pressure less than 0.2.

Calculation of Tortuosities

The tortuosity factor accounts for the fact that pores are not always parallel to the flow direction nor of cylindrical shape. For solids of practical interest, the value of δ is usually between 1 and 10 [2]. To determine the tortuosity factors, a pore model must be assumed. The model applied is the "parallel pore" model as described in the modeling

section. In this model, all pores are assumed to be cylindrical and of the same diameter. The effective diffusivity is given by:

$$D_e = \frac{\epsilon D}{\delta} \tag{15}$$

For a given model of diffusion in the capillaries, D may be calculated. With calculated values for D and ϵ, and experimentally determined values of D_e, the tortuosity δ can be evaluated for the three catalyst supports.

For diffusion in capillaries at low pressure, Knudsen [31] has derived the following expression for D_k:

$$D_k = \frac{4r}{3}\sqrt{\frac{2RT}{\pi M}}\,\frac{(2-f)}{f} \tag{41}$$

where D_k = Knudsen diffusivity (cm^2/s).

f = fraction of molecules which stick to the pore wall

M = molecular weight

r = pore radius (cm)

R = gas constant

T = Temperature (K)

For practical applications, the sticking coefficient, f, is usually taken to be 1 and Equation 41 is simplified in cgs units to [2]:

$$D_k = 9700\,\bar{r}\sqrt{\frac{T}{M}} \tag{42}$$

where $\bar{r}$ is the average pore size.

The major problem with the application of Equation 42 is the question of the proper choice for the mean pore radius. To calculate this with a combination of the surface area and total pore volume, one can use:

$$\bar{r} = \frac{2\,PV}{S} \tag{43}$$

In principle, pore diameter values calculated via Equation 43 will agree for cylindrical pores only. With beds of uniformly sized spheres, Equation 43 may be reduced to a function of the sphere diameter and porosity only [31]:

$$\bar{r} = \frac{\epsilon}{3(1-\epsilon)} \, d_s \tag{44}$$

where d_s is the diameter of the unimodal spheres.

Table 6 presents the results obtained using Equation 44 to calculate $\bar{r}$ for the $\epsilon = 0.38$ unimodal spheres and Equation 43 for the $\epsilon = 0.48$ and 0.61 bimodal spheres. Equation 43 was used for the bimodal spheres because a single sphere size could not be determined for use in Equation 44. Equation 42 was used to calculate D_k and Equation 15 was used with the calculated effective diffusivities and porosities to determine the tortuosities.

Table 6. Calculated Knudsen Diffusivities and Tortuosities.

Porosity	$\bar{r}$ (nm)	D_k (cm^2/s)	δ
Unimodal Spheres			
0.38	21.8±1.2	4.1×10^{-2}	7.4±0.8
Bimodal Spheres			
0.48	10.8±0.4	2.0×10^{-2}	3.6±1.1
0.61	22.2±1.3	2.5×10^{-2}	10.1±2.8

The values for solids of practical interest are usually between 1 and 10 [2]. In Table 6, all the tortuosities lie in this range. The $\epsilon = 0.61$ bimodal spheres seem to have a high value of δ. This could be from the uncertainty of calculating the proper mean pore radius for the bimodal spheres.

Constant Pressure Flow Method

Diffusion Coefficients

An attempt was made to match several different models to experimental adsorption data. Figure 20 shows the excellent reproducibility for two experimental uptake curves.

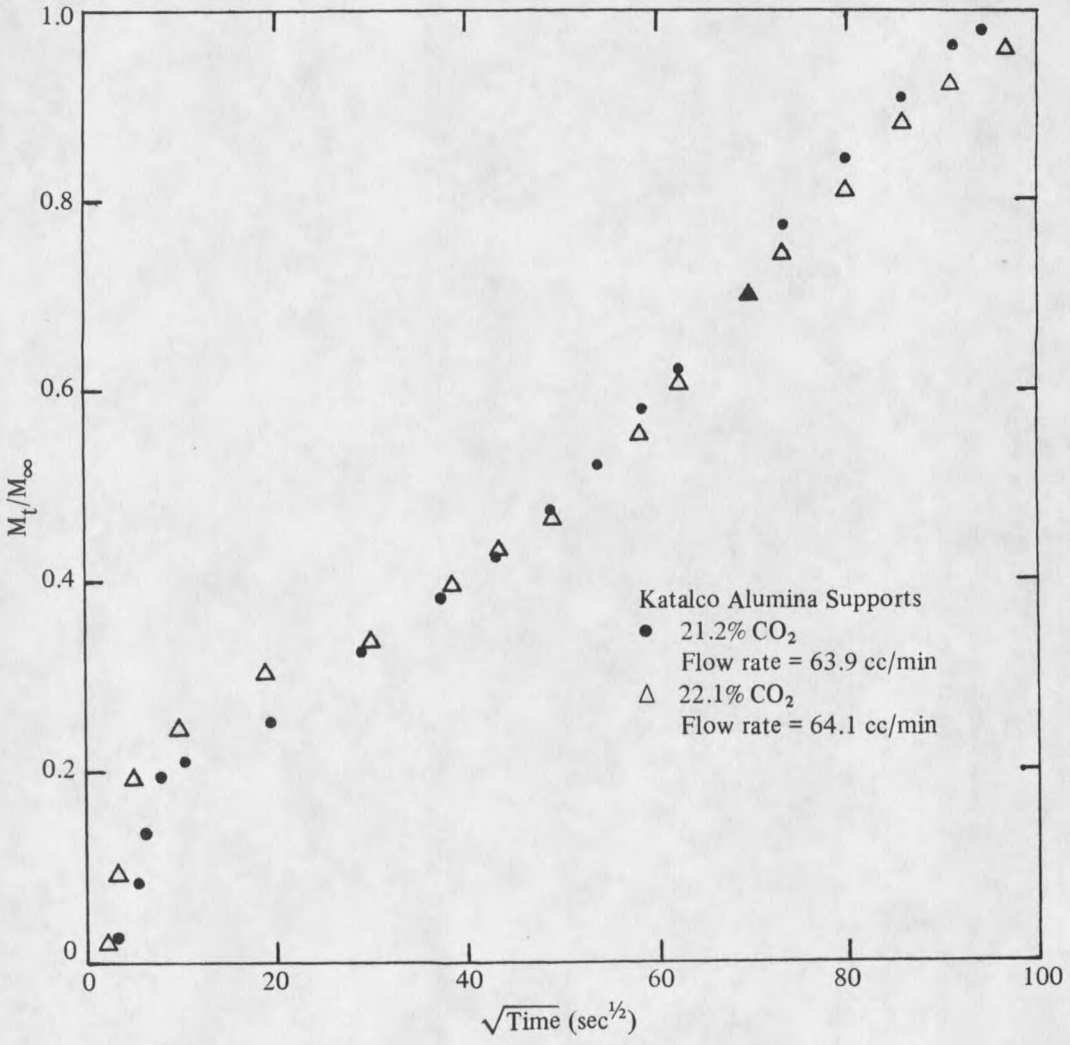

Figure 20. Reproducibility of experimental uptake curves for the flow method.

The uptake curves were determined using 21.2 and 22.1% CO_2 at 303 K on Katalco alumina supports.

With each step change in the inlet carbon dioxide concentration, there was a period in which the concentration in the diffusion cell was changing until it reached its new equilibrium concentration. To determine an effective diffusivity for the Katalco alumina supports, a physical model describing the system was assumed. Because of the changing concentration in the diffusion cell, the "unipore" model with variable surface concentration was the first choice. The solution to this model is presented in the modeling section, Equation 31. Using Equations 28 and 33, the diffusivity was calculated by means of moment analysis. The diffusivity calculated was 2.7×10^{-7} cm^2/s. This was put back into the solution, Equation 31, and compared in Figure 22 with the experimental data. As demonstrated by comparing the calculated uptake curve to the experimental data, this model does not fit the experimental sorption curve at values of $M_t/M_\infty < 0.4$.

Another model was attempted because of possible diffusion into the upper portion of the system through the opening in the diffusion cell for the sample hangdown wire from the null-beam balance. This opening possibly allows CO_2 to diffuse into the bell jar housing the null-beam balance. This model assumes diffusion into the bell jar is limiting, and diffusion into the catalyst support is instantaneous. This is analogous to parallel continuous stirred tank reactors (CSTR), hence this model is referred to as the parallel CSTR model. Figure 21 is a flow diagram of the parallel CSTR model.

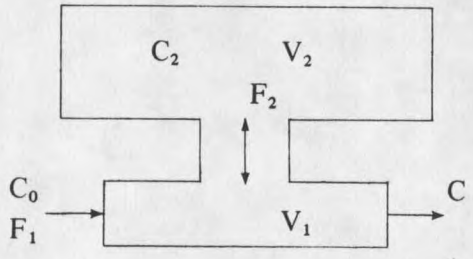

Figure 21. Flow diagram for the parallel CSTR model.

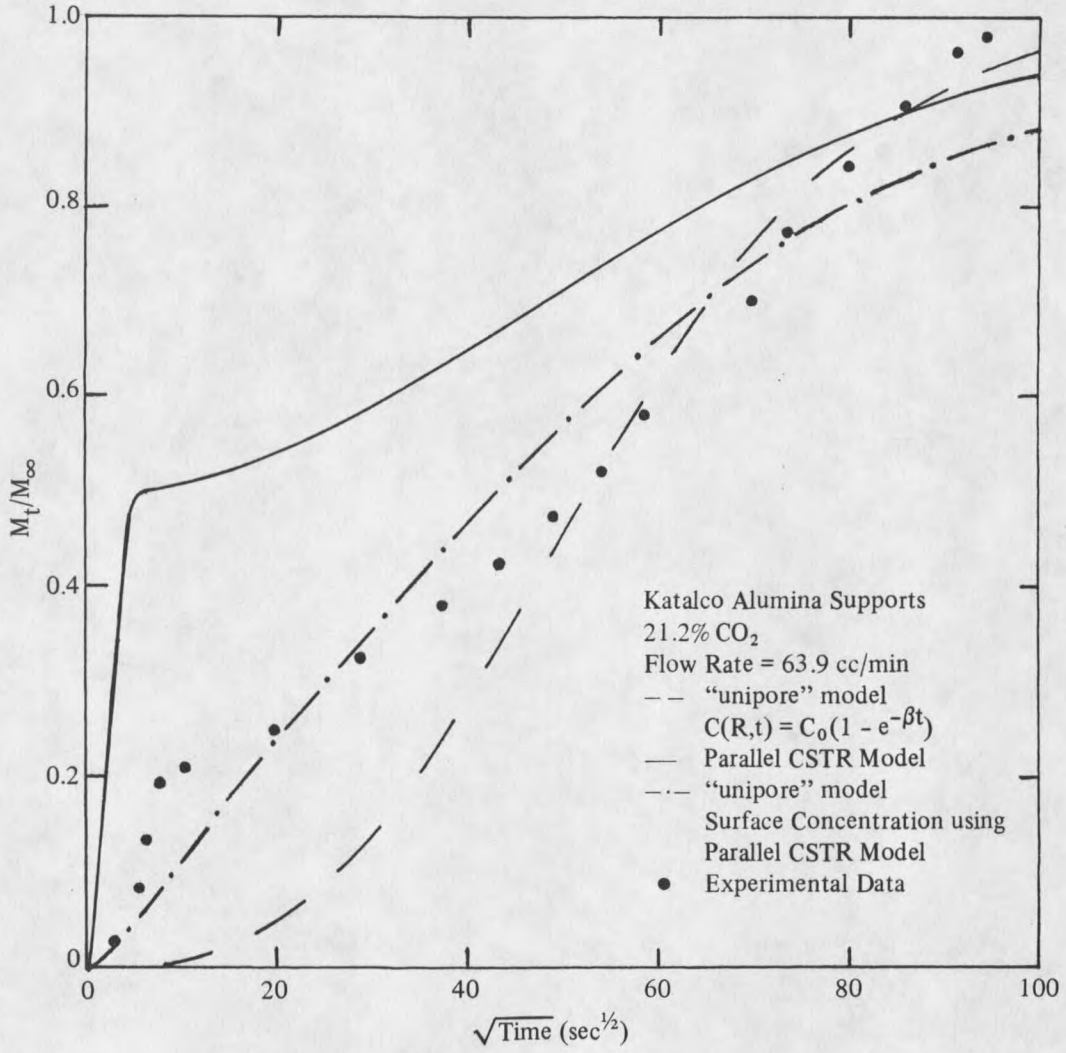

Figure 22. Comparison of models with experimental sorption data.

The governing equations are:

$$F_1 C_0 - F_1 C = V_1 \frac{dC}{dt} + F_2 (C - C_2) \tag{45}$$

$$F_2 (C - C_2) = V_2 \frac{dC_2}{dt} \tag{46}$$

where F_1 = flow into the diffusion cell

C_0 = the initial concentration into the diffusion cell

F_2 = the flow into the upper chamber

C_2 = the concentration in the upper chamber

C = the exit concentration out of the system

The solution to Equations 45 and 46 via Laplace transform techniques is:

$$\frac{M_t}{M_\infty} = \frac{F_1}{V_1 (b-a)} (e^{-at} - e^{-bt}) + \frac{F_1 F_2}{V_1 V_2 ab(a-b)} (be^{-at} - ae^{-bt} + a - b) \tag{47}$$

where:

$$a = \frac{2F_1 F_2}{(V_1 + V_2)F_2 + F_1 V_2 + \left\{ [(V_1 + V_2)F_2 + F_1 V_1]^2 - 4F_1 F_2 V_1 V_2 \right\}^{1/2}} \tag{48}$$

$$b = \frac{(V_1 + V_2)F_2 + F_1 V_2 + \left\{ [(V_1 + V_2)F_2 + F_1 V_1]^2 - 4F_1 F_2 V_1 V_2 \right\}^{1/2}}{2V_1 V_2} \tag{49}$$

A full derivation is given in Appendix 1. This solution is compared to an experimental sorption curve in Figure 22. As demonstrated by comparing the calculated sorption curve to the experimental data, this model does not fit, but it does have the same general shape.

The last model that was proposed was one using the parallel CSTR model to represent the surface concentration in the "unipore" model with variable surface concentration. If the initial concentration in the cylinder is zero and that at the surface is $\phi(t)$, the solution is [27]:

$$C(r,t) = \frac{2\,D_e}{R} \sum_{n=1}^{\infty} e^{-D_e\alpha_n^2 t} \frac{\alpha_n J_o(r\alpha_n)}{J_1(R\alpha_n)} \int_o^t e^{D_e\alpha_n^2 t} \phi(\lambda)\,d\lambda \qquad (50)$$

where the α_ns are the roots of $J_o(R\alpha_n)$. Letting $\phi(\lambda$, equal Equation 47, the sorption-time curve is given by:

$$\frac{M_t}{M_\infty} = \frac{4}{R^2} \sum_{n=1}^{\infty} \left\{ \frac{F_1}{V_1(b-a)} \left[\frac{e^{-at} - e^{-D_e\alpha_n^2 t}}{\alpha_n^2 - a/D_e} + \frac{e^{-D_e\alpha_n^2 t} - e^{-bt}}{\alpha_n^2 - b/D_e} \right] + \right.$$

$$+ \frac{1}{(a-b)} \left[\frac{be^{-at} - be^{-D_e\alpha_n^2 t}}{\alpha_n^2 - a/D_e} + \frac{ae^{-D_e\alpha_n^2 t} - ae^{-bt}}{\alpha_n^2 - b/D_e} \right] +$$

$$\left. + \left[\frac{1 - e^{-D_e\alpha_n^2 t}}{\alpha_n^2} \right] \right. \qquad (51)$$

Equation 51 has two unknowns, D_e and F_2. The solution is compared to the experimental sorption curve in Figure 22. This model clearly fits the experimental data better than the other two models proposed. Since there are two unknowns and only one equation. a unique solution for the effective diffusivity is not possible with this model.

More complex models can be attempted, but the disadvantage is that there will be an increased number of parameters and they will not give a single answer for an effective diffusivity.

Comparison of Batch and Flow Methods

In the batch method surface areas were determined from equilibrium data, and it was found that the uptake curves could be modeled using the "unipore" model allowing calculation of effective diffusivities. With the flow system an attempt was made to match the uptake curves generated with three different models. The results were inconclusive with respect to determining an effective diffusivity. The two main reasons are: (1) A catalyst support with a bidisperse pore structure was used which necessitates a more complex

model. With a more complex model the number of parameters is increased so a unique solution for an effective diffusivity cannot be obtained. (2) Possible diffusion into the upper bell jar may have introduced error into the experimental data.

SUMMARY

1. A variable pressure batch method was developed which allowed the simultaneous measurement of effective diffusivities and surface areas of several "model" spherical catalyst supports.
2. Surface areas were obtained by applying the BET equation to equilibrium adsorption isotherms. The adsorption isotherms can be extended to calculate pore size distribution. A rate of approach to equilibrium curve was obtained at each pressure increment. A pore diffusion model was assumed to match this experimental uptake curve. From this diffusion model, effective diffusivities were determined.
3. The "unipore" model was appropriate for determining effective diffusivities in assemblages of silica spheres. Initial slope and moment model matching techniques were employed to determine the effective diffusivities.
4. Tortuosities were calculated for the assemblages of silica spheres. The analysis is complicated by uncertainty concerning the characteristic pore size in the catalyst support.
5. A constant pressure flow method was attempted to measure effective diffusivities and pore structure (i.e., surface area and pore-size distribution) for Katalco alumina supports using carbon dioxide.
6. Three models were applied to determine an effective diffusivity for the Katalco alumina supports. The results were inconclusive for determining an effective diffusivity.

RECOMMENDATIONS FOR FUTURE RESEARCH

1. Determination of a proper characteristic pore size and tortuosity for assemblages of silica spheres.
2. Continued investigation of real catalyst supports using the batch method.
3. Refinement of the flow method employing a "model" catalyst support.
4. The flow apparatus could be modified to eliminate diffusion into the upper bell jar, for example by placing baffles between the bell jar and the diffusion cell. Eliminating this unwanted diffusion would simplify the mathematical modeling of the system.
5. Develop equilibrium adsorption isotherms using the flow method for the determination of surface areas and pore-size distributions.

REFERENCES CITED

REFERENCES CITED

1. Perry, R. H. and Chilton, C. H., Chemical Engineers Handbook, McGraw-Hill, 5th ed., 4-32 (1973).

2. Satterfield, C. N., Mass Transfer in Heterogeneous Catalysis, MIT Press, 1970.

3. Dubinin, M. M., Proc. Conf. Ind. Carb. Graph., S.C.I., 219 (1958).

4. Polanyi, M., Verh. Dtsch. Phys. Ges., 16, 1012 (1914).

5. Branauer, S., Emmett, P. H. and Teller, E., J. Am. Chem. Soc., 60, 309 (1938).

6. Gregg, S. J. and Sing, K. S. W., Adsorption, Surface Area and Porosity, Academic Press, London and New York, 1967.

7. Brunauer, S., "Solid Surfaces and the Gas Solid Interface," Adv. in Chem. Series, 33, Washington, D.C. (1961).

8. Lowell, S., Introduction to Powder Surface Area, Wiley-Interscience, 1979.

9. Emmett, P. H. and Brunauer, S., J. Amer. Chem. Soc., 59, 1553 (1937).

10. Lee, V. H., "Methane Recovery From Coalbeds; Effects of Monolayer Capacity and Pore Structure on Gas Content," M.S. Thesis, University of New Mexico (1982).

11. Livingston, H. K., J. Colloid Sci., 4, 447 (1949).

12. Thomson, W. T., Philos. Mag., 42, 448 (1871).

13. de Boer, J. H., The Structure and Properties of Porous Materials, Butterworth, London, p. 68, 1958.

14. Zigmondy, A., Z. Anorg. Chem., 71, 356 (1911).

15. McBain, J. W., J. Am. Chem. Soc., 57, 699 (1935).

16. Cohan, L. H., J. Am. Chem. Soc., 60, 433 (1938).

17. Foster, A. G., J. Chem. Soc., 1806 (1952).

18. Wicke, E. and Kallenback, R., Koiloid Z., 97, 135 (1941).

19. Smith, D. M., "Methane Diffusion and Desorption in Coal," Ph.D. Thesis, University of New Mexico, 66, 1982.

20. Smith, J. M., Chemical Engineering Kinetics, McGraw-Hill, 3rd ed., 1982.

21. Satterfield, C. N. and Cadle, P. J., Ind. Eng. Chem. Process Des. Dev., 7, No. 2, 256 (1968).

22. Kocirik, M. and Zikanova, A., Ind. Eng. Chem. Process Des. Dev., 22, 168 (1974).

23. Smith, D. M., Ind. Eng. Chem. Fund., 23, No. 2, 265 (1984).

24. Garza, G. and Rosales, M. A., Ind. Eng. Chem. Process Des. Dev., 22, No. 1 (1983).

25. Massoth, F. E., Chemtech, vol. 2, 285 (1972).

26. Wheeler, A., Advances in Catalysis—Vol. III, Academic Press, p. 250, 1951.

27. Crank, J., The Mathematics of Diffusion, Clarendon Press, 1956.

28. Carslaw, H. S. and Jaeger, J. C., Conduction of Heat in Solids, Oxford University Press, 1959.

29. Huizenga, D. G., "Knudsen Diffusion in Beds of Monodisperse Silica Spheres," Master's Thesis, Montana State University, 1984.

30. Andersen, L. B., Chem. Eng. 173 (1963).

31. Smith, D. M. and Huizenga, D. G., "Simulation of Knudsen Diffusion in Porous Media," Presented before the Applied Simulation and Modeling IASTED International Conference, San Francisco, June 4-6, 1984.

32. Wylie, C. R. and Barrett, L. C., Advanced Engineering Mathematics, McGraw-Hill, Inc., p. 401, 1982.

APPENDICES

APPENDIX 1

DIFFUSION MODELS

APPENDIX 1

DIFFUSION MODELS

To determine the effective diffusivity in porous media, appropriate models describing the system must be developed. These models consist of partial differential equations which are transformed into the Laplace domain. Expressions are obtained for the first absolute moment which are used for calculation of effective diffusivities. What follows are derivations for slab, cylindrical, and spherical geometries.

Slab

The rate of change of the concentration of an adsorbing species inside a porous solid is given by the corresponding mass balance equation, assuming slab geometry:

$$D_e \frac{\partial^2 C}{\partial r^2} = \frac{\partial C}{\partial t} \tag{A.1}$$

with initial and boundary conditions

$$C(r,0) = 0, \quad C(R,t) = C_o(1 - e^{-\beta t}), \quad \frac{\partial C}{\partial r}(0,t) = 0 \tag{A.2}$$

Transforming A.1 and A.2 into the Laplace domain [32]:

$$D_e \frac{\partial^2 \tilde{C}}{\partial r^2} - s\tilde{C} = 0 \tag{A.3}$$

$$\tilde{C}(r,0) = 0, \quad \tilde{C}(R,t) = \frac{C_o \beta}{s(s+\beta)}, \quad \frac{\partial \tilde{C}}{\partial r}(0,t) = 0 \tag{A.4}$$

The general solution to the ordinary differential equation given by A.3 is:

$$\tilde{C}(r) = \frac{C_o \beta \cosh(\sqrt{s/D_e}\, r)}{s(s+\beta)\cosh(\sqrt{s/D_e}\, R)} \tag{A.5}$$

Since gravimetric measurements give information about the overall rather than the local weight gain, the average concentration inside the adsorbate can be taken as:

$$\frac{\tilde{M}_t}{\tilde{M}_\infty} = \frac{\int_0^R \tilde{C}(r,s)\, dr}{\int_0^R \tilde{C}(\infty,s)\, dr} \tag{A.6}$$

From Equations A.5 and A.6, one obtains

$$\frac{\tilde{M}_t}{\tilde{M}_\infty} = \frac{C_o}{\phi}\left(1 + \frac{s}{s+\beta}\right)\tanh\phi \tag{A.7}$$

where $\phi = \sqrt{s/D_e}\, R$. The zeroth and first moments are calculated introducing Equation A.7 into Equation 26

$$m_i = (-1)^i \left.\frac{d^i(\tilde{M}_t/\tilde{M}_\infty)}{ds^i}\right|_{s=0} \tag{26}$$

which yields

$$\mu_1 \equiv \frac{m_1}{m_0} = \frac{1}{\beta} + \frac{R^2}{3\, D_e} \tag{A.8}$$

where μ_1 is the first absolute moment.

Cylinder

The governing equation is:

$$\frac{D_e}{r}\frac{\partial}{\partial r}\left(r\frac{\partial C}{\partial r}\right) = \frac{\partial C}{\partial t} \tag{A.9}$$

with the initial and boundary conditions

$$C(r,0) = 0, \quad C(R,t) = C_o(1 - e^{-\beta t}), \quad \frac{\partial C}{\partial r}(0,t) = 0 \tag{A.2}$$

Transforming A.9 and A.10 into the Laplace domain gives

$$\tilde{C}(r,0) = 0, \quad \tilde{C}(R,t) = \frac{C_o \beta}{s(s+\beta)}, \quad \frac{\partial \tilde{C}}{\partial r}(0,t) = 0 \tag{A.4}$$

and

$$D_e \frac{\partial^2 \tilde{C}}{\partial r^2} + \frac{D_e}{r} \frac{\partial C}{\partial r} - s\tilde{C} = 0 \tag{A.10}$$

Solving Equation A.10 one obtains

$$\tilde{C}(r,s) = \frac{C_o \beta I_o(\sqrt{s/D_e}\, r)}{s(s+\beta) I_o(\sqrt{s/D_e}\, R)} \tag{A.11}$$

The average concentration is obtained by

$$\frac{\tilde{M}_t}{\tilde{M}_\infty} = \frac{\int_0^R r \tilde{C}(r,s)\, dr}{\int_0^R r \tilde{C}(r,\infty)\, dr} \tag{A.12}$$

Substituting A.11 into A.12 and solving yields

$$\tilde{M}_t/\tilde{M}_\infty = 2A \frac{I_1(\Phi)}{(\Phi^3 + \Phi A) I_o(\Phi)} \tag{A.13}$$

where $\Phi = \sqrt{s/D_e}\, R$ and $A = R^2\beta/D_e$. Thus from Equations 26 and A.13

$$\mu_1 \equiv \frac{m_1}{m_0} = \frac{1}{\beta} + \frac{R^2}{8 D_e} \tag{A.14}$$

Sphere

The diffusion equation is:

$$\frac{D_e}{r^2} \frac{\partial}{\partial r}\left(r^2 \frac{\partial C}{\partial r}\right) = \frac{\partial C}{\partial t} \tag{A.15}$$

with the initial and boundary equations

$$C(r,0) = 0, \quad C(R,t) = C_o(1 - e^{-\beta t}), \quad \frac{\partial C}{\partial r}(0,t) = 0 \tag{A.2}$$

Taking Laplace transform with respect to t gives

$$D_e \left(\frac{\partial^2 \tilde{C}}{\partial r^2} + \frac{2}{r}\frac{\partial \tilde{C}}{\partial r}\right) - s\tilde{C} = 0 \tag{A.16}$$

With the boundary equations

$$\tilde{C}(r,0) = 0, \quad \tilde{C}(R,t) = \frac{C_o \beta}{s(s+\beta)}, \quad \frac{\partial \tilde{C}}{\partial r}(0,t) = 0 \tag{A.4}$$

one obtains

$$\tilde{C}(r,s) = \frac{1}{s}\frac{R\,C_o}{\sinh(\Phi)}\frac{1}{r}\sinh(\sqrt{s/D_e}\,r) \tag{A.17}$$

where $\Phi = \sqrt{s/D_e}\,R$. Thus,

$$\frac{\tilde{M}_t}{\tilde{M}_\infty} = \frac{\int_0^R r^2\,\tilde{C}(r,s)\,dr}{\int_0^R r^2\,\tilde{C}(r,\infty)\,dr}$$

$$= \frac{3\,C_o}{\Phi^2}\,s\left(\frac{1}{s} - \frac{1}{s+\beta}\right)[\Phi\coth(\Phi) - 1] \tag{A.18}$$

From Equation 26 and A.13 one obtains

$$\mu_1 \equiv \frac{m_1}{m_0} = \frac{1}{\beta} + \frac{R^2}{15\,D_e} \tag{A.19}$$

Parallel CSTR Model

The governing equations are

$$F_1 C_0 - F_1 C = V_1 \frac{dC}{dt} + F_2(C - C_2) \tag{45}$$

$$F_2(C - C_2) = V_2 \frac{dC_2}{dt} \tag{46}$$

With the initial conditions

$$C(0) = 0, \quad C_2(0) = 0 \tag{A.20}$$

Taking the Laplace transform with respect to t gives:

$$\frac{F_1 C_0}{s} - F_1 \tilde{C} + F_2 \tilde{C}_2 - F_2 \tilde{C} = V_1 s \tilde{C} \tag{A.21}$$

$$F_2(\tilde{C} - \tilde{C}_2) = V_2 s \tilde{C}_2 \tag{A.22}$$

Solving Equation A.22 for $\tilde{C}_2$ and putting into Equation A.21 one obtains

$$\frac{F_1 C_0}{s} - F_1 \tilde{C} + \frac{(F_2)^2 \tilde{C}}{V_2 s + F_2} - F_2 \tilde{C} = V_1 s \tilde{C} \tag{A.23}$$

Solving for $\tilde{C}$ gives

$$\tilde{C} = \frac{V_2 F_1 C_0}{(V_1 s + F_2)(V_2 s + F_2) + F_1(V_2 s + F_2) - F_2^2} + \frac{F_1 F_2 C_0}{s[(V_1 s + F_2)(V_2 s + F_2) + F_1(V_2 s + F_2) - F_2^2]} \tag{A.24}$$

Taking the inverse Laplace of Equation A.24 gives

$$C(t) = \frac{F_1 C_0}{V_1(b-a)}(e^{-at} - e^{-bt}) + \frac{C_0}{(a-b)}(be^{-at} - ae^{-bt} + a - b) \tag{A.25}$$

where

$$a = \frac{2 F_1 F_2}{(V_1 + V_2)F_2 + F_1 V_2 + \{[(V_1 + V_2)F_2 + F_1 V_1]^2 - 4F_1 F_2 V_1 V_2\}^{1/2}} \tag{A.26}$$

$$b = \frac{(V_1 + V_2)F_2 + F_1 V_2 + \{[(V_1 + V_2)F_2 + F_1 V_1]^2 - 4F_1 F_2 V_1 V_2\}^{1/2}}{2 V_1 V_2} \tag{A.27}$$

$$\frac{M_t}{M_\infty} = \frac{F_1}{V_1(b-a)}(e^{-at} - e^{-bt}) + \frac{1}{(a-b)}(be^{-at} - ae^{-bt} + a - b) \tag{A.28}$$

APPENDIX 2

COMPUTER ALGORITHMS

```
c<<<<<<<<<<<<<<<<<<<<<<<<<<<<<<<>>>>>>>>>>>>>>>>>>>>>>>>>>>>c
c            This program calculates the surface             c
c            area for porous media using the BET             c
c        equation with 2,2-dimethylpropane at 273 K.         c
c<<<<<<<<<<<<<<<<<<<<<<<<<<<<<<<>>>>>>>>>>>>>>>>>>>>>>>>>>>>c
      implicit real*8 (a-h,o-z)
      dimension x(100),y(100),p(100),v(100),w(100)
c     nrun is the run number
      nrun=1
c     den is the gas density(g/cm**3) at STP
      den=.003219
c     psat is the saturation pressure (mm hg) at operating
c     temperature.
      psat=531.96
c     num is the number of adsorption points with
c     0.05< P/Po <0.35 (ie. 27< P <186 mm hg).
      num=5
c     samp is the sample weight(g)
      samp=0.4986
c     cross is the cross-sectional area of the adsorbent
      cross=62.
c     p and w are the experimental data, p=pressure
c     (mm hg), w=weight adsorbed(g).
c
      p(1)=31.
      p(2)=61.
      p(3)=105.
      p(4)=148.
      p(5)=190.
      w(1)=.01205
      w(2)=.01951
      w(3)=.02748
      w(4)=.03375
      w(5)=.03988
      do 50 i=1,num
c     v is the volume STP.
      v(i)=w(i)/den/samp
c     x is the relative pressure.
      x(i)=p(i)/psat
      y(i)=p(i)/v(i)/(psat-p(i))
50    continue
      call least(num,x,y,a,b)
c     c is the heat of adsorption.
      c=1.+a/b
c     vm is the monolayer capacity.
      vm=1./(c*b)
      area=vm*6.023*10.**23*cross/(22400*10.**20)
      write(1,60) nrun
60    format(' run number     = ',i3)
```

```
      write(1,70) samp
70    format(' sample weight = ',f6.4,' g.')
      write(1,80)
80    format(' adsorbent     = neopentane')
      write(1,100) vm
100   format(' monolayer capacity = ',1pd10.3,' cm**3/g')
      write(1,110) c
110   format(' heat of adsorption = ',1pd10.3,' kcal/mol')
      write(1,120) area
120   format(' surface area       = ',1pd10.3,' m**2/g')
      write(1,130)
130   format(' p/psat',9x,'p/v/(psat-p) exp',5x,'p/v/(psat
     &-p) bet')
      do 150 i=1,num
      dum=a*x(i)+b
      write(1,140) x(i),y(i),dum
150   continue
140   format(f7.4,8x,1pd12.3,10x,1pd12.3)
      end
c
      subroutine least(n,x,y,a,b)
c     This subroutine fits the data set(x,y) to a straight
c     line, y=ax+b.
      real*8 x(100),y(100),a,b,z(2,3),dum
      z(1,1)=n
      z(1,2)=0.
      z(1,3)=0.
      z(2,2)=0.
      z(2,3)=0.
      do 100 i=1,n
      z(1,2)=z(1,2)+x(i)
      z(1,3)=z(1,3)+y(i)
      z(2,2)=z(2,2)+x(i)**2
      z(2,3)=z(2,3)+x(i)*y(i)
100   continue
      z(2,1)=z(1,2)
      dum=z(2,1)/z(1,1)
      a=(z(2,3)-dum*z(1,3))/(z(2,2)-dum*z(1,2))
      b=(z(1,3)-a*z(1,2))/z(1,1)
      return
c<<<<<<<<<<<<<<<<<<<<<<<<<<<<<<<<>>>>>>>>>>>>>>>>>>>>>>>>>>>>c
      end
```

```
c<<<<<<<<<<<<<<<<<<<<<<<<<<<<<>>>>>>>>>>>>>>>>>>>>>>>>>>>>c
c           This program calculates the surface          c
c           area for porous media using the BET          c
c             equation with nitrogen at 77 K.            c
c<<<<<<<<<<<<<<<<<<<<<<<<<<<<<>>>>>>>>>>>>>>>>>>>>>>>>>>>>c
c
      implicit real*8 (a-h,o-z)
      dimension x(100),y(100),p(100),v(100),w(100)
c     nrun is the run number
      nrun=1
c     den is the gas density(g/cm**3) at STP
      den=.001250
c     psat is the saturation pressure(mm hg) at the
c     operating temperature.
      psat=642.
c     num is the number of adsorption points with
c     0.05< P/Po <.35 (i.e. 32< P <225).
      num=3
c     samp is the sample weight(g)
      samp=.94128
c     cross is the cross-sectional area of the adsorbent
c     in anstroms.
      cross=16.2
c     p and w are the experimental data,
c     p=pressure(mm hg), w=weight adsorbed(g).
      p(1)=36.
      p(2)=74.
      p(3)=117.
      w(1)=.00362
      w(2)=.00443
      w(3)=.00476
      do 50 i=1,num
c     v is the gas volume at STP.
      v(i)=w(i)/den/samp
c     x is the relative pressure.
      x(i)=p(i)/psat
      y(i)=p(i)/v(i)/(psat-p(i))
50    continue
      call least(num,x,y,a,b)
c     c is the heat of adsorption.
      c=1.+a/b
c     vm is the monolayer capacity.
      vm=1./(c*b)
      area=vm*6.023*10.**23*cross/(22400*10.**20)
      write(1,60) nrun
60    format(' run number    = ',i3)
      write(1,70) samp
70    format(' sample weight = ',f6.4,' g.')
      write(1,80)
```

```
80     format(' adsorbent       = nitrogen')
       write(1,100) vm
100    format(' monolayer capacity = ',1pd10.3,' cm**3/g')
       write(1,110) c
110    format(' heat of adsorption = ',1pd10.3,' kcal/mol')
       write(1,120) area
120    format(' surface area       = ',1pd10.3,' m**2/g')
       write(1,130)
130    format(' p/psat',9x,'p/v/(psat-p) exp',5x,'p/v/(psat
      &-p) bet')
       do 150 i=1,num
       dum=a*x(i)+b
       write(1,140) x(i),y(i),dum
150    continue
140    format(f7.4,8x,1pd12.3,10x,1pd12.3)
       end
c
       subroutine least(n,x,y,a,b)
c      This subroutine fits the data set(x,y) to a
c      straight line, y=ax+b.
       real*8 x(100),y(100),a,b,z(2,3),dum
       z(1,1)=n
       z(1,2)=0.
       z(1,3)=0.
       z(2,2)=0.
       z(2,3)=0.
       do 100 i=1,n
       z(1,2)=z(1,2)+x(i)
       z(1,3)=z(1,3)+y(i)
       z(2,2)=z(2,2)+x(i)**2
       z(2,3)=z(2,3)+x(i)*y(i)
100    continue
       z(2,1)=z(1,2)
       dum=z(2,1)/z(1,1)
       a=(z(2,3)-dum*z(1,3))/(z(2,2)-dum*z(1,2))
       b=(z(1,3)-a*z(1,2))/z(1,1)
       return
c<<<<<<<<<<<<<<<<<<<<<<<<<<<<<<<<<<<<>>>>>>>>>>>>>>>>>>>>>>>>>>>>>>>>c
       end
```

```
C<<<<<<<<<<<<<<<<<<<<<<<<<<<<>>>>>>>>>>>>>>>>>>>>>>>>>>>>C
C     THIS PROGRAM IS A MEANS OF COMPUTING THE PORE       C
C     VOLUME DISTRIBUTION OF A POWDER FROM ISOTHERM       C
C      DATA DURING EITHER ADSORPTION OR DESORPTION.       C
C     FOR THE EXACT DERIVATION THE USER IS REFERENCED     C
C    TO THE BOOK "INTRODUCTION TO POWDER SURFACE AREA"    C
C                        BY S. LOWELL.                    C
C<<<<<<<<<<<<<<<<<<<<<<<<<<<<>>>>>>>>>>>>>>>>>>>>>>>>>>>>C
      DIMENSION P(50),VL(50),RK(50),F(50),RP(50)
      DIMENSION RKAV(50),RPAV(50),DELF(50),DELVL(50)
      DIMENSION SA(50),SUMSA(50),EXPOS(50),POREVOL(50)
C     PO IS THE SATURATION PRESSURE.
C     N IS THE NUMBER OF DATA POINTS.
C     GRAMS IS THE ADSORBENT SAMPLE WEIGHT (GMS).
      READ (2,*),PO,N,GRAMS
C     THE AMBIENT PRESSURE (SAME UNITS AS DATA POINTS)
C     NUMBER OF DATA POINTS, AND ADSORBENT SAMPLE
C     WEIGHT (IN GRAMS) MUST BE IN THE ABOVE ORDER IN
C     THE FIRST LINE OF THE DATA FILE. THE SUCCESSIVE
C     DATA PAIRS (PRESSURE, ADSORBENT WEIGHT) ARE THEN
C     READ FROM THE FILE.
      DO 10 I=1,N
C     PD IS THE PRESSURE.
C     W IS THE WEIGHT GAIN OF ADSORBATE ON ADSORBENT.
      READ (2,*),PD,W
      P(I)=PD/PO
C     VL IS THE VOLUME OF CONDENSED ADSORBED GAS.
      VL(I)=1.235*W/GRAMS
C     RK IS THE KELVIN RADIUS.
      RK(I)=9.566/(-ALOG(P(I)))
C     F IS THE ADSORBED LAYER THICKNESS.
      F(I)=3.54*((5.0/(-ALOG(P(I))))**.33333)
C     RP IS THE RADIUS OF THE PORE.
      RP(I)=RK(I)+F(I)
10    CONTINUE
C     THE PREVIOUS LOOP CALCULATES:
C       1)THE RELATIVE ADSORPTION PRESSURE,
C       2)THE VOLUME OF CONDENSED ADSORBED GAS FROM
C         IT'S DENSITY (NITROGEN), AND GRAM NORMALIZES
C         ALL SUCESSIVE CALCULATIONS,
C       3)THE KELVIN PORE RADIUS (ASSUME A ZERO
C         WETTING ANGLE FOR NITROGEN),
C       4)THE ADSORBED FILM THICKNESS FROM THE HALSEY
C         EQUATION (IN ANGSTROMS),
      SA(0)=0.0
      SUMSA(0)=0.0
      EXPOS(0)=0.0
      DO 20 I=1,N-1
C     RKAV IS THE AVERAGE KELVIN RADIUS.
```

```
      RKAV(I)=(RK(I)+RK(I+1))/2.0
C     RPAV IS THE AVERAGE PORE RADIUS.
      RPAV(I)=(RP(I)+RP(I+1))/2.0
C     DELF IS THE CHANGE IN FILM DEPTH.
      DELF(I)=F(I)-F(I+1)
C     DELVL IS THE CHANGE IN ADSORBED VOLUME BETWEEN
C     SUCCESSIVE P/Po VALUES.
      DELVL(I)=VL(I)-VL(I+1)
C     EXPOS REPRESENTS THE VOLUME CHANGE OF THE ADSORB-
C     ED FILM REMAINING ON THE WALLS OF THE PORES FROM
C     WHICH THE CENTER CORE HAS PREVIOUSLY EVAPORATED.
      EXPOS(I)=DELF(I)*SUMSA(I-1)*.0001
C     POREVOL IS THE ACTUAL PORE VOLUME.
      POREVOL(I)=((RPAV(I)/RKAV(I))**2.0)*
     &(DELVL(I)-(EXPOS(I)))
C     SA IS THE SURFACE AREA OF THE PORE WALLS.
      SA(I)=20000.*POREVOL(I)/RPAV(I)
C     SUMSA IS THE SUM OF THE PREVIOUS SURFACE AREAS.
      SUMSA(I)=SUMSA(I-1)+SA(I)
20    CONTINUE
C     THIS LOOP CALCULATED THE AVERAGE PORE AND KELVIN
C     RADII, AND THE CHANGE IN FILM THICKNESS & VOLUME
C     ADSORBED FOR EACH INTERVAL; AS WELL AS THE
C     EXPOSED VOLUME OF FILM FOR EACH INTERVAL. THE
C     PORE VOLUME IS COMPUTED FROM GEOMETRIC CONSIDER-
C     ATIONS, AS IS THE SURFACE AREA AND RUNNING
C     SUMMATION OF THE SURFACE AREA.
      WRITE(3,21)
21    FORMAT(2X,'P/PO',2X,'VLIQUID',1X,'RKELVIN',2X,
     &  'RPORE',4X,'FILM',3X,'RK AVE',2X,'RP AVE',3X,
     &  'DELF',2X,'DELVL',2X,'S AREA',2X,'EXPOS',4X,
     &  'SUMSA',1X,'POREVOL',1X,'RPORE AVE',/)
      WRITE(3,22)
22    FORMAT(8X,'CM3/GR',4X,'A.',7X,'A.',6X,'A.',6X,
     &  'A.',6X,'A.',6X'A.'3X,'CM3/GR',2X,'M2/GR',2X,
     &  'CM3/GR',3X,'M2/GR',2X,'CM3/GR',4X,'A.',//)
      DO 30 I=1,N
      WRITE(6,40)P(I),VL(I),RK(I),RP(I),F(I),RKAV(I),
     &  RPAV(I),DELF(I),DELVL(I),SA(I),EXPOS(I),
     &  SUMSA(I),POREVOL(I),RPAV(I)
      WRITE(3,40)P(I),VL(I),RK(I),RP(I),F(I),RKAV(I),
     &  RPAV(I),DELF(I),DELVL(I),SA(I),EXPOS(I),
     &  SUMSA(I),POREVOL(I),RPAV(I)
30    CONTINUE
40    FORMAT(F6.3,1X,F6.3,2X,F8.3,1X,F8.3,1X,F6.3,/,
     &  40X,F7.3,1X,F7.3,1X,F6.3,2X,F5.3,1X,F7.3,2X,
     &  F6.4,1X,F7.3,2X,F6.4,1X,F7.3)
C<<<<<<<<<<<<<<<<<<<<<<<<<<<<<<<<>>>>>>>>>>>>>>>>>>>>C
      END
```

```
c<<<<<<<<<<<<<<<<<<<<<<<<<<<<>>>>>>>>>>>>>>>>>>>>>>>>>>>>>>c
c        This program evaluates the first through         c
c                      fourth moments                     c
c<<<<<<<<<<<<<<<<<<<<<<<<<<<<>>>>>>>>>>>>>>>>>>>>>>>>>>>>>>c
c
      implicit real*8(a-h,o-z)
      dimension v(200),t(200),dt(200)
      write(6,*)
      pi=4.*datan(1.d0)
      write(6,*)'This program will read Time(sec),',
     &' Voltage(volt) for'
      write(6,*)'data in file FOR003.DAT.  It will then',
     &' analyze this'
      write(6,*)'data for the 1st, 2nd, 3rd and 4th',
     &' moments.'
      write(6,*)
      write(6,10)
10    format(' ',' Enter the number of data pairs,',
     &' (integer) ')
c     npoint is the number of data points.
      read(5,*) npoint
      do 40 i=1,npoint
c     t is the time and v is the voltage obtained from
c     the data file for003.dat.
40    read(3,*) t(i),v(i)
      write(6,*)' To normalize the data inter 0'
      read(5,*)nor
      if(nor.ne.0)goto 55
      f1=v(npoint)-v(1)
      f2=v(1)
      do 50 i=1,npoint
50    v(i)=(v(i)-f2)/f1
55    write(6,*)'To offset Time data, input T-offset(sec),'
      write(6,*)'      (0 for no offset)  '
c     t1 is the time value to offset the time scale.
      read(5,*)t1
      if(t1.eq.0)goto 100
c     Calculation of the first through forth moments.
      do 60 i=1,npoint
60    t(i)=t(i)-t1
100   write(6,*)
c     This loop calculates the change for the normalized
c     weight gain.
      do 102 i=1,npoint
102   v(i)=1.-v(i)/v(npoint)
c     This loop calculates the change for successive
c     time increments.
      do 130 i=2,npoint
130   dt(i)=t(i)-t(i-1)
```

```
      t0=0.
c     Calculation for the first moment.
      do 135 i=2,npoint
135   t0=t0+.5*(v(i)+v(i-1))*dt(i)
      n1=1
      write(6,400)n1,t0
c     calculation of the second through forth moments.
      do 300 n=1,3
      tsum=0.
      do 200 i=2,npoint
c     t(i)**n is the weighting factor for the absolute
c     moments (i.e. 1, 2, 3 for the second, third and
c     forth moments respectively).
      d1=.5*t(i)**n
      d2=.5*t(i-1)**n
200   tsum=tsum+(v(i)*d1+v(i-1)*d2)*dt(i)
      n1=n+1
300   write(6,400) n1,tsum
400   format('  moment# ',i1,' = ',1pd10.3)
c<<<<<<<<<<<<<<<<<<<<<<<<<<<>>>>>>>>>>>>>>>>>>>>>>>>>>>>>>>>>>c
      end
```

```
c<<<<<<<<<<<<<<<<<<<<<<<<<<<<<<>>>>>>>>>>>>>>>>>>>>>>>>>>>>>>>c
c                  Diffusion model for a slab                   c
c                      Non-steady state                         c
c                Constant surface concentration                 c
c<<<<<<<<<<<<<<<<<<<<<<<<<<<<<<>>>>>>>>>>>>>>>>>>>>>>>>>>>>>>>c
c
       implicit real*8(a-h,o-z)
       pi=3.14159
       j=0
       write(6,*)
       write(6,10)
10     format(' ','Input De(cm**2/s) for initial slope',
     &' and moment')
c      diffl is the diffusion coeff. from initial slope
c      method. diff2 is the diffusion coeff. from moment
c      analysis.
       read(5,*) diffl,diff2
       write(6,20)
20     format(' ',' Input diffusion length(cm)')
c      rlen is 1/2 the path length.
       read(5,*) rlen
       write(6,30) diffl,rlen
       write(7,30) diffl,rlen
30     format(' ',' De (initial slope) = ',1pd10.3,'  length = '
     &,1pd10.3/)
15     write(7,*)
       write(6,*)
       j=j+1
       if(j.ne.2) goto 37
       write(6,31) diff2,rlen
       write(7,31) diff2,rlen
31     format(' ',' De (moment)        = ',1pd10.3,
     &'  length = ',1pd10.3/)
37     if(j.eq.1) diff=diffl
       if(j.eq.2) diff=diff2
       if(j.gt.2) go to 1000
       write(6,40)
       write(7,40)
       write(7,*)
       write(6,*)
40     format(' time(sec)     [time(sec)]**.5',
     &'        V/V-inf')
c*****************************************************c
c       Calculation of M/M-inf vs. time values        c
c*****************************************************c
       do 100 i=1,40
       ds=float(i)
       time=ds**2
       sum=0.
```

```
      dum1=time*pi**2*diff/4./rlen**2
      dum2=8./pi**2
c     This loop calculates the series part of the
c     solution.
      do 50 n=0,50
      rl=float(2*n+1)
50    sum=sum+dum2*dexp(-dum1*rl**2)/rl**2
c     Sum is the M/M-inf value.
      sum=1.-sum
      write(6,70)time,ds,sum
      write(7,70)time,ds,sum
70    format(1pd9.2,8x,1pd9.2,10x,1pd10.3)
100   continue
      go to 15
1000  write(6,*)
c<<<<<<<<<<<<<<<<<<<<<<<<<<<<<<<<>>>>>>>>>>>>>>>>>>>>>>>>>>c
      end
```

```
c<<<<<<<<<<<<<<<<<<<<<<<<<<<<<<>>>>>>>>>>>>>>>>>>>>>>>>>>>c
c                Diffusion model for a slab               c
c                     Non-steady state                    c
c              variable surface concentration             c
c<<<<<<<<<<<<<<<<<<<<<<<<<<<<<<>>>>>>>>>>>>>>>>>>>>>>>>>>>c
c
       implicit real*8(a-h,o-z)
       pi=3.14159
       write(6,*)
       write(6,10)
10     format(' ','Input De(cm**2/s), Beta, r(cm) ')
c      diff is the diffusion coefficient.
c      beta is the flow rate divided by the diffusion
c      cell volume.
c      rlen is 1/2 the path length.
       read(5,*) diff,beta,rlen
       write(6,*)'  Input # of iterations, ds'
c      ds6 is a multiplier for the square root of time.
       read(5,*)nl,ds6
       write(6,30) diff,beta
       write(7,30) diff,beta
30     format(' ',' De (initial slope) = ',1pd10.3,
     &'  beta = '
     &,1pd10.3/)
       write(7,*)
       write(6,*)
       write(6,40)
       write(7,40)
       write(7,*)
       write(6,*)
40     format(' time(sec)     [diff*time/R**2]**.5',
     &'     V/V-inf')
c*******************************************************c
c       Calculation of M/M-inf vs. time values          c
c*******************************************************c
       do 100 i=1,nl
c      ds is the square root of time.
       ds=float(i)*ds6
       time=ds**2
       sum=0.
       r1=0.
       r2=0.
       r3=0.
       dum1=exp(-1.0*beta*time)*(diff/beta/rlen**2)**.5*
     &tan((beta*rlen**2/diff)**.5)
       dum2=8./pi**2
c      This loop claculates the series part of the
c      solution.
       do 50 n=0,50
```

```
        r1=(2.0*float(n)+1.0)**2
        r2=exp(-1.0*r1*pi**2*diff*time/4.0/rlen**2)
        r3=r1*(1.-(r1*(diff*pi**2/(4.*beta*rlen**2))))
50      sum=sum+ r2/r3
c       Sum is the M/M-inf value.
        sum=1.-dum1-dum2*sum
        write(6,70)time,(diff*time/rlen**2)**.5,sum
        write(7,70)time,(diff*time/rlen**2)**.5,sum
70      format(1pd9.2,8x,1pd9.2,10x,1pd10.3)
100     continue
        write(6,*)
c<<<<<<<<<<<<<<<<<<<<<<<<<<<<<>>>>>>>>>>>>>>>>>>>>>>>>>>>>>>>>c
        end
```

```
c<<<<<<<<<<<<<<<<<<<<<<<<<<<<<>>>>>>>>>>>>>>>>>>>>>>>>>>>>>>c
c                Diffusion model for a cylinder            c
c                      Non-steady state                    c
c                constant surface concentration            c
c<<<<<<<<<<<<<<<<<<<<<<<<<<<<<>>>>>>>>>>>>>>>>>>>>>>>>>>>>>>c
c
        implicit real*8(a-h,o-z)
        real ml,m
        write(6,*)
        write(6,10)
10      format(1x,'Input De(cm**2/s), radius(cm)')
c       diff is the diffusion coefficient.
c       r is the radius of the cylinder.
        read(5,*) diff,r
        write(6,*)
        write(6,*)'Input # of iterations'
        read(5,*)n8
        write(6,*)
        write(6,20)diff,r
        write(3,20)diff,r
20      format(1x,' Diffusity = ',1pd10.3,'   r = ',
     &1pd10.3)
        write(6,*)
        write(3,*)
        write(6,30)
        write(3,30)
30      format(1x,'  Time(sec)     (diff*time/r**2)**.5',
     &'      v/v-inf')
        write(6,*)
        write(3,*)
        do 100 i = 1,n8
        dum1=0.0
        ds=float(i)
        time=ds**2
c       x1 initializes the starting point to find the
c       zeros for Jo(alphn*R).
        x1 = 2.40
        m1=0.
        do 200 j = 1,50
c***********************************************************c
c             Newton-Raphson for finding zeros              c
c***********************************************************c
        loop=0
1       call bess0(x1,0,f)
        call bess0(x1,1,fslope)
        xn=x1+(f/fslope)
        call bess0(xn,0,Y3)
        IF (ABS(Y3).LT.0.0001) GO TO 150
        loop=loop+1
```

```
        if(loop.gt.60) goto 1000
        xl=xn
        goto 1
c       alphns are the roots of Jo(R*alphn)=0.
150     alphn=xn/r
        xl=xn+3.0
c*****************************************************c
c                Calculate summation values           c
c*****************************************************c
        r3=exp(-1.0*diff*(alphn)**2*time)
        r4=4.0/alphn**2/r**2
        ml=ml+r3*r4
200     continue
c               Calculation of the M/M-inf value.
        M=1.0 - ml
c*****************************************************c
c                        Print routine                c
c*****************************************************c
        write(6,89)time,(diff*time/r**2)**.5,M
        write(3,89)time,(diff*time/r**2)**.5,M
89      format(2x,1pd9.2,11x,1pd9.2,10x,1pd10.3)
100     continue
        write(6,*)
        write(3,*)
c<<<<<<<<<<<<<<<<<<<<<<<<>>>>>>>>>>>>>>>>>>>>>>>>c
1000    end
```

```
c<<<<<<<<<<<<<<<<<<<<<<<<<<<<<>>>>>>>>>>>>>>>>>>>>>>>>>>>>>>>c
c                 Diffusion model for a cylinder             c
c                      Non-steady state                      c
c                 variable surface concentration             c
c<<<<<<<<<<<<<<<<<<<<<<<<<<<<<>>>>>>>>>>>>>>>>>>>>>>>>>>>>>>>c
c
        implicit real*8(a-h,o-z)
        real m1,m
        write(6,*)
        write(6,10)
10      format(1x,'Input De(cm**2/s), beta and the',
     &' radius(cm)')
c       diff is the diffusion coefficient.
c       beta is the flow rate divided by the diffusion
c       cell volume.
c       r is the diameter of the pellet.
        read(5,*) diff,beta,r
        write(6,*)
        write(6,*)'Input # of iterations, ds'
c       s25 is the multiplier for the square root
c       increment.
        read(5,*)n8,s25
        write(6,*)
        write(6,20)diff,beta
        write(3,20)diff,beta
20      format(1x,' Diffusity = ',1pd10.3,'   Beta',
     &' = ',1pd10.3)
        write(6,*)
        write(3,*)
        write(6,30)
        write(3,30)
30      format(1x,'  Time(sec)    (diff*time/r**2)**5',
     &'   v/v-inf')
        write(6,*)
        write(3,*)
        do 100 i = 1,n8
        dum1=0.0
        ds=float(i)*s25
        time=ds**2
        r1=(beta*r**2/diff)**0.5
c       Calculation of Jo(r1).
        call bess0(r1,0,y1)
c       Calculation of J1(r1).
        call bess0(r1,1,y2)
        dum1=(2*y2*exp(-1.*beta*time))/(r1*y1)
c       x1 initializes the starting point to find the
c       zeroes for Jo(alphn*R).
        x1 = 2.40
        m1=0.
```

```
        do 200 j = 1,65
c*************************************************************c
c             Newton-Raphson for finding zeros                c
c*************************************************************c
        loop=0
1       call bess0(x1,0,f)
        call bess0(x1,1,fslope)
        xn=x1+(f/fslope)
        call bess0(xn,0,Y3)
        IF (ABS(Y3).LT.0.0001) GO TO 150
        loop=loop+1
        if(loop.gt.60) goto 1000
        x1=xn
        goto 1
c       alphns are the roots of Jo(R*alphn)=0
150     alphn=xn/r
        x1=xn+3.0
c*************************************************************c
c                  Calculate summation values                 c
c*************************************************************c
        r3=exp(-1.0*diff*(alphn)**2*time)
        r4=alphn**2*(((alphn**2/(beta/diff))-1.0))
        m1=m1+r3/r4
200     continue
c       calculation of the M/M-inf value.
        M=1.0 - dum1 + (4.0/r**2)*m1
c*************************************************************c
c                           Print routine                     c
c*************************************************************c
        write(6,89)time,(diff*time/r**2)**.5,M
        write(3,89)time,(diff*time/r**2)**.5,M
89      format(2x,1pd9.2,7x,1pd9.2,8x,1pd10.3)
100     continue
        write(6,*)
        write(3,*)
c<<<<<<<<<<<<<<<<<<<<<<<<<<<<>>>>>>>>>>>>>>>>>>>>>>>>>>>>>c
1000    end
```

```
c<<<<<<<<<<<<<<<<<<<<<<<<<<<<<<<<>>>>>>>>>>>>>>>>>>>>>>>>>>>>c
c                  Diffusion model for a sphere                c
c                        Non-steady state                      c
c                  Constant surface concentration              c
c<<<<<<<<<<<<<<<<<<<<<<<<<<<<<<<<>>>>>>>>>>>>>>>>>>>>>>>>>>>>c
c
      implicit real*8(a-h,o-z)
      real n2
      write(6,*)'Input D/a**2, # of iterations'
c     diff is the diffusion coefficient divided by the
c     path length.
      read(5,*) diff,n
      write(3,15)
15    format(3x,'Sphere with constant surface',
     &' concentration')
      write(3,*)
      pi2 = 3.14159**2
c     This loop calculates the series part of the
c     solution.
      do 1 i=0,n
      ds=float(i)*.5
      time=ds**2
      sum=0.0
      do 2 m=1,100
      n2=float(m)**2
      r1=exp(-1.0*n2*diff*pi2*time)
      sum=sum+r1/n2
2     continue
      sum1=1.0-(6.0/pi2)*sum
      write(3,30) time,(diff*time)**.5,sum1
      write(6,30) time,(diff*time)**.5,sum1
30    format(5x,1pd9.2,5x,1pd9.3,5x,1pd10.3)
1     continue
c<<<<<<<<<<<<<<<<<<<<<<<<<<<<<<<<>>>>>>>>>>>>>>>>>>>>>>>>>>>>c
      end
```

```
c<<<<<<<<<<<<<<<<<<<<<<<<<<<<<<>>>>>>>>>>>>>>>>>>>>>>>>>>>>>>>c
c                   Diffusion model for a sphere               c
c                         Non-steady state                     c
c                  Variable surface concentration              c
c<<<<<<<<<<<<<<<<<<<<<<<<<<<<<<>>>>>>>>>>>>>>>>>>>>>>>>>>>>>>>c
c
        implicit real*8(a-h,o-z)
        real N2
        pi2=3.14159**2
5       write(6,10)
10      format(1x,'Input D/(R**2)(s**-1)')
c       diff is the diffusion coefficient divided by the
c       path length.
        read(5,*) diff
        write(6,*)
        write(6,20)
20      format(1x,'Input F/V (s**-1),  # of iterations
     &, ds')
c       beta is the flow rate cc/s divided by the
c       diffusion cell volume.  n is the number of
c       iterations and s is the multiplier for the square
c       root increment.
        read(5,*) beta,n,s
        write(6,*)
        write(7,30) diff,beta
        write(6,30) diff,beta
30      format(1x,' Diffusity = ',p1d10.3,'    Beta
     &= ',p1d10.3)
        write(6,*)
        write(7,*)
        write(6,40)
        write(7,40)
40      format(1x,'  Time(sec)     (De*t/R**2)**.5
     &    V/V-inf')
        write(6,*)
        write(7,*)
        do 100 I = 1,n
c       ds is the square root of time.
         ds=s*float(I)
         time=ds**2
         dim=(diff*time)**0.5
         sum=0.0
         dum1=(3.0*diff/beta)*exp(-1.0*beta*time)
         dum2=(1.-(beta/diff)**0.5*(1.0/tan((beta/diff
     &)**0.5)))
         dum3=(6.*beta)/(pi2*diff)
        do 200 m=1,50
         n2=float(m)**2
         r1=exp(-1.*diff*n2*pi2*time)
```

```
          r2=n2*(n2*pi2-beta/diff)
200       sum=sum+r1/r2
         sum1=1.0-dum1*dum2+dum3*sum
         write(6,70) time,(diff*time)**.5,sum1
         write(7,70) time,(diff*time)**.5,sum1
70       format(2x,1pd9.2,6x,1pd9.2,6x,1pd10.3)
100      continue
         go to 5
c<<<<<<<<<<<<<<<<<<<<<<<<<<<<<<>>>>>>>>>>>>>>>>>>>>>>>>>>>>>>>>>>c
         end
```

```
c<<<<<<<<<<<<<<<<<<<<<<<<<<<<<>>>>>>>>>>>>>>>>>>>>>>>>>>>>>>>c
c                 2 CSTR's in parallel model                  c
c<<<<<<<<<<<<<<<<<<<<<<<<<<<<<>>>>>>>>>>>>>>>>>>>>>>>>>>>>>>>c
c
        implicit real*8(a-h,o-z)
        real M
        write(6,*)
        write(6,*)'Input F1 and F2 (cc/s)'
c       f1 and f2 are the flow rates into the lower and
c       upper chambers respectively.
        read(5,*) f1,f2
        write(6,*)'Input # of iterations'
        read(5,*) n8
c       v1 is the diffusion cell volume.
        v1=15.0
c       v2 is the upper chamber volume.
        v2=2400.0
        x1=f1*v2 + (v1+v2)*f2
        x2=f1*f2
        x3=v1*v2
        a=(2.0*x2)/(x1+sqrt(x1**2-4.0*x2*x3))
        b=(x1+sqrt(x1**2-4.0*x2*x3))/(2.0*x3)
        z1=f1/(v1*(b-a))
        z2=1.0/(a-b)
        write(6,*)
        write(6,19)f1,f2
        write(3,19)f1,f2
19      format(2x,'F1 = ',1pd9.2,'  F2 = ',1pd9.2/)
        write(3,*)
        write(6,*)
        write(6,10)
        write(3,10)
10      format(1x,'   Time(sec)    [Time(sec)]**.5',
     &'     v/v-inf')
        write(3,*)
        write(6,*)
c*************************************************************c
c          Calculation of M/M-inf vs. time values             c
c*************************************************************c
        do 100 i=0,n8
        ds=float(i)*3
        time=ds**2
        r1=exp(-1.0*a*time)-exp(-1.0*b*time)
        r2=b*exp(-1.0*a*time)-a*exp(-1.0*b*time)+a-b
c       M = M/M-inf value.
        M=z1*r1+z2*r2
        write(6,20) time,ds,M
        write(3,20) time,ds,M
20      format(3x,1pd9.2,7x,1pd9.2,8x,1pd10.3)
```

```
100     continue
        write(6,*)
        write(3,*)
c<<<<<<<<<<<<<<<<<<<<<<<<<<<>>>>>>>>>>>>>>>>>>>>>>>>>>>c
        end
```

```
c<<<<<<<<<<<<<<<<<<<<<<<<<<<>>>>>>>>>>>>>>>>>>>>>>>>>>>>>>c
c             Diffusion model for a cylinder              c
c                  Non-steady state                       c
c        2 CSTR model as the surface concentration        c
c<<<<<<<<<<<<<<<<<<<<<<<<<<<>>>>>>>>>>>>>>>>>>>>>>>>>>>>>>c
c
        implicit real*8(a-h,o-z)
        real ml,m
        write(6,*)
        write(6,10)
10      format(1x,'Input De(cm**2/s), F1 and F2 (cc/s),',
     &' V2')
c       diff is the diffusion coefficient.
c       f1 and f2 are the flow rates into the diffusion
c       cell and the upper chamber respectively.
c       v2 is the upper chamber volume.
        read(5,*) diff,f1,f2,V2
c       r is the radius of the cylinder.
        r=0.045
c       v1 is the diffusion cell volume.
        v1=15.0
        x1=f1*v2 + (v1+v2)*f2
        x2=f1*f2
        x3=v1*v2
        a=(2.0*x2)/(x1+sqrt(x1**2-4.0*x2*x3))
        b=(x1+sqrt(x1**2-4.0*x2*x3))/(2.0*x3)
        z1=f1/(v1*(b-a))
        z2=1.0/(a-b)
        write(6,*)
        write(6,*)'Input # of iterations'
        read(5,*)n8
        write(6,*)
        write(6,20)diff,f1,f2
        write(4,20)diff,f1,f2
20      format(1x,' Diffusity = ',p1d10.3,' F1 = ',
     &1pd9.2,' F2 = ',1pd9.2)
        write(6,*)
        write(4,*)
        write(6,30)
        write(4,30)
30      format(1x,'  Time(sec)    [Time(sec)]**.5',
     &'     v/v-inf')
        write(6,*)
        write(4,*)
c*********************************************************c
c        Calculation of M/M-inf vs. time values           c
c*********************************************************c
        do 100 i = 0,n8
        ds=float(i)*3
```

```
        time=ds**2
c       xl initializes the starting point to find the
c       zeroes for Jo(alphan*R)
        xl = 2.40
        ml=0.
        do 200 j = 1,50
c*************************************************************c
c            Newton-Raphson for finding zeros                 c
c*************************************************************c
        loop=0
1       call bess0(xl,0,f)
        call bess0(xl,1,fslope)
        xn=xl+(f/fslope)
        call bess0(xn,0,Y3)
        IF (ABS(Y3).LT.0.0001) GO TO 150
        loop=loop+1
        if(loop.gt.60) goto 1000
        xl=xn
        goto 1
c       alphns are the roots of Jo(R*alphn)=0.
150     alphn=xn/r
        xl=xn+3.0
c*************************************************************c
c                 Calculate summation values                  c
c*************************************************************c
        r1=exp(-1.0*a*time)
        r2=exp(-1.0*diff*alphn**2*time)
        r3=exp(-1.0*b*time)
        r4=alphn**2-a/diff
        r5=alphn**2-b/diff
        r6=alphn**2
        dum1 = z1*((r1-r2)/r4 + (r2-r3)/r5)
        dum2 = z2*((b*r1-b*r2)/r4 + (a*r2-a*r3)/r5)
        dum3 = (1.0 - r2)/r6
        ml=ml + dum1+dum2+dum3
200     continue
c           Calculation of the M/M-inf values
        M=(4.0/r**2)*ml
c*************************************************************c
c                   Print routine                             c
c*************************************************************c
        write(6,89)time,ds,M
        write(4,89)time,ds,M
89      format(2x,1pd9.2,7x,1pd9.2,8x,1pd10.3)
100     continue
        write(6,*)
        write(4,*)
c<<<<<<<<<<<<<<<<<<<<<<<<<<<<>>>>>>>>>>>>>>>>>>>>>>>>>>>>>>>>>>c
1000    end
```

```
1  REM  THIS PROGRAM SAMPLES TIME

2  REM  VERSUS VOLTAGE DATA FROM
3  REM  DIFFUSION EXPERIMENTS WIT
     H
4  REM  THE KAHN ELECTROBALANCE.
10  DIM V(1000),T(1000)
20  REM  C=ANALOG I/O CHANNEL
30 C = 1
40  PRINT "INPUT RUN#"
50  INPUT R1
55  REM  THIS LOOP ZEROES THE SCA
     LE
60  PRINT "ZERO VOLTAGE SETTING"
70  FOR I = 1 TO 20
80  & AIN,(TV) = V,(C#) = C
90  PRINT 5 * (V - 2048) / 2048
95  & PAUSE = 1
100  NEXT I
790  PRINT "INPUT SORPTION #"
791  REM  R2 IS THE SORPTION #
795  INPUT R2
797 V0 = 0.
798 VM = 0.
800  & TIME TO HR,MN,SC
801  HGR2
803  & ALTSET
804  & OUTLINE
805  REM  SETS UP SCREEN FOR PLOT
     MODE
806 PLT =  PEEK (966) +  PEEK (96
     7) * 256
807  POKE PLT,0
810 N = 1
815  REM  ST IS THE SAMPLE TIME I
     NTERVAL
820 ST = 1.0
830  & PAUSE = ST
835 D = 0
840  FOR I = 1 TO 100
850  & ASUM,(TV) = D,(C#) = C
860  NEXT I
870 V(N) = D / 100.
880  & TIME TO H1,M1,S1
905 NT = N
```

```
908  REM  RANGE OF THE INSTRUMENT

909 P1 = .25 * (V(N) - 2048)
910  IF P1 > 100 THEN P1 = 100
911  IF P1 < 0 THEN P1 = 0
913  & NXTPLT = P1
920  & BIN,(TV) = B
930  IF B < 65535 THEN  GOTO 999
935 N = N + 1
936 T(N - 1) = 3600 * (H1 - HR) +
     60 * (M1 - MN) + S1 - SC
937  IF T(N - 1) > 180 THEN ST =
     10
938  IF T(N - 1) > 500 THEN ST =
     25
939  IF T(N - 1) > 1000 THEN ST =
     100
940  GOTO 830
999  TEXT
1000  REM  LETS YOU VIEW DATA
1002  PRINT "FINAL VOLTAGE = ";V9
     ;" VOLTS"
1004  PRINT "SORPTION RUN # =",R2

1010  PRINT "# OF DATA POINTS=";N
     T
1011  PRINT
1012  PRINT "FIRST PRINT HARD COP
     Y OF THE GRAPH."
1013  PRINT "THEN VIEW RAW DATA A
     ND NORMALIZE IT."
1015  PRINT "INPUT 0 TO HARD COPY
      GRAPH"
1020  PRINT "TO VIEW RAW DATA, IN
     PUT 1"
1030  PRINT "TO STORE RAW DATA, I
     NPUT 2"
1035  PRINT "TO HARD COPY RAW DAT
     A, INPUT 3"
1040  PRINT "TO START ANOTHER RUN
     , INPUT4"
1050  PRINT "TO END EXPERIMENT, I
     NPUT 5"
1060  INPUT IC
1070  IF IC = 5 THEN  GOTO 2000
```

```
1080  IF IC = 4 THEN  GOTO 790
1085  IF IC = 3 THEN  GOTO 1700
1090  IF IC = 2 THEN  GOTO 1410
1092  IF IC = 0 THEN  GOTO 1900
1100  PRINT "INPUT 1ST AND LAST P
     OINTS TO BE VIEWED"
1110  INPUT Z1,Z2
1120 L = (Z2 - Z1) / 10 + 1
1130  FOR J = 1 TO L
1135  PRINT "TIME(SEC)
      VOLTS"
1140 Z3 = Z1 + 9
1150  FOR J1 = Z1 TO Z3
1160  PRINT T(J1),V(J1)
1170  NEXT J1
1175  & PAUSE = 10
1180 Z1 = Z3 + 1
1190  NEXT J
1195  IF VM > 0 THEN  GOTO 1350
1200  PRINT "TO ZERO VOLTAGE,INPU
     T THE DESIRED OFFSET,0 FOR N
     O OFFSET"
1210  INPUT V0
1220  PRINT "TO NORMALIZE, INPUT
     MAX. VOLTS,0 FOR NO NORMALIZ
     ATION"
1230  INPUT VM
1240  IF V0 > 0 THEN  GOTO 1270
1250  IF VM > 0 THEN  GOTO 1270
1260  GOTO 1350
1270  FOR I = 1 TO NT
1280 V(I) = (V(I) - V0) / (VM - V
     0)
1290  NEXT I
1300  PRINT "TO OFFSET TIME DATA,
      INPUT T-OFFSET(SEC), 0 FOR
     NO OFFSET"
1310  INPUT T0
1320  FOR I = 1 TO NT
1330 T(I) = T(I) - T0
1340  NEXT I
1350  PRINT
1351  PRINT "INPUT 1 TO VIEW DATA
     "
1355  PRINT "INPUT 2 TO HARD COPY
      RESULTS"
```

```
1360  PRINT "INPUT 3 TO STORE DAT
      A"
1370  PRINT "INPUT 4 FOR A NEW RU
      N"
1375  PRINT "INPUT 5 TO END EXPER
      IMENT"
1380  INPUT I9
1390  IF I9 = 5 THEN  GOTO 2000
1395  IF I9 = 2 THEN  GOTO 1800
1400  IF I9 = 1 THEN  GOTO 1100
1405  IF I9 = 4 THEN  GOTO 790
1410  REM  DATA STORAGE SECTION
1411  PRINT
1420 D$ = "": REM   THERE IS A CO
      NTROL-D BETWEEN THE QUOTES
1421  PRINT
1423  PRINT "INPUT NAME OF DATA F
      ILE"
1425  INPUT Z$
1440  PRINT
1442  PRINT "MAKE SURE THAT A DIS
      K IS IN THE DRIVE"
1443  & BUZZ ON
1444  & PAUSE = 5
1445  & BUZZ STOP
1450  PRINT D$;"OPEN ";Z$
1460  PRINT D$;"WRITE ";Z$
1470  PRINT R1
1480  PRINT R2
1485  PRINT NT
1490  FOR I = 1 TO NT
1500  PRINT T(I)
1505  PRINT V(I)
1510  NEXT I
1520  PRINT D$;"CLOSE DATA"
1530  GOTO 1350
1699  REM  HARD COPY OF RAW DATA
1700  PR# 1
1705  PRINT
1710  PRINT "RUN # =";R1
1720  PRINT "SORPTION # =";R2
1721  PRINT "RAW DATA"
1722  PRINT "ZERO VOLTS = ";V0
1723  PRINT "MAX. VOLTS = ";VM
```

```
1724  PRINT "#OF DATA PAIRS = ";N
      T
1725  PRINT
1730  PRINT "TIME(SEC)        VOLT
      S"
1735  PRINT
1740  FOR I = 1 TO NT
1750  PRINT  TAB( 4);T(I); TAB( 1
      3);V(I)
1760  NEXT I
1770  PR# 0
1775  PRINT
1780  GOTO 1015
1800  REM  NORMALIZED DATA
1801  PR# 1
1805  PRINT
1810  PRINT "RUN # =";R1
1820  PRINT "SORPTION # =";R2
1825  PRINT "FINAL VOLTAGE =",V9
1830  PRINT "NORMALIZED DATA"
1840  PRINT "TIME(SEC)      V/V-IN
      F"
1845  PRINT
1850  FOR I = 1 TO NT
1860  PRINT  TAB( 4);T(I); TAB( 1
      3);V(I)
1870  NEXT I
1880  PR# 0
1890  GOTO 1350
1900  REM . PLOTTING ROUTINE
1902  PRINT "PLOT OF WEIGHT GAIN
      VS TIME": PRINT
1903  PRINT "RUN # = ";R1
1904  PRINT "SORPTION # = ";R2
1905  PRINT "# OF DATA POINTS SAM
      PLED = ";NT
1906  PRINT
1907  POKE 10,76: POKE 11,00: POKE
      12,96
1910  PRINT  CHR$ (4);"BLOAD EPSO
      N.HIRES.OBJ"
1920  PRINT  USR (1101)
1930  GOTO 1015
2000  END
```

APPENDIX 3

EQUILIBRIUM ADSORPTION DATA

APPENDIX 3

EQUILIBRIUM ADSORPTION DATA

Table 7. Data For Equilibrium Adsorption Experiments for Katalco Alumina Supports.

Sorption #	Pressure (kPa)	Total Wt. Gain (mg)
	Run #1†[a]	
1	4.7	2.90
2	8.8	4.07
3	12.1	4.70
4	15.9	5.36
5	19.7	6.08
	Run #2†[b]	
1	3.9	3.29
2	7.6	4.36
3	11.2	5.09
4	14.7	5.76
5	17.9	6.32
6	21.6	6.93
	Run #3‡[c]	
1	1.5	5.51
2	4.1	12.05
3	8.1	19.51
4	14.0	27.48
5	19.7	33.75
6	25.3	39.88

† Adsorbate used was carbon dioxide at 273 K.
‡ Adsorbate used was 2,2-dimethylpropane at 273 K.
[a] Adsorbent weight = 0.4041gms.
[b] Adsorbent weight = 0.4786 gms.
[c] Adsorbent weight = 0.4986 gms.

Table 8. Data For Equilibrium Adsorption Experiments for ϵ = 0.48 Bimodal Spheres.

Sorption #	Pressure (kPa)	Total Wt. Gain (mg)
	Run #1*	
1	1.5	1.78
2	2.9	2.72
3	5.2	4.15
4	7.3	5.37
5	9.9	6.72
6	12.4	7.69
7	14.0	8.82
8	18.8	9.86
9	20.0	10.79
10	22.8	11.66
11	23.6	12.36
12	31.5	14.51
13	35.9	16.12
14	38.8	16.99
15	40.4	18.13
16	45.1	19.59
17	47.9	21.43
18	50.7	22.46
	Run #2*	
1	3.5	3.20
2	7.7	5.74
3	10.5	7.15
4	13.6	8.63
5	16.7	9.94
6	19.3	10.89
7	22.0	11.93

*Adsorbate used was 2,2-dimethylpropane at 273 K; adsorbent weight = 0.6011 gms.

Table 9. Data For Equilibrium Adsorption Experiments for ϵ = 0.61 Bimodal Spheres.

Sorption #	Pressure (kPa)	Total Wt. Gain (mg)
	Run #1*	
1	3.6	1.26
2	8.1	2.56
3	11.2	3.49
4	14.5	4.47
5	16.7	5.24
6	20.7	5.88
7	22.9	6.34
	Run #2*	
1	–	1.62
2	4.3	1.94
3	7.9	3.15
4	12.7	4.48
5	17.1	5.68
6	20.1	6.24
7	23.9	6.94
8	29.1	8.03
9	34.8	9.19
10	38.8	9.89
11	42.5	10.77
12	49.2	11.27
13	54.7	12.81
14	57.9	19.07
15	61.2	15.26
16	64.0	17.08
17	69.6	17.89
	Run #3*	
1	2.1	1.56
2	5.3	2.70
3	9.7	4.09
4	16.7	5.85
5	21.5	6.83
6	25.3	7.62

*Adsorbate used was 2,2-dimethylpropane at 273 K; adsorbent weight = 0.441 gms.

Table 10. Data For Equilibrium Adsorption Experiments for $\epsilon = 0.28$ Unimodal Spheres.

Sorption #	Pressure (kPa)	Total Wt. Gain (mg)
	Run #1†a	
1	2.7	0.41
2	6.0	0.68
3	9.3	0.90
4	13.2	1.28
5	16.4	1.56
6	20.9	1.86
7	23.5	2.05
	Run #2†b	
1	3.6	0.82
2	8.8	1.58
3	12.5	2.21
4	16.9	2.83
5	20.8	3.34
6	24.9	3.75
7	28.7	4.31
	Run #3†b	
1	3.9	0.91
2	7.2	1.43
3	10.8	2.04
4	13.9	2.50
5	17.9	3.08
6	24.1	4.03
7	29.5	4.79
8	34.0	5.31
9	36.8	5.71
10	40.1	6.11
11	44.3	6.73
12	48.9	7.54
13	53.5	8.34
14	57.9	9.07
15	61.2	9.92
16	64.0	10.45
17	66.4	10.92
18	69.6	11.56

Table 10 (continued).

Sorption #	Pressure (kPa)	Total Wt. Gain (mg)
	Run #4‡c	
1	2.7	2.98
2	4.8	3.62
3	9.9	4.43
4	15.6	4.76
5	23.5	5.07
6	29.1	5.23
	Run #5†d	
1	0.9	0.12
2	2.7	0.36
3	4.8	0.61
4	8.7	1.08
5	12.0	1.40

† Adsorbate used was 2,2-dimethylpropane at 273 K.
‡ Adsorbate used was nitrogen at 77 K.
[a] Adsorbent weight = 0.4621 gms.
[b] Adsorbent weight = 1.1707 gms.
[c] Adsorbent weight = 0.9413 gms.
[d] Adsorbent weight = 0.7073 gms.

 Drake, M. C.
A study of new methods for the simultaneous measurement ...